STATOR FLUX VECTOR BASED MODULATION AND CONSTANT SWITCHING FREQUENCY DIRECT TORQUE CONTROL OF AC MACHINES

ANSHUMAN TRIPATHI

NATIONAL UNIVERSITY OF SINGAPORE

2004

STATOR FLUX VECTOR BASED MODULATION AND CONSTANT SWITCHING FREQUENCY DIRECT TORQUE CONTROL OF AC MACHINES

ANSHUMAN TRIPATHI
(M. Tech., IIT Kanpur, India)

A THESIS SUBMITTED FOR THE DEGREE OF DOCTOR OF PHILOSOPHY

DEPARTMENT OF ELECTRICAL & COMPUTER ENGINEERING,
NATIONAL UNIVERSITY OF SINGAPORE

2004

Acknowledgments

In my tenure as research student, I have come across several people who have been my teachers, colleagues, supervisors and friends. Dr. Ashwin M Khambadkone, first and foremost, has been all of these. The ideal supervisor and teacher I could have wished for, he is actively involved in the work of all his students and clearly always has their best interest in mind. Thank you Sir, for pushing me. Time after time, his easy grasp in the area of power electronics and control of industrial drives at its most fundamental level, helped me in the struggle for my own understanding. On the personal side, he did not hesitate to invite me to become an extended part of his schedule. Without any exaggeration, I owe to him, whatever little I know in the area of drives.

I thank Prof Sanjib K Panda, for constantly encouraging me during the course of my stay in the National University of Singapore. His constant encouragement and his advice regarding part time work as graduate tutor were very valuable. It helped me to stay with my family in Singapore.

My sincere thanks to Prof. Ramesh Oruganti, Director, Center for Power Electronics, and Dr. Abdullah Al Mamun for their encouragement and faith in my

abilities to pursue the PhD degree. Thank you Sir, for giving me this opportunity. I was lucky to work with Prof Oruganti for a brief period during the PEDS 2001. His expertise in the area of power electronics is second to none. He has always been encouraging and asking about me, my family, my work and my career.

Mr. Woo and Mr. Chandra, Lab officers of the Machine and Drives Laboratory, Mr. Teo of the PE lab and Mr. Seow of the Power systems lab have been a great help. Thank you all. The ever smiling face of Mr. Woo, always cheers one up. He kept on encouraging me when my spirits nose dived. He has a parental attitude towards the lab guys that dilutes the pressure. The lab is blessed by his presence.

In my Lab here in NUS, I was surrounded by friendly people who helped me daily. My Lab mates Sahooji, Krishna, Qing Hua, Amit, Wang Wei, Wu Xinhui, Dong Jing, Laurent, Phyu are knowledgeable bunch of guys. I am fortunate to know them and learn from them. I will never forget, Sahooji's brotherly attention and advice full of wisdom, regarding the matters of my job and research, Amit's patience in going through my dissertation draft and helping me out in many ways than one and Krishna's help in day to day things. Knowing people like Ravinder P, Xu Xinyu, Kong Xin, Siew Chong and Echo of the PE lab has been a great feeling. RP's sense of humor pulled me up even under stressed conditions. Thank you all for being my friends and teachers.

I thank the National University of Singapore for providing me with the research facility, the scholarship and part-time employment as graduate tutor. I feel honored to be a student of this institute.

Finally, I would like to thank those closest to me, whose presence helped make the completion of my work possible. My wife Deepshikha at home was constant source of encouragement. My Son Avi kept me awake and always on my toes. My friend Satya, his wife Reetha and their daughter Malu have been like family to me. They made me feel like being at home. My friend K. Viswanathan, kept pushing me and inspiring me at the same time. Vijay and his family has supported me every time and in every way they could.

Most of all, I would like to thank Shri SAINATH, who planned all this, my brother and his wife back in India and especially my parents, for their absolute confidence in me. Despite of adversities back home, they continued to encourage me to carry on. Probably, the knowledge that they will always be there to pick up the pieces is what allows me to repeatedly risk exploring new avenues.

Contents

Summary

Direct method of torque control is a major research area for control of speed and torque of AC machine drives. The advantages of classical direct torque control (DTC) methods over field oriented current control methods have been their rapid dynamic response, well defined torque ripple and simple to implement control structure. The problems of these methods are, variation of switching frequency with drive speed, requirement of very high sampling rates for digital implementation and absence of current control. More recent approaches towards direct torque control have been proposed that achieve torque control at constant switching frequency. These schemes use space vector modulation (SVM) to realize the voltage vector required for control and therefore are called DTC-SVM methods. However, the methods to obtain appropriate voltage vector requires computationally intensive control algorithms and approximations. Moreover, the existing DTC-SVM methods, have not demonstrated a dynamic performance, that matches with the classical DTC methods using hysteresis controllers.

The DTC-SVM method proposed in this work uses predictive stator flux vector control. This makes the torque and stator flux vector control algorithm simple. Torque ripple analysis has been carried out for all regions of operation. In

the overmodulation region, the proposed method of switching produces zero phase error in a fundamental cycle. As a result, steady state torque and stator flux vector control is possible in spite of the inverter voltage limit. A large signal algorithm is proposed, that helps to achieve a dynamic response similar to classical DTC methods. Steady state and dynamic torque control analysis is extended to the field weakening region and the theory developed is verified using experimental results.

Direct control of torque comes with an apprehension of excessive currents, specially during dynamic operating conditions. This is because the current vector is not directly controlled. Current vector dynamics are studied for a dynamic condition in torque. Using fundamental equations of the machine, it is shown how the current vector is inherently controlled in DTC schemes. Simulation and test results are provided to assist the analysis. By exploiting the structure of the proposed DTC-SVM method a current limiting DTC is also implemented.

In all, this dissertation has proposed a constant switching frequency DTC method and studied the steady state and dynamic torque control characteristics of the scheme. Theoretical developments have been appropriately supported with analytical and experimental results.

List of Tables

List of Figures

List of symbols

m_e	normalized motor torque
m_e^*	normalized reference torque
$\Delta m_{e(av)}(k)$	average torque error in a sampling period
$m_{e(av)}(k)$	average torque in a sample
$m_{e(av)}(sec)$	average torque in a sector
$\Delta m_{e(ovm)}$	average magnitude of torque pulsation in a sector
f_{sw}	switching frequency
t	time (sec)
τ	normalized time
τ_a, τ_b, τ_0	normalized switching state times
$\tau_{a1}, \tau_{b1}, \tau_{01}$	modified switching state times

$p.u.$	per unit
$\boldsymbol{u}_s$	normalized stator voltage vector
$\boldsymbol{u}_{an,bn,cn}$	normalized phase voltages of the motor
$\boldsymbol{u}_a, \boldsymbol{u}_b$	normalized voltage vectors constituting a sector
$\boldsymbol{u}_0$	normalized zero voltage vector
U_{dc}	DC-link voltage of the inverter
$\boldsymbol{i}_s$, $\boldsymbol{\psi}_s$	normalized stator current vector and stator flux vector
$\boldsymbol{\psi}_r$	normalized rotor flux vector
$\boldsymbol{\psi}_s^*$	normalized reference stator flux vector
$\boldsymbol{\psi}_{ps}^*$	normalized predicted reference stator flux vector
$\boldsymbol{\Delta\psi}_s$	stator flux vector displacement
$\lvert\boldsymbol{\Delta\psi}_s\rvert_{max}$	maximum magnitude of the flux error vector
$\boldsymbol{\Delta\psi}_s^*$	reference stator flux error vector compensated for $\boldsymbol{i_s}r_s$ drop
$\boldsymbol{\Delta\psi}_{s(samp)}^*(k)$	Error vector between values of $\boldsymbol{\psi}_s^*$ at two sampling instants
$\lvert\boldsymbol{\psi}_s(k)\rvert_{av}$	average magnitude of the flux vector in a sampling period
$\psi_{s\alpha}(thd)$	total harmonic distortion in the flux waveform
$\psi_{s\alpha(rms)}$	root mean square value of the alpha component of the flux vector

r_s	normalized stator phase winding resistance
r_r	normalized rotor phase winding resistance
l_s	normalized stator inductance
l_r	normalized rotor inductance
l_h	normalized magnetizing inductance
k_s	$\frac{l_h}{l_s}$
k_r	$\frac{l_h}{l_r}$
σ	$1 - \frac{l_h^2}{l_r l_s}$
$\omega_{s(inst)}$	normalized instantaneous stator angular frequency
ω_{sR}	nominal value of stator angular frequency
ω	normalized rotor angular velocity
ω_s	normalized stator angular frequency
ω_r	normalized slip
$\omega_{s(av)}(k)$	average angular velocity of $\boldsymbol{\psi}_s$ in a sampling period
$\omega_{s(av)}(sec)$	average angular velocity of $\boldsymbol{\psi}_s$ in a sector
ω^*	reference rotor angular velocity

ϵ	angle of the stator flux vector
ϵ^*	angle of the reference stator flux vector
α_h	hold angle
γ	angle of the flux error vector in a sector w.r.t $\boldsymbol{u}_a$
φ	angular displacement of the flux error vector
k	sampling instant
λ	factor used in overmodulation I
J	inertia of rotor

Chapter 1

Introduction

Electromagnetic torque m_e of an AC machine is produced by the interaction between the stator and rotor flux vectors. Field oriented control (FOC) and direct torque control (DTC) methods are the two main approaches of achieving torque control of AC machines. In FOC, torque is controlled by controlling the stator current vector $\boldsymbol{i}_s$ of the motor. This is done in a co-ordinate system that moves at synchronous angular velocity. Every space vector of the machine is expressed with respect to the rotor flux vector and therefore this method of current vector control is called rotor field oriented control method. The basic idea of this method is shown in figure 1.1(a). Magnitude of the rotor flux vector $\boldsymbol{\psi}_r$ is maintained constant, while the angular position δ of the stator flux vector $\boldsymbol{\psi}_s$ is changed as per the torque control requirement. For this, the torque component i_q and flux component i_d of the stator current vector $\boldsymbol{i}_s$ are controlled by applying a suitable voltage vector $\boldsymbol{u}_s^*$ using a pulse width modulation (PWM) technique. Figure 1.1(b) shows the second approach, ie. DTC. The errors in torque and stator flux vector

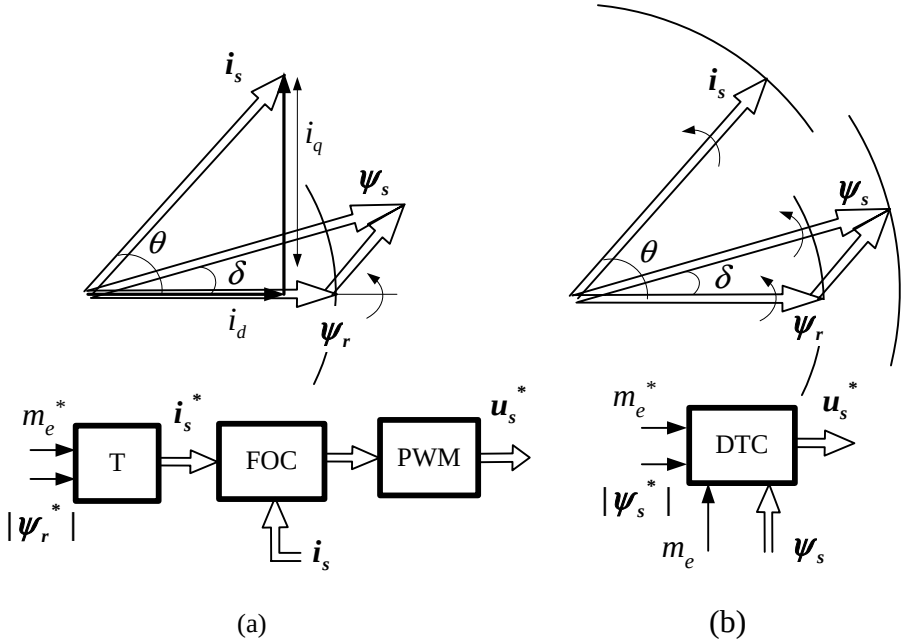

Figure 1.1: Two main approaches of torque control of AC-machines

magnitude directly decide the voltage vector $\boldsymbol{u}_s^*$ and therefore the motion of stator flux vector $\boldsymbol{\psi}_s$. Control of torque is achieved in the stationary co-ordinate system using hysteresis controllers.

The FOC principle tries to replicate the control philosophy of a separately excited fully compensated DC motor. However, a significant difference between the FOC concept and the DC motor torque control is the need for precise information of motor parameters, in case of an ac machine. The transformations and control algorithms presume accurate knowledge of various resistances and inductances within the machine. In a dc motor, small parameter errors will alter the output torque but not the decoupling. In an ac machine, parameter errors will alter the transformation and will cause an oscillatory torque response, [2].

Conventional DTC has two versions, namely, the Direct Torque Control

(DTC) method and the Direct Self Control (DSC) method. These methods were originally designed to be implemented in a continuous time domain and as such when digitally configured, require very high sampling rates. The dynamic torque response is physically the fastest due to complete exploitation of the voltage and current capability of the inverter. However, the switching frequency of the inverter varies with the operating angular velocity and hence for a considerable operating range, the switching capability of the inverter remain unutilized.

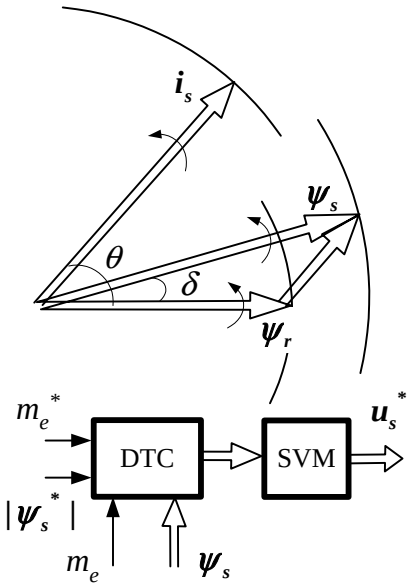

Figure 1.2: DTC at constant switching frequency

As a remedy to the variable switching frequency problem, constant switching frequency DTC methods have been proposed. Figure 1.2 shows the control philosophy. Errors in torque and stator flux vector are processed by the controller to define the voltage vector required for torque control. This voltage vector is implemented using a fixed switching frequency PWM. Most of the methods use space vector modulation (SVM) to realize the voltage vector $\boldsymbol{u}_s^*$ and therefore are also

called DTC-SVM methods of torque control. The distinct advantages of DTC-SVM methods over the conventional DTC methods are (1) Torque control can be achieved at a lower sampling frequency and (2) Switching capabilities of the inverter can be fully exploited. However, most of the schemes with DTC-SVM, have a computationally intensive control structure. Some of them even require co-ordinate transformations to achieve torque control. This defeats the purpose of the basic DTC philosophy of simple implementation and good steady state and dynamic control. Besides this, some of the important issues related to the control of torque, like steady state torque quality, dynamic torque control at high angular velocities and behavior of the current vector during steady state and dynamic control of torque have not been analyzed.

This thesis focuses on the development and implementation of a DTC-SVM method. All the above issues related to the direct control of torque have been considered. Unlike the previous computationally intensive approaches, a simple method of DTC-SVM is proposed, that retains the fast dynamic response of the conventional DTC scheme. Following are the contributions of this work.

- The first important contribution is the development of a predictive closed loop stator flux vector control method, that works in the entire speed range of the drive system. Switching states of the inverter are selected to compensate the sampled error between the reference and the stator flux vectors. Problems of closed loop stator flux vector control in the overmodulation region have been brought out and a method to overcome them has been discussed and verified

with analytical and experimental results. The overmodulation algorithms are devised such that they can be implemented in real time, with a simple and low cost processor. A comparison between the proposed method of modulation using the stator flux error vector and some other methods shows the superiority of the proposed method. Finally, a speed control strategy that uses the stator flux vector control is described with experimental results. Besides this, the problem of estimation of the stator flux vector has been discussed and a simple algorithm for detection and elimination of the DC-bias in the measured variables is proposed.

- The second contribution is the development of a torque control method, that utilizes the stator flux vector control principle, to achieve direct control of torque in all regions of operation. Comprehensive analysis to evaluate the quality of torque during steady state operation has been carried out. Control of torque in the overmodulation region and dynamic performance of the proposed method are explained. A comparison with the conventional/contemporary methods is given to weigh the performance of the proposed method in the context of steady state torque quality and dynamic response.

- Current vector $\boldsymbol{i}_s$ is not controlled deliberately in a direct torque control method. The third significant contribution has been to study the behavior of the current vector under dynamic operating conditions when a step change of torque or stator flux vector is applied. Using an analytical approach,

the inherent current control ability of the proposed DTC-SVM scheme has been shown. Control of torque and stator flux vector inherently controls the current vector. Moreover, the peak value of the current vector is well within the short time ratings of the inverter. The entire analysis is supported with experimental and simulation results.

- Analytical and experimental verifications are presented to show that both steady state and dynamic control of torque can be achieved in the constant power region. The advantage of the proposed method is that torque control in the entire field weakening operation is performed in the six-step mode without imposing any limit on the current vector. Hence, the voltage and current ratings of the drive can be fully exploited. At the same time the current vector magnitude during dynamics, is within the short time current limit of the motor.

Altogether, this dissertation attempts to describe a constant switching frequency direct torque control method, that is easy to implement in real time and can be used for any frequency of operation from zero to the field weakening range. There are seven chapters in this dissertation, each with a specific focus. The organization of the thesis is as follows.

- The next chapter will give a literature survey of different torque control methods. The performance of these control schemes in terms of steady state torque quality and dynamic response in different operating regions has been criti-

cally evaluated. This will help to bring out the focus of the present work and also to recognize the problems.

- Starting from the basic concepts, the third chapter develops the closed loop stator flux vector control method. Stator flux vector based SVM is introduced and the closed loop control is extended to the six-step range. Steady state and dynamic performance are discussed with experimental verification.

- Fourth chapter describes the proposed torque control method and discusses the steady state and dynamic performance in different regions of operation.

- In the fifth chapter, the performance of the proposed torque control method at high angular velocities and in the field-weakening region of operation is described.

- The sixth chapter describes the experimental platform and the DSP processor that has been used for experimental work.

- In the seventh chapter some of the salient features of this work have been summarized.

Chapter 2

Background and problem definition

2.1 Torque control methods

High performance speed and torque control of AC machines has been a focus of research since the early seventies, [3], [2]. The invention of field oriented vector control (FOC) by Blaschke, [4] and Hasse [5] made it possible to control an induction motor in a manner similar to a separately excited and fully compensated DC machine. The basic principle of FOC is to properly and independently distribute the magnetizing flux and torque producing components of the stator currents, for both during steady state and dynamic conditions of drive operation. By independently controlling each component with a high performance linear current controller, a fast change in motor torque is achieved. Vector control methods employ constant switching frequency pulse width modulation (PWM) techniques and

hence are suitable for digital implementation, [6], [7]. However, since the rotor flux observer is sensitive to the rotor resistance and inductance variations, a suitable parameter adaptation is needed, [8], [9], [10].

Another approach towards the control of torque is by using nonlinear controllers. Methods employing nonlinear controllers can be classified into two categories, namely, flux trajectory based direct torque control (DTC) methods and current trajectory based FOC methods. Classical DTC methods have two versions, (1) Direct Self Control (DSC) by Depenbrock [11] and (2) Direct Torque Control (DTC) by Takahashi [12]. In the original form, these methods were implemented in a continuous time domain and produce switching states depending on the instantaneous trajectory of the stator flux vector and instantaneous value of torque. Hence the digital implementation of these schemes require high sampling rates e.g. $40\mu s$ with TMS32C2x [13]. DSC has been employed mainly in low switching frequency high power applications like in traction drives while DTC based upon switching tables, [12], is used mainly for industrial drives. On the other hand, a current trajectory based torque control was proposed by Stadtfeld and Holtz, [14]. In this method, a predictive current control is implemented in stator co-ordinates. Subsequently, a field oriented PWM method was proposed using switching tables [15], [16]. References [15] and [17] apply the largest single vector to achieve the fastest dynamic and show a similar torque response as in DSC [11]. All these trajectory based control methods can be classified as feedback PWM as they use the state variable feedback to generate the switching state vec-

tors [18]. Therefore, they show a variable switching frequency at constant state variable error. The switching frequency is maximum at half the rated speed or modulation index, [17], [19], implying that the switching capability of the inverter is not utilized in a major portion of the operating region.

To obtain a constant switching frequency operation, Casadei et. al in reference [20], propose a method whereby in addition to the six active switching vectors, some vectors are added to the voltage space by using a fixed time PWM. In this method, the authors use only few states that result from the quantization of the voltage space. Hence the complete voltage space as in classical space vector modulation [18], is not utilized. These additional vectors which are combination of the three vertex vectors of a switching sector, are switched using a five-level hysteresis. This makes the scheme very complicated and at the same time results in a poor torque quality. The results show low frequency torque ripple, as the instantaneous torque is not strictly reaching the error bands in every switching interval as in earlier trajectory based methods [13], [16] and [17]. One distinct advantage of the scheme [20] is, torque control can be achieved at lower sampling rate than classical DTC. Similarly, Acarnley et. al in [21] propose a strategy to limit the switching rate in each leg of inverter while increasing the control update rate. Such limitation is natural in trajectory based schemes as [14] and [17] as they use a minimum commutation criteria in steady state operation.

It can therefore be said that, the trajectory based schemes will not have optimal utilization of the inverter switching capacity under steady state conditions.

The true advantage of such schemes is their response time during transients. DSC was proposed to exploit the limited switching regimes in high power drives and yet achieve a well defined torque ripple and fastest possible dynamics to suit the needs of traction drives. However, the use of nonlinear hysteresis controllers and low switching frequency operation resulted in higher current distortion, [18].

The disadvantages of the trajectory based methods using non-linear controllers can be overcome by adopting fixed switching frequency PWM. To this end, a direct torque control scheme proposed by Habetler, [1] uses the stator flux and torque references to generate a voltage reference $\boldsymbol{u}_s^*$. The voltage reference $\boldsymbol{u}_s^*$ is realized by using the principle of space vector modulation (SVM) to get the inverter switching states. However, to obtain $\boldsymbol{u}_s^*$, quadratic equations are solved in every sampling period. These equations have sinusoidal quantities in the denominators and therefore will result in indeterminant values at the point of singularities. Hence a suitable approximation has to be employed. Moreover, as the authors control the stator flux vector in stator coordinates, a phase error between the reference and stator flux vector appears, which is proportional to the sub-cycle period of SVM. To solve this problem, torque control with predictive control of stator flux vector [22], is carried out. The scheme in [22] however, does not exploit the installed DC-link capability of the inverter, resulting in a slower dynamic response.

To achieve constant switching frequency operation, Sul et. al incorporate a "torque ripple minimization" controller in the basic DTC control structure, [23]. This controller finds out the time instant at which the voltage vector selected by

the DTC logic is to be applied. In doing so, a quadratic equation is solved in every sampling period to decide the switching time instant that minimizes the torque ripple function. This time consuming algorithm decides the switching purely on the basis of torque ripple information and no concern is given for the flux magnitude control. Moreover, the equation to calculate the switching instant requires accurate knowledge of all machine parameters. This increases the parameter sensitivity of the method. Another method to produce DTC-SVM is proposed by Lascu et.al [24], wherein the flux controller produces a d-axis component of the voltage vector and the torque controller a q-axis component. PI controllers are used in both cases. Though a simple structure, the authors acknowledge that the PI controllers saturate at large errors (as in high dynamics or high speeds) and the scheme cannot guarantee six-step operation. Moreover the scheme has a variable structure as it switches to classical DTC whenever the PI controllers saturate, but no discussion on the stability of variable structure is provided. From the results given, it is difficult to identify in which regions the scheme operates under SVM and in which region it operates as DTC. Further, the scheme uses current model to estimate the stator flux vector. As this involves the rotor parameters, the estimation itself is parameter sensitive.

In all, the trend of research in the area of speed and torque control is heading towards developing control schemes that can be implemented digitally using a low cost processor. Besides this, the method should be able to exploit the installed switching and power capabilities of the inverter. This will result in a good steady

state torque quality and rapid dynamic response. In this regard, the DTC-SVM methods have succeeded in utilizing the inverter switching capabilities. However, since these methods use a modulator to switch the inverter, the dynamic response that can be obtained, depends on the abilities of both the controller and the modulator to exploit the voltage and current capabilities of the drive. This requirement becomes even more important when steady state torque control is carried out at large angular velocities or when a rapid dynamic response is required.

2.2 Switching techniques employed in constant switching frequency drives and operation in overmodulation region

Constant switching frequency FOC uses either the carrier based sine-triangle methods, [25] or SVM, [18] for switching. Due to simplicity in digital implementation, DTC-SVM schemes use conventional space vector modulation, for switching the inverter, [26]. An inverter has three distinct operating regions. First is the normal region in which the fundamental voltage desired by the controller, is equal to the one that is obtained in a sampling period. The voltage gain is always linear in a sampling cycle and hence in a fundamental cycle. The second operating region is the overmodulation region in which the voltage gain reduces due to the fixed DC-link inverter voltage. Finally, there is the six-step region in which the fundamental component obtainable is maximum in an operating cycle. The normal and six-step operating regions of a modulator can be easily programmed, but to

maintain a continuity between these two regions, overmodulation is required. To this end, several methods of achieving overmodulation are suggested.

Holtz et. al in reference [27], divide the overmodulation range in two sub-regions and the inverter switching is defined based upon the unique characteristics of the two regions. In the first sub-region, a pre-processor modifies the magnitude of the reference voltage vector before it is being processed by the conventional space vector modulator. In the second sub-region, the pre-processor modifies both the angle and magnitude of the reference voltage vector. To avoid the solution of nonlinear equations, two look up tables are used and continuous control of voltage is obtained until six-step region. While the fundamental voltage cannot be obtained in every sampling period, the authors of reference [27] get it in a fundamental cycle. The other overmodulation schemes reported in references [28], [29], [30], [31] use the basic geometrical understanding provided in [27]. However, these methods differ from each other in the manner they implement the overmodulation switching strategy. In terms of processing time, the method given by Bolognani et. al in [30] is the fastest. However, due to large harmonic content in the voltage waveform, it results in distorted current and flux waveforms. The method described by Jain et. al in [28] uses artificial intelligence based classification algorithms to achieve overmodulation. Instead of pre-processing the voltage vector as suggested in the reference [27], the authors of references [29] and [31] use approximated piecewise linearized equations to achieve overmodulation switching. All these methods have effectively extended the DC-bus utilization of the inverter until the six-step mode

but are tested for the open loop V/f drives.

During overmodulation, lower order harmonics are added to improve the fundamental cycle voltage gain of the modulator. However, when used in a closed loop torque and flux vector control scheme like FOC, these harmonics interfere with the working of linear current controllers making even the steady state operation difficult. Khambadkone and Holtz in reference [32], proposed a method of compensation that uses an inverse model to estimate the harmonic component of the current vector during overmodulation. This harmonic content is then cancelled from the inputs to the linear controllers. Hence the linear current controllers see the average current which allows for a higher bandwidth of control.

During dynamic operation at high angular velocities (or overmodulation), the voltage vector required for control is more than that an inverter can provide. The inverter voltage limit is geometrically expressed as a hexagon of side $2/3\ U_{dc}$, [27]. Since the required voltage vector cannot be obtained, it is approximated by a voltage vector on the hexagonal boundary. The method developed by Mochikawa et. al, [33], selects the voltage vector such that the difference in magnitudes of the reference voltage vector and the selected voltage vector is minimum. This is achieved by projecting the reference voltage vector tip point on the closest inverter hexagon side. Another method implemented by Seidl et al. [34], uses neural networks for selection of the voltage vector as proposed by [33]. This approach however fails to utilize the voltage capability and requires a computationally intensive control algorithm. In another approach, by Jul et. al [35], the vector formed

by the superposition of PI current controller output vector and the motor back-emf vector is intersected with the hexagon side. The intersection point defines the tip of the modified reference voltage vector. This approach has a marginally better performance than the other methods but at the same time is complex in real time implementation, [36]. Similarly, in the method developed in the reference [37] the reference vector tip point is projected on the inverter voltage vector closest to the reference vector. The modified voltage vector is the point on the hexagon side which the projection line intersects. As analyzed in reference [36], this method is similar in performance and implementation complexity to the above methods. All the above methods apply the overmodulation technique only during the dynamic operation of the drive. Therefore these methods are also called dynamic overmodulation methods, [36].

Besides the SVM based overmodulation methods discussed in the above paragraphs, a class of discontinuous PWM methods [38] have been described that extend the linear range of operation using the sine-triangle PWM scheme. In this category, the popular methods tested for V/f induction motor drives are the ones by Depenbrock [39] and by Ogasawara [40]. A hybrid method that combines the advantages of these methods has been developed by Hava et. al in [38]. However, the steady state FOC drive performance using most of these methods in the overmodulation range is shown to be oscillatory, [36]. On the other hand, Kerkman et. al in reference [41] attempt to overcome the adverse affect of the nonlinear gain on the linear current controllers by utilizing the nonlinear inverter gain function

model.

Most of the existing overmodulation algorithms are either tested for an FOC scheme or for open loop V/f drives. Only reference [1], uses the overmodulation strategy during the dynamic operation with a DTC-SVM scheme. Though the method of dynamic overmodulation as proposed in [1] is simple in implementation, it results in a slower dynamic response. This is because the switching strategy adopted during dynamic overmodulation fails to exploit the voltage and current capabilities of the inverter.

2.3 Torque control in the field weakening range

At low speeds, back emf of the machine is small and the control strategy can easily apply a voltage vector for fast dynamic torque control. However at very high speeds, the voltage reserve for torque and flux vector control is very small due to a large magnitude of the back emf vector. Therefore, it becomes very important to fully exploit the installed voltage capability of the inverter.

Most of the FOC and DTC-SVM schemes for torque control in the field-weakening range, do not operate in overmodulation. References [42], [43], [44] and [45] exploit only the linear voltage region of inverter operation, resulting in poor utilization of the installed voltage capability. A reduced voltage capability implies, reduced magnitudes of the controllable d-axis and q-axis currents. Besides this, schemes by Sul et. al, [42], and by Harnefors et. al, [43] use co-ordinate transforms

and their control structure depends upon rotor parameters. The rotor inductance changes rapidly as the machine comes out of saturation, in the field weakening range.

Problem of parameter sensitivity can be reduced by employing DTC methods. DSC method by Depenbrock, [11] exploits the inverter voltage limit to the maximum as it works in a six-step mode during field weakening. On the other hand, the DTC-SVM methods like the one by Griva et. al, [44] and by Casadei et. al, [45] need co-ordinate transformation and the inverter voltage utilization is limited to a maximum value of 0.907 per unit (p.u). Unlike [11], these schemes result in a complex approach which is highly sensitive to parameter variations. Only the steady state torque control performance has been given in the field weakening range. Due to under utilization of the inverter voltage capability, dynamic response of the drive will be slow and the controllable speed range, smaller.

2.4 Problems at low operating angular velocity

Accurate estimation of stator flux vector is a key factor in the hardware implementation of any DTC/DTC-SVM control scheme. Common methods of stator flux vector estimation are those using voltage model or the current model, [46]. For robust torque and flux vector control schemes, voltage model is used because the only machine parameter involved is stator resistance. For angular velocities greater than a few Hz, the fundamental voltage has a large value. However, as the angular

velocity reduces, the effects of DC-offset and thermal drift become more and more prominent causing error in flux vector estimation using the voltage model. Hence the integration of the induced emf results in drift and initial value problems [47], [48], [49]. Besides this, the unequal gains of the anti aliasing analog filters used for current measurement, result in torque pulsations. These problems are minimized by using a low pass filter instead of a pure integrator but this results in a magnitude and phase angle error in the estimated flux vector. In the approach followed by [47], the magnitude of the stator flux vector is maintained at the required value by clipping of excess amplitude caused by drift. To obtain the correct phase angle of $\pi/2$ with respect to the induced emf, a PI controller is made use of. However, this method has not been tested in a closed loop scheme. In a computationally involved approach, [49] derives a nonlinear inverter model for estimation of the DC-bias.

References [48] and [50] use inverse magnitude and phase angle gains to compensate for the error created due to low pass filtering. The poles of this modified low pass filter are made to change with respect to the angular velocity of operation. However, the extent of shifting of poles needs to be decided by trial and error. Using these methods, accurate estimation is achieved for operating frequencies higher than a few Hz, but around zero speed (less than 50 RPM), these methods fail to properly estimate the flux vector, because the magnitude of dc offset and other disturbances become much more pronounced than the induced emf. This deteriorates the steady state torque quality of schemes like Direct Torque Control (DTC) as it leads to pulsations in torque, [51].

2.5 Summary

This chapter has briefly summarized the advanatages and disadvantages of different torque and stator flux vector control methods. From FOC to DTC-SVM method, the area of high performance control of torque has seen the evolution of different and improved methods. Given their distinct advantages over FOC schemes the recent trend is to develop and improve upon the conventional approach of achieving direct torque control methods. In all, state of the art direct methods of torque control can be broadly divided in two classes (a) those having simple to implement control algorithm with the fastest torque dynamic but requiring high sampling rate and having variable switching frequency operation like [12], [11] and (b) those requiring considerable processing time and approximations as well as having a parameter sensitive control structure, with not as good a dynamic response as the conventional versions but having constant switching frequency operation. This category includes [1], [22], [24], [20]. While conventional DTC schemes are proven to have a high performance torque control during dynamic operating conditions as well as during operation at large angular velocities, DTC-SVM methods are still in the emerging stage and therefore offer extensive research opportunities. Issues like torque quality, dynamic response, operation in the overmodulation range, and operation at large angular velocities are the ones that need immediate attention. This will help in solving the problems associated with these methods and their commercialization.

Proposed DTC-SVM method has been implemented using closed loop predictive stator flux vector control. Next chapter is devoted in the development and analysis of the stator flux vector control method for all operating angular velocities.

Chapter 3

Closed Loop Stator Flux Vector Control

3.1 Introduction

In conventional Direct torque control (DTC) methods, [11], [12], nonlinear hysteresis controllers act on the instantaneous values of torque and stator flux vector magnitude. The inverter switching information for torque and stator flux vector control is obtained directly from the magnitudes of the errors. The advantages of these methods are their simple control structure, easy implementation and rapid dynamic response. However, they have the problem of variable switching frequency and require very large sampling rates for real time digital implementation. On the other hand, the constant switching frequency DTC methods like [1] require large processing times and approximations. Moreover, the DC-link voltage is not fully utilized.

The constant switching frequency DTC scheme explained in this dissertation, retains the dynamic performance of classical DSC/DTC, and is implemented in the form as shown in the figure 3.1. Normalized quantities have been used in this dissertation and the normalization is done as described in the reference [52]. Torque

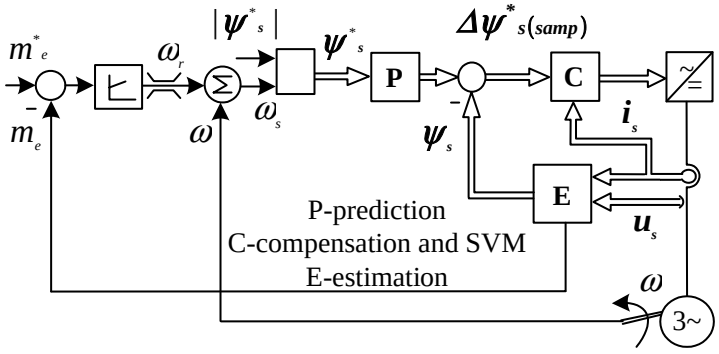

Figure 3.1: Block diagram of the control scheme

reference m_e^* is compared with estimated torque m_e and the error is processed by the torque controller to obtain the slip angular frequency ω_r. The sum of ω_r and the rotor angular velocity ω defines the angular velocity ω_s, of the reference stator flux vector. The reference stator flux vector $\boldsymbol{\psi}_s^*$ has a circular trajectory and the error vector between the reference and the estimated stator flux vector $\boldsymbol{\psi}_s$ defines the switching states of the inverter, for torque and stator flux vector control. Stator flux vector $\boldsymbol{\psi}_s$ and torque m_e are estimated using the sensed voltage and current vectors, $\boldsymbol{u}_s$ and $\boldsymbol{i}_s$ respectively. Estimation of stator flux vector is dealt with, in a later section.

This chapter will focus on stator flux vector control that forms the inner loop of the proposed DTC scheme. The magnitude of the reference stator flux vector $\boldsymbol{\psi}_s^*$ depends upon whether the operation is below or above base speed and the angular

velocity ω_s will be given as the command value. The functions of blocks **P**, **C** and **E** will be discussed in detail in the following sections. The issues related with closed loop stator flux vector control that are discussed in this chapter are,

- Predictive dead-beat closed loop steady state control of the stator flux vector in the normal region.
- Effect of voltage vector limit of the inverter on control of stator flux vector. Problems associated with closed loop stator flux vector control during the overmodulation region of operation and solution to these problems.
- Performance evaluation of the proposed method of overmodulation switching and its comparison with different PWM schemes. The criterion of this comparison is to ascertain closed loop stator flux vector control capability of these schemes, with zero phase error in a fundamental operating cycle.
- Dynamic control of the stator flux vector and a switching strategy that ensures fast dynamic response.
- Problems in estimation of the stator flux vector and a solution to eliminate the DC-bias in the measured variables.
- Experimental verification of all characteristics of closed loop stator flux vector control and a simple closed loop speed control.

3.2 Principle of closed loop flux vector control

3.2.1 Brief review of fundamentals

Stator flux vector control method is based upon Faraday's law. When expressed using space vectors, this law can be written as, $\boldsymbol{u}_i^* = d\boldsymbol{\psi}_s/d\tau$, ie. rate of change of flux vector $\boldsymbol{\psi}_s$ is equal to the induced voltage vector. With the assumption of negligible resistance, this voltage is equal to the applied voltage vector $\boldsymbol{u}_s^*$. In discrete time domain, this equation can be interpreted as

$$\boldsymbol{\Delta\psi}_s(k) = \boldsymbol{u}_s^*(k)\tau_s \tag{3.1}$$

A vector displacement $\boldsymbol{\Delta\psi}_s(k)$ in flux vector $\boldsymbol{\psi}_s$ can be obtained by applying a voltage vector $\boldsymbol{u}_s^*(k)$ for a time τ_s that is equal to the sampling period. This basic principle can be used for controlling the stator flux vector magnitude and angle. Here, the designation τ is used for the normalized time in radians and is given as $\omega_{sR}t$, where ω_{sR} is the rated angular frequency of the machine in rad/sec and t is the time in *sec*.

In a three phase AC machine controlled by a voltage source inverter (figure 3.2) , the voltage vector $\boldsymbol{u}_s^*$ is defined as [52],

$$\boldsymbol{u}_s^* = \frac{2}{3}(u_{an} + \mathbf{a}u_{bn} + \mathbf{a}^2u_{cn}) \tag{3.2}$$

where, u_{an}, u_{bn} and u_{cn} are the line to neutral voltages applied across the motor terminals. The available switching state combinations, s_a, s_b, s_c result in six active vectors, 100, 110 etc. and two zero vectors 111 and 000 as shown in the figure

3.2. All active vectors have a magnitude of $\frac{2}{3}U_{dc}$ and they form a set of six equal triangular sectors, $(0-5)$. Here, U_{dc} is the DC-link voltage. Any voltage vector $\boldsymbol{u}_s^*$ within the inscribed circle of the hexagon can be obtained in a normalized sampling time period τ_s, by the volt-sec equality principle and is given as,

$$\boldsymbol{u}_s^*\tau_s = \boldsymbol{u}_a\tau_a + \boldsymbol{u}_b\tau_b + \boldsymbol{u}_0\tau_0 \tag{3.3}$$

Here τ_a, τ_b and τ_0 are switching times of the voltage vectors $\boldsymbol{u}_a$, $\boldsymbol{u}_b$ and $\boldsymbol{u}_0$ that constitute the sector in which $\boldsymbol{u}_s^*$ is located. Angle γ represents the location of this vector in a sector, with respect to the vector $\boldsymbol{u}_a$, figure 3.2 (b). The time taken

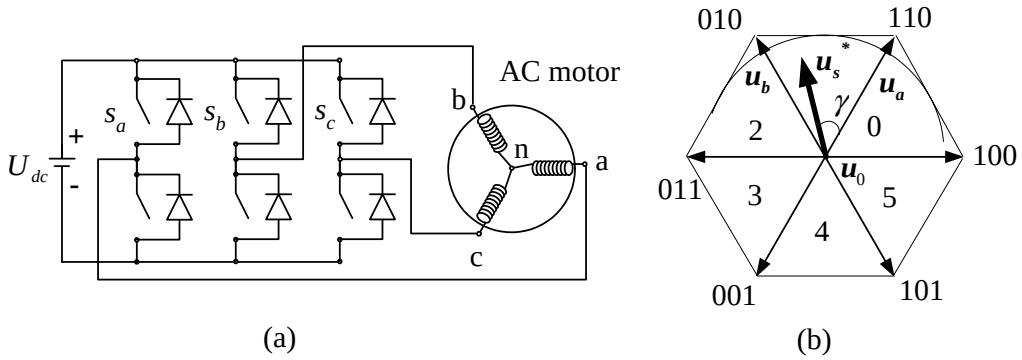

Figure 3.2: Three phase inverter and the voltage vectors for different switching combinations of s_a s_b and s_c

to compensate the flux displacement vector, equation (3.1), will depend upon the DC-link voltage and also upon the ability of the modulation scheme to exploit this installed capacity. The maximum voltage vector magnitude $|\boldsymbol{U}_s^*|_{max}$, that can be applied in a phase is given as,

$$|\boldsymbol{U}_s^*|_{max} = \frac{2}{3}U_{dc} \tag{3.4}$$

For normalizing voltages, the maximum value of the fundamental component during six-step operation is taken as base value [18]. This value is $\frac{2}{\pi}U_{dc}$. Hence, the

normalized value of DC-link voltage becomes $\frac{\pi}{2}$ while the normalized magnitude of every active switching state vector is,

$$|\boldsymbol{u}_a| = |\boldsymbol{u}_b| = \frac{\frac{2}{3}U_{dc}}{\frac{2}{\pi}U_{dc}} = \frac{\pi}{3} \tag{3.5}$$

Therefore, the maximum possible volt-sec or the maximum possible magnitude of vector displacement $|\boldsymbol{\Delta\psi}_s|_{max}$ in the stator flux vector error that can be obtained in a sampling time period is given as,

$$|\boldsymbol{\Delta\psi}_s(k)|_{max} = \frac{\pi}{3}\tau_s \tag{3.6}$$

This vector displacement will be along one of the voltage vectors selected for switching in that sampling period.

Principle of volt-sec equality will be exploited to obtain the switching state times of the inverter states required to compensate the error between reference and stator flux vectors.

3.2.2 Definition of flux error vector and problem of phase delay

Before the actual control strategy is described, it is important to observe the trajectories of the flux vectors and define the flux error vector. Figure 3.3 (a), shows the reference stator flux vector trajectory. As the control is carried out in discrete time domain, the sampled reference stator flux vector moves in discrete steps as shown in figure 3.3 (a). The vector displacement between the values of reference stator flux vector at any two consecutive sampling instants is given as,

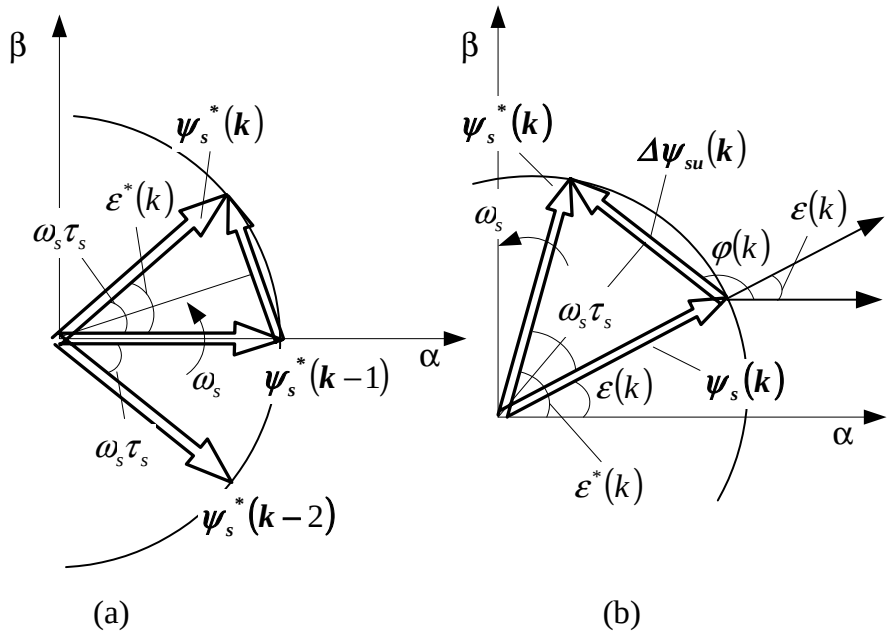

Figure 3.3: (a) Trajectory of the reference stator flux vector (b) Uncompensated flux vector error

$2|\psi_s^*(k)| \sin \frac{\omega_s \tau_s}{2}$. Here, ω_s is the synchronous angular velocity of the reference stator flux vector. In steady state, the angular velocity ω_s will be constant. For small values of the sampling time interval, the product $\omega_s \tau_s$ will be very small. Therefore, $\sin \frac{\omega_s \tau_s}{2} \approx \frac{\omega_s \tau_s}{2}$. For example, if the sampling time period is 1 ms, then the difference between the actual value $\sin \frac{\omega_s \tau_s}{2}$ and the approximate value $\frac{\omega_s \tau_s}{2}$ is less than 0.25% at an angular velocity $\omega_s = 1.0\ p.u.$ Therefore, the vector displacement between any two sampling instants of the reference stator flux vector will be, $|\psi_s^*(k)| \omega_s \tau_s$.

For a fixed value of reference stator flux vector magnitude and sampling period τ_s, the magnitude of the vector displacement between any two consecutive values of the reference stator flux vector is directly proportional to the angular velocity ω_s.

For control, the error between the reference stator flux vector $\boldsymbol{\psi}_s^*(k)$ and the stator flux vector $\boldsymbol{\psi}_s(k)$ given by $\Delta\boldsymbol{\psi}_{su}(k)$ in figure 3.3 (b), should be zero at the k^{th} sampling instant.

This will result in the condition,

$$\boldsymbol{\psi}_s(k) \;=\; \boldsymbol{\psi}_s^*(k) \tag{3.7}$$

However, the error $\Delta\boldsymbol{\psi}_{su}(k)$ between the two vectors at any instant k can only be compensated in the $(k+1)^{th}$ instant. This is because, the required volt-secs computed for the k^{th} sampling instant can be realized at the $(k+1)^{th}$ instant. Therefore, at the k^{th} sampling instant the stator flux vector will be,

$$\boldsymbol{\psi}_s(k) \;=\; \boldsymbol{\psi}_s^*(k-1) \tag{3.8}$$

Hence, the stator flux vector will always lag the reference stator flux vector by

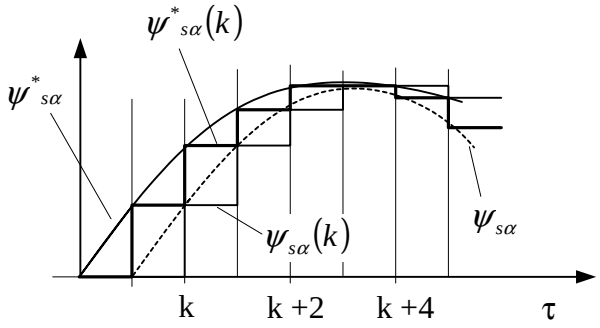

Figure 3.4: phase delay

one sample period. The resulting phase error can be observed in terms of the α-components of the flux vectors as illustrated in figure 3.4. Stator flux vector $\boldsymbol{\psi}_s$ lags behind the reference stator flux vector. This affect becomes more prominent with the increase in ω_s.

To ensure that no phase error is produced, predictive control of the stator flux vector is necessary.

3.2.3 Predictive control of the stator flux vector

In polar coordinates, linear prediction of the reference stator flux vector can be carried out. The reference stator flux vector in polar coordinates can be expressed as

$$\boldsymbol{\psi}_s^* = |\boldsymbol{\psi}_s^*| e^{j\epsilon^*} \tag{3.9}$$

here ϵ^* is the angular position of the reference stator flux vector at any instant of time. In steady state operation, only the angle of the stator flux reference vector will change and not its magnitude. This is because the angular velocity of the reference flux vector ω_s is constant. Hence, the stator flux reference vector at time τ_s in future can be predicted as follows,

$$\boldsymbol{\psi}_{ps}^* = |\boldsymbol{\psi}_s^*| e^{j(\epsilon^* + \omega_s \tau_s)} \tag{3.10}$$

Block **P** of figure 3.1, implements the prediction in discrete time using a sampling period of τ_s. Therefore at the k^{th} sampling instant, the predicted stator flux reference is given as

$$\boldsymbol{\psi}_{ps}^*(k) \;=\; |\boldsymbol{\psi}_s^*| e^{j(\epsilon^*(k) + \omega_s \tau_s)} \tag{3.11}$$

or

$$\boldsymbol{\psi}_{ps}^*(k) \;=\; \boldsymbol{\psi}_s^*(k) e^{j\omega_s \tau_s} \tag{3.12}$$

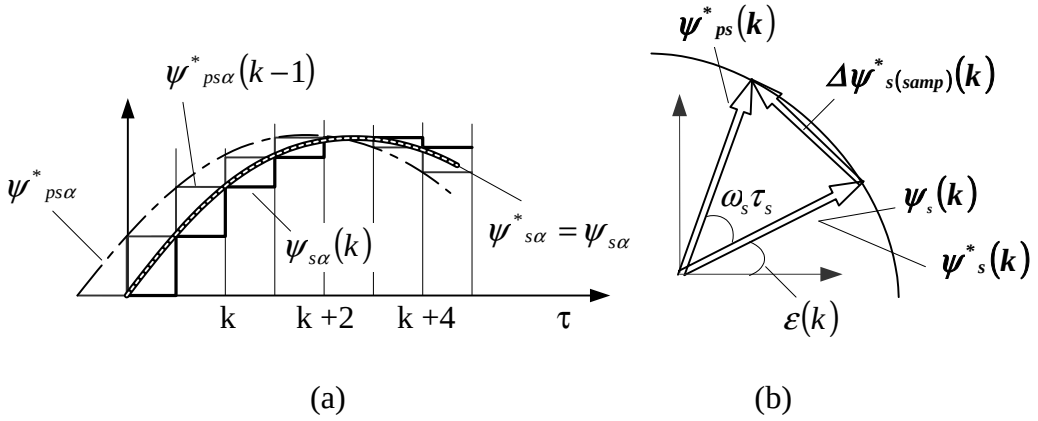

Figure 3.5: Phase delay compensation using predictive control

Predictive control of the stator flux vector is shown in figure 3.5. In figure 3.5 (a) the dotted curve represents the α-component of the predicted reference stator flux vector and the white curve is the α-component of the stator flux vector. The stator flux vector follows the reference stator flux vector without any delay. Figure 3.5 (b) shows the vector relationship between the predicted reference stator flux vector $\boldsymbol{\psi}^*_{ps}(k)$ and the stator flux vector $\boldsymbol{\psi}_s(k)$ at the k^{th} sampling instant. Here vector $\boldsymbol{\Delta\psi}^*_{s_{(samp)}}(k)$ is the desired vector displacement for control and will be compensated by using the appropriate switching states of the inverter. As the predicted reference stator flux vector and the stator flux vector rotate, the error vector $\boldsymbol{\Delta\psi}^*_{s_{(samp)}}(k)$ also rotates at a constant angular velocity ω_s. Hence, the vector $\boldsymbol{\Delta\psi}^*_{s_{(samp)}}(k)$ has a circular trajectory.

3.3 Calculation of switching state times for predictive stator flux vector control

Switching state times required for closed loop stator flux vector control with zero average error will be obtained, using the basic volt-sec equality criterion of the conventional SVM.

Stator voltage equation of an induction machine in a sampling period τ_s can be written as,

$$\boldsymbol{u}_s^*(k) = \frac{\boldsymbol{\Delta\psi}^*_{s_{(samp)}}(k)}{\tau_s} + \boldsymbol{i}_s(k) r_s \tag{3.13}$$

here, $\boldsymbol{i}_s$ is the space vector of current and r_s is the stator winding resistance. Desired rate of change of the stator flux vector in a sampling period is given as $\boldsymbol{\Delta\psi}^*_{s_{(samp)}}(k)/\tau_s$.

Expressing the above equation in volt-seconds,

$$\boldsymbol{u}_s^*(k)\tau_s = \boldsymbol{\Delta\psi}^*_{s_{(samp)}}(k) + \boldsymbol{i}_s(k) r_s \tau_s \tag{3.14}$$

The left hand side (LHS) quantity in equation (3.14) has the units of flux and it can be expressed as the stator flux error vector compensated for the resistive drop. The stator flux vector displacement required for control is now equal to $\boldsymbol{\Delta\psi}^*_s(k)$ and is expressed as,

$$\boldsymbol{\Delta\psi}^*_s(k) = \boldsymbol{\Delta\psi}^*_{s_{(samp)}}(k) + \boldsymbol{i}_s(k) r_s \tau_s \tag{3.15}$$

Hence, to obtain a vector displacement $\boldsymbol{\Delta\psi}^*_{s_{(samp)}}(k)$, of the stator flux vector

$\boldsymbol{\psi}_s$, the reference stator flux error vector $\boldsymbol{\Delta\psi}_s^*(k)$ should be used for selecting the switching states.

Reference stator flux error vector $\boldsymbol{\Delta\psi}_s^*(k)$ is compensated by switching of active voltage vectors. Figure 3.6 illustrates the idea. Resistive drop compensation appears in the form of a vector, figure 3.6 (a). The trajectory followed by the

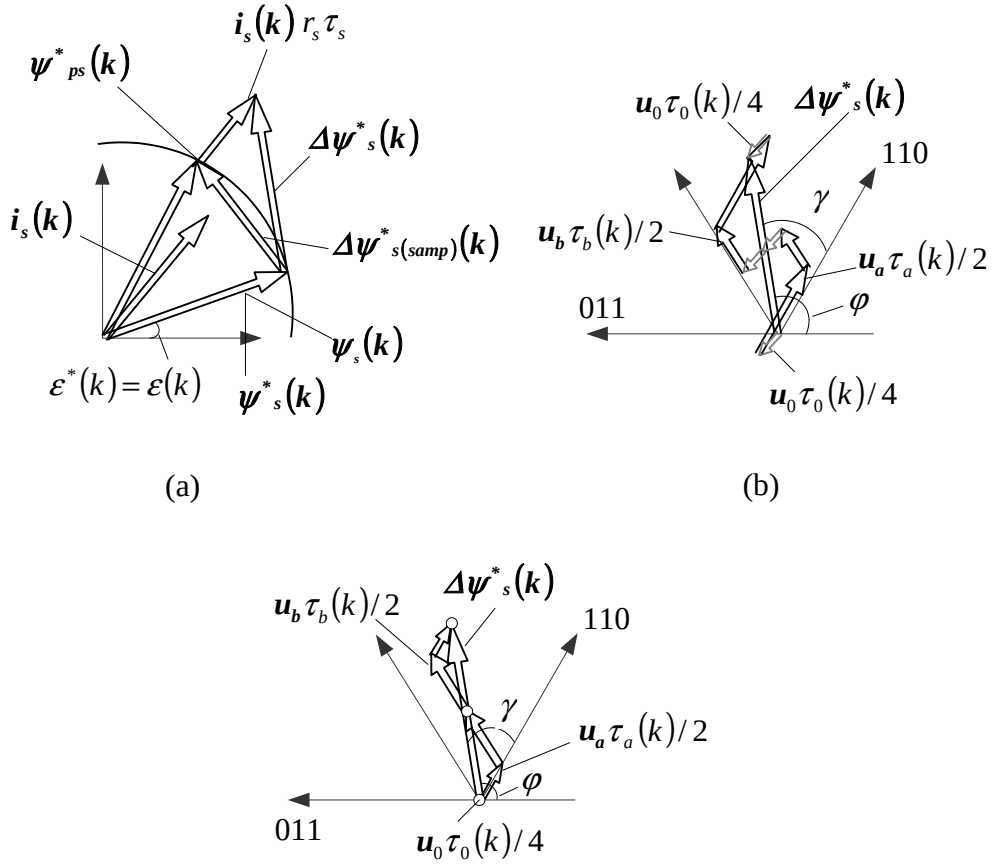

Figure 3.6: Switching state times selection for predictive control of stator flux vector (a)Resistive drop compensation (b) stator flux vector movement when the resistive drop is significant (c) stator flux vector movement when the resistive drop is negligible

stator flux vector depends upon the switching pattern used. In present work, the switching sequence adopted is same as that of the conventional SVM. Thus, one

cycle of sampling time period τ_s, is subdivided in a set sub cycle and a reset sub cycle. In the set sub cycle the sequence is, $\frac{\tau_0}{4} - \frac{\tau_a}{2} - \frac{\tau_b}{2} - \frac{\tau_0}{4}$ while in the reset sub cycle it is, $\frac{\tau_0}{4} - \frac{\tau_b}{2} - \frac{\tau_a}{2} - \frac{\tau_0}{4}$.

Figure 3.6 (b) shows the mapping of the reference stator flux error vector $\boldsymbol{\Delta\psi}_s^*(k)$ on the voltage vector space. When a zero vector is switched, the stator flux vector moves along the vector $-\boldsymbol{i}_s r_s$ while the switching of active vectors moves it along their respective directions, figure 3.6 (b). Motion of the stator flux vector due to the switching of a zero vector is shown as grey vectors. The affect of $\boldsymbol{i}_s r_s$ drop is fully compensated in a sampling cycle .

On the other hand, if the stator resistance drop is considered to be negligible, the switching of zero vectors will almost stop the stator flux vector. This is represented in figure 3.6 (c) as white circles.

The switching state times $\tau_a(k)$ and $\tau_b(k)$ for control can be obtained by the following volt-sec equality,

$$\boldsymbol{\Delta\psi}_s^*(k) = \boldsymbol{u}_a\tau_a(k) + \boldsymbol{u}_b\tau_b(k) \tag{3.16}$$

where $\boldsymbol{u}_a$ and $\boldsymbol{u}_b$ are the adjacent active voltage vectors in the sector where reference stator flux error vector $\boldsymbol{\Delta\psi}_s^*(k)$, is located. The sector of operation is obtained from the angular displacement φ of the stator flux error vector (figure 3.6 (b),(c)) using,

$$sector = \text{int}(\frac{\varphi}{\pi/3}) \tag{3.17}$$

and the angle γ within the sector can be obtained using

$$\gamma = \pi/3 \cdot \big(\varphi \mathrm{mod}(\pi/3)\big) \tag{3.18}$$

Once the sector and the angle γ are known, the reference stator flux error vector $\boldsymbol{\Delta\psi}_s^*(k)$ can be placed in the complex switching vector plane as shown in figure 3.6(b). Equating the real and imaginary parts of the equation (3.16),

$$\begin{aligned} |\boldsymbol{\Delta\psi}_s^*(k)| \cos\gamma &= \frac{\pi}{3}\tau_a(k) + \frac{\pi}{3}\cos(\pi/3)\tau_b(k) \\ |\boldsymbol{\Delta\psi}_s^*(k)| \sin\gamma &= \frac{\pi}{3}\sin(\pi/3)\tau_b(k) \end{aligned} \tag{3.19}$$

where normalized value $\pi/3$ of the voltage vector magnitudes $|\boldsymbol{u}_a|$ and $|\boldsymbol{u}_b|$ has been used. The normalized on times can be obtained as,

$$\begin{aligned} \tau_a(k) &= \frac{3}{\pi}\frac{|\boldsymbol{\Delta\psi}_s^*(k)| \sin(\pi/3 - \gamma)}{\sin(\pi/3)} \\ \tau_b(k) &= \frac{3}{\pi}\frac{|\boldsymbol{\Delta\psi}_s^*(k)| \sin(\gamma)}{\sin(\pi/3)} \\ \tau_0(k) &= \tau_s - \tau_a(k) - \tau_b(k) \end{aligned} \tag{3.20}$$

Reference stator flux error vector $\boldsymbol{\Delta\psi}_s^*(k)$, has been utilized to obtain the switching state times instead of the open loop value of the reference voltage vector $\boldsymbol{u}_s^*$. With this approach, switching states are directly selected based upon the stator flux error vector, achieving direct control of the stator flux vector magnitude and angle. Therefore this approach falls in the category of feedback PWM [18].

3.4 Motion of the stator flux vector with SVM switching: Steady state operation

Before the motion of stator flux vector is described, it will be useful to understand the extent of influence of the stator resistance drop on the trajectory of the stator flux vector.

3.4.1 Effect of stator resistance

The reference stator flux error vector $\boldsymbol{\Delta\psi}_s^*(k)$ is given by equation (3.15). For large angular velocities, the error vector $\boldsymbol{\Delta\psi}_{s_{(samp)}}^*(k)$ is large in comparison with the factor, $\boldsymbol{i}_s(k)r_s\tau_s$ and hence the latter can be neglected. However, for

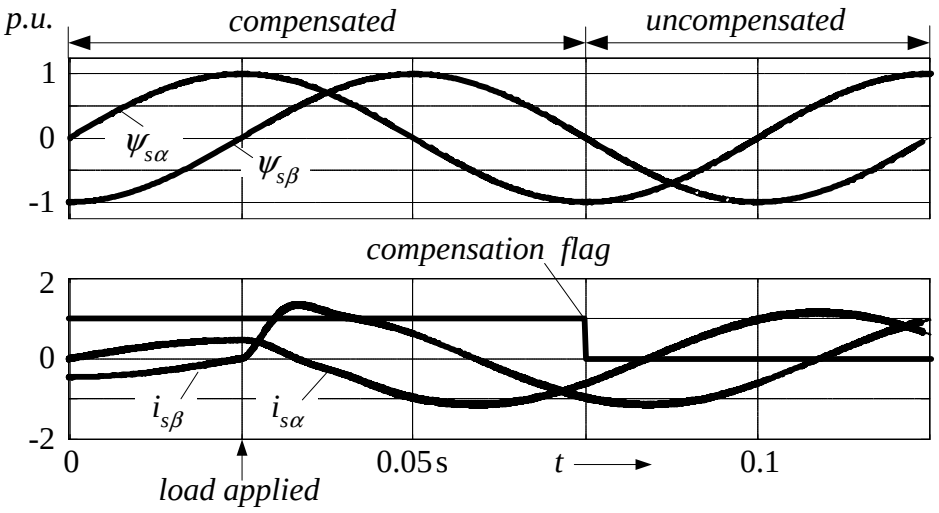

Figure 3.7: Effect of stator resistance

lower angular velocities and under the conditions of heavy loading, the influence of the resistive drop needs to be observed. Figure 3.7 gives a simulation study for operation at an angular velocity ω_s of 0.05 $p.u.$ and a sampling frequency of 1 kHz.

A load of 1.25 *p.u.* is applied at $t = 0.025$ s when the compensated reference stator flux error vector $\boldsymbol{\Delta\psi}_s^*(k)$ was used for switching. At $t = 0.075$ s, the compensation factor is removed and just $\boldsymbol{\Delta\psi}^*_{s_{(samp)}}(k)$ is used for switching. It is observed that the influence of stator resistance under these conditions is not significant. Hence for the sake of analysis the stator resistance drop will be considered negligible.

3.4.2 Concept of average angular velocity control

During steady state, the reference stator flux vector $\boldsymbol{\psi}_s^*$ moves at a constant angular velocity ω_s. This means, $\omega_s(k) = \omega_s(k-1)$. On the other hand, switching of active and zero states results in a non uniform motion of the stator flux vector $\boldsymbol{\psi}_s$. Its instantaneous angular velocity, $\omega_{s(inst)}$ can be obtained, by differentiating the angle ϵ with respect to time. When a zero vector is switched, the rate of change of this angle is negligible and hence the instantaneous angular velocity is almost zero. However, when an active vector is switched, the instantaneous angular velocity has a value equal to $\omega_{s(inst)} \approx \frac{|\boldsymbol{u}_s|}{|\boldsymbol{\psi}_s|}$. The average angular velocity in a sampling period 'k' can be expressed as $\omega_{s(av)}(k)$ and is obtained by finding out the angle traversed by the stator flux vector in a sampling time period. For this, the angular displacement of the stator flux vector brought about by switching of the inverter states is calculated.

Figure 3.8 explains the idea. Since the switching state times $\tau_a(k)$ and $\tau_b(k)$

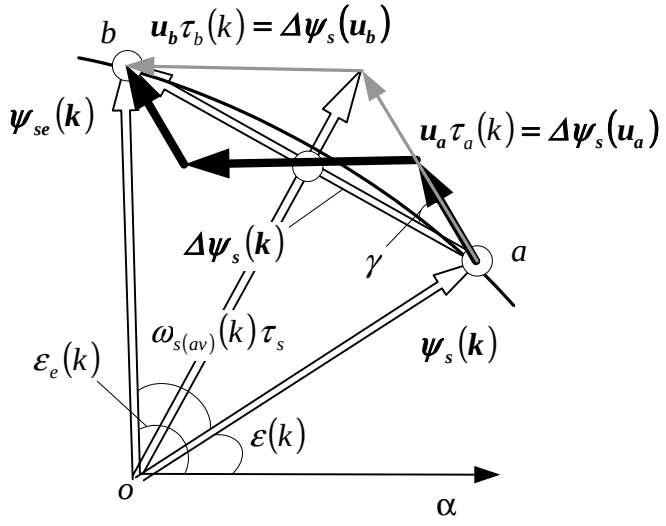

Figure 3.8: Calculating angular velocity of the stator flux vector

are known, the stator flux vector $\boldsymbol{\psi}_{se}(k)$ can be estimated as,

$$\boldsymbol{\psi}_{se}(k) = \boldsymbol{\psi}_s(k) + \boldsymbol{u}_a\tau_a(k) + \boldsymbol{u}_b\tau_b(k) \tag{3.21}$$

The average angular velocity is therefore given as,

$$\omega_{s(av)}(k) = \frac{\epsilon_e(k) - \epsilon(k)}{\tau_s} \tag{3.22}$$

Here, $\epsilon_e(k) - \epsilon(k)$ is the angle subtended at the center o in a sampling time interval τ_s. As shown in figure 3.8, this angle depends upon the switching of active states and therefore is proportional to the vector displacement $\boldsymbol{\Delta\psi}_s(k)$. Here $\boldsymbol{\Delta\psi}_s(k)$ is given as,

$$\boldsymbol{\Delta\psi}_s(k) = \boldsymbol{u}_a\tau_a(k) + \boldsymbol{u}_b\tau_b(k) \tag{3.23}$$

or from figure 3.8,

$$\boldsymbol{\Delta\psi}_s(k) = \boldsymbol{\Delta\psi}_s(\boldsymbol{u}_a) + \boldsymbol{\Delta\psi}_s(\boldsymbol{u}_b) \tag{3.24}$$

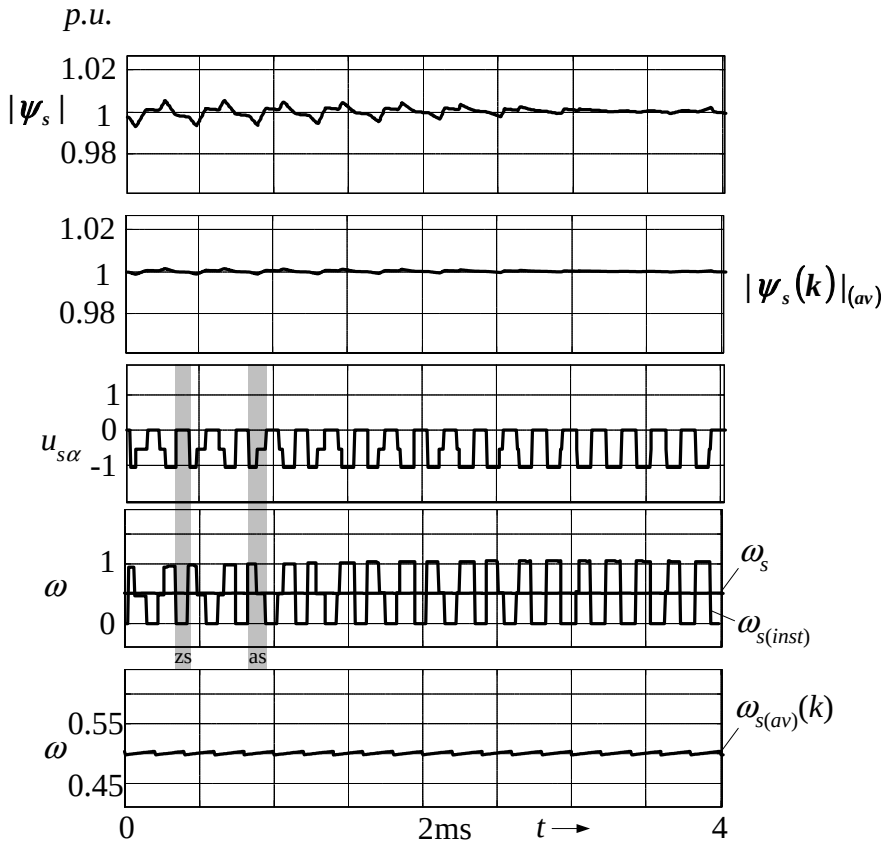

Figure 3.9: Result showing the instantaneous and average angular velocity for the angular velocity ω_s equal to 0.5 *p.u.* Sampling time, $T_s = 400\mu s$

For control, the vector displacement in the stator flux vector brought about by the switching states of the inverter should be equal to the reference stator flux error vector. At the same time, the average magnitude of the stator flux vector in a sampling period should be equal to the reference. If the resistive drop is considered to be negligibly small, the reference stator flux error vector is directly proportional to the angular velocity ω_s, (section 3.2.2). Therefore the switching state vectors should move the stator flux vector at the same average angular velocity, as the reference stator flux vector.

Figure 3.9 shows the relation between the instantaneous angular velocity

$\omega_{s(inst)}$ of the stator flux vector and the α-component of the stator voltage. To obtain $\omega_{s(inst)}$, the angle ϵ of the stator flux vector is estimated at a sampling rate that is 100 times faster than τ_s. The affect of zero vector switching (region 'zs') and active vector switching (region 'as') can be observed on the instantaneous angular velocity. The average angular velocity $\omega_{s(av)}(k)$ closely matches with the reference value when conventional SVM is employed for switching, figure 3.9. Moreover, the average stator flux vector magnitude $|\boldsymbol{\psi}_s(k)|_{av}$ is equal to the reference stator flux vector magnitude of 1.0 $p.u.$ Hence the proposed method of switching based on the reference stator flux error vector, results in the control of the stator flux vector magnitude and angle.

As the reference angular velocity ω_s increases, the reference stator flux error vector $\boldsymbol{\Delta\psi}_s^*(k)$ also increases, equation (3.15). Therefore, the compensating volt-sec vectors $\boldsymbol{u}_a\tau_a$ and $\boldsymbol{u}_b\tau_b$ should increase to achieve the desired average angular velocity. Since the magnitudes of active states are fixed to $\frac{\pi}{3}$, their switching times increase to bring about this compensation. Hence, for constant switching time interval, the time for switching the zero states reduces. The reduced switching time of the zero vector implies an increased average angular velocity of the stator flux vector.

Figure 3.10 shows the affect of increasing angular velocity ω_s on the $\boldsymbol{\Delta\psi}_s^*$ vector. The circular trajectory of this vector grows and becomes an inscribed circle to a hexagon of side $\frac{\pi}{3}\tau_s$ at $\omega_s = 0.907$ $p.u.$ It should be noted that $\frac{\pi}{3}\tau_s$ is the maximum magnitude of the stator flux vector displacement that is possible in a

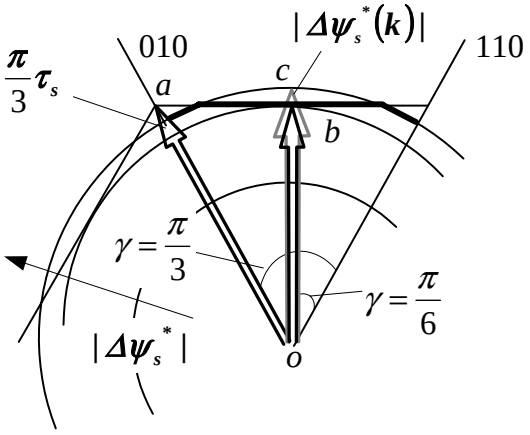

Figure 3.10: Maximum magnitude of $|\boldsymbol{\Delta\psi}_s(k)|$ depends upon the voltage vector limit

sampling period, equation (3.6). Under these conditions the stator flux vector moves at the maximum angular velocity of 1.0 $p.u.$ Therefore, the maximum vector displacement corresponds to the maximum angular velocity of the stator flux vector. Until $\omega_s = 0.907$ $p.u.$, average angular velocity control can be easily achieved using the switching times given by equation (3.20). However for values of reference angular velocity greater than 0.907 $p.u.$, the circular $\boldsymbol{\Delta\psi}_s^*$ trajectory moves out of the hexagon. In a sector, this happens around $\gamma = \pi/6$. For the region in which the circular trajectory is outside, switching state time τ_0 has a negative value and therefore only active vectors can be switched. In so doing, the vector displacement $\boldsymbol{\Delta\psi}_s$ trajectory moves along the hexagon. On the other hand, the region in which the circular trajectory is still inside the hexagon, zero vectors can be switched as defined by equation (3.20) and the error $\boldsymbol{\Delta\psi}_s^*(k)$ can be compensated. Hence the trajectory of the $\boldsymbol{\Delta\psi}_s$ is circular in the region when the trajectory of $\boldsymbol{\Delta\psi}_s^*$ is inside the hexagon, while it moves along the hexagonal boundary for the duration when $\boldsymbol{\Delta\psi}_s^*$ is outside the hexagon and τ_0 is less than zero. Therefore the $\boldsymbol{\Delta\psi}_s$ trajectory

gets distorted. Such trajectory is shown by the thick black curve in figure 3.10.

The average angular velocity reduction begins at a reference angular velocity of $\omega_s = 0.907\ p.u.$ This particular value of the reference angular velocity is equal to the value of modulation index at which the normal range operation of conventional SVM ends. Therefore the proposed method of feedback SVM using the stator flux error vector, is similar to the conventional method of feed-forward SVM, that uses the voltage vector reference to generate the switching states. Hence, the region of operation within this critical value of ω_s can likewise be termed as normal region of operation.

3.5 Problem of control in overmodulation and the proposed solution

3.5.1 Problem

For reference angular velocities greater than 0.907 p.u., the stator flux error vector $\boldsymbol{\Delta\psi_s^*}(k)$ cannot be compensated in a given sampling period. This is because of the inverter voltage limit. Figure 3.11 explains the problem. Loci of $\boldsymbol{\Delta\psi_s^*}$ and $\boldsymbol{\Delta\psi_s}$ are shown in this figure. $\boldsymbol{\Delta\psi_s^*}$ is always circular, whereas, the locus of $\boldsymbol{\Delta\psi_s}$ is polygonal depending on the switching times and switching states. When zero vector is not switched, the locus of $\boldsymbol{\Delta\psi_s}$ vector is along the hexagon. Two regions of operation are typical in every sector. Region P, in which the available volt-sec in every sampling period is less than the stator flux error vector $\boldsymbol{\Delta\psi_s^*}(k)$ and region Q

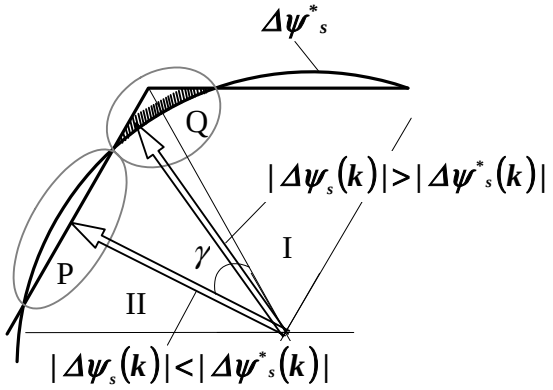

Figure 3.11: Problem during overmodulation, trajectories of $\Delta\psi_s^*$ and $\Delta\psi_s$

where there are still enough volt-secs available that the stator flux error vector can be compensated. Figure 3.12 shows the affect of voltage vector limit on the average

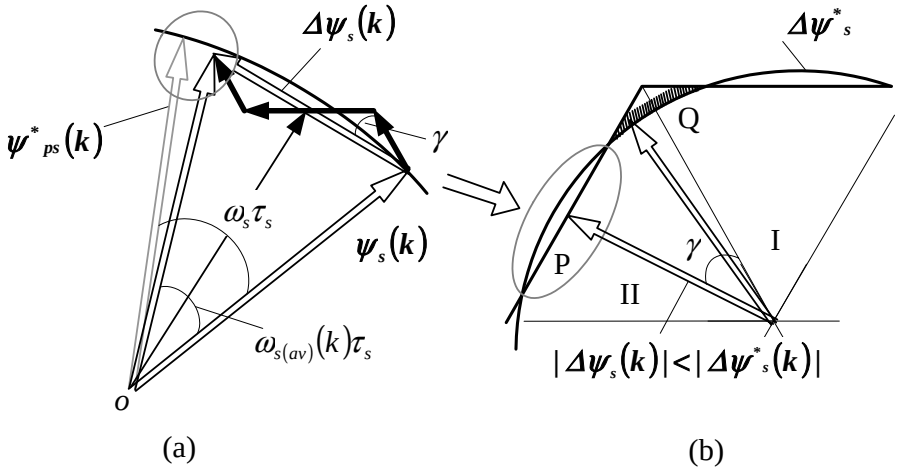

Figure 3.12: Stator flux vector magnitude and angular velocity reduction, corresponding to region P of figure 3.11, trajectory of flux vector ψ_s in a sampling time period

magnitude and angular velocity of the stator flux vector in region P. The grey vector in figure 3.12(a) represents the desired value $\psi_{ps}^*(k)$ at the k^{th} sampling instant. This results in a reference stator flux error vector $\Delta\psi_s^*(k)$. Vector $\Delta\psi_s^*$ traces a circular trajectory as shown in figure 3.12 (b). Due to lack of volt-secs in region P, the resulting vector displacement $\Delta\psi_s$, is less than $\Delta\psi_s^*$ for every sampling

period in the region P. Hence in region P, the average angular velocity $\omega_{s(av)}(k)$ in every sampling period will be less than the reference value of ω_s. Moreover, due to lack of compensating volt-secs in region P, the average magnitude of the stator flux vector is also reduced. This creates phase angle and magnitude error. At $\gamma = \frac{\pi}{6}$ in every sector, figure 3.12 (b), the volt-sec available is minimum. Hence minimum vector displacement is possible at this value of γ and therefore the reduction in the average angular velocity and average magnitude of the stator flux vector is the maximum.

In region Q, it is still possible to obtain the required volt-sec balance and to compensate the stator flux error vector. The average angular velocity of the stator flux vector $\boldsymbol{\psi}_s$ in this region is therefore equal to that of the reference. However, due to the reduction in angular velocity in regions P of all the sectors, the average angle traversed by $\boldsymbol{\psi}_s$ in a fundamental cycle gets reduced. Moreover, the average magnitude is also less than the reference stator flux vector. In order to eliminate both angle and magnitude error for operation in a fundamental cycle, the extra volt-sec margin available in region Q is utilized. Hence in region Q, the stator flux vector is deliberately moved at an average angular velocity $\omega_{s(av)}(k)$, that is more than the reference value. As shown in figure 3.13, switching in region Q is such that the actual vector displacement $\boldsymbol{\Delta\psi}_s(k)$ in this region is in excess of the required value, $\boldsymbol{\Delta\psi_s^*}(k)$ (shaded area of region Q). This mode of operation is called overmodulation I. Figure 3.13 shows the affect of the proposed switching strategy. Once again the grey vector in figure 3.13 (a) represents the desired value

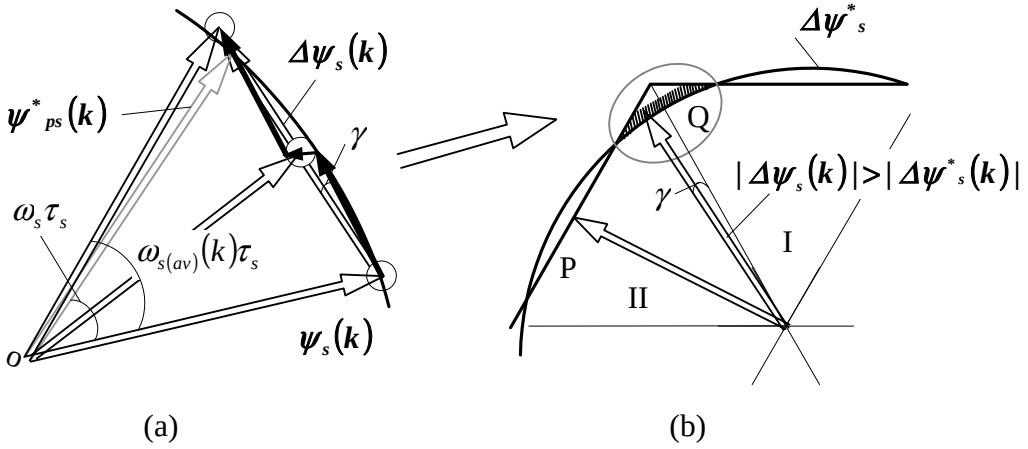

Figure 3.13: Compensation of the volt-sec loss corresponding to region Q of figure 3.11

and switching is such that the stator flux vector value exceeds the reference value both in magnitude and phase angle. This not only increases the average magnitude of the stator flux vector but also accelerates it. The average magnitude and phase angle control is now achieved in a **sector**. On the other hand in the normal range ($\omega_s < 0.907$), the same control was possible in a **sampling period**.

3.5.2 Switching state times calculation in overmodulation I region

Before the switching states in overmodulation I region are calculated, the limit of overmodulation I region will be found. The maximum possible reduction in the vector displacement for overmodulation I occurs in region P and is given as,

$$|\boldsymbol{\Delta\psi}_s|_{-max} = |\boldsymbol{\Delta\psi}^*_s(k)|_{max} - 0.907|\boldsymbol{\Delta\psi}_s(k)|_{max} \tag{3.25}$$

where $|\boldsymbol{\Delta\psi}_s|_{-max}$ represents the maximum possible loss in volt-secs and $|\boldsymbol{\Delta\psi}^*_s(k)|_{max}$ is the unknown magnitude of $\boldsymbol{\Delta\psi}^*_s$ where overmodulation I ends. The value

$|\boldsymbol{\Delta\psi}_s^*(k)|_{max}$ occurs at a particular unknown angular velocity of the reference stator flux vector. $|\boldsymbol{\Delta\psi}_s(k)|_{max}$ is the maximum possible magnitude of the vector displacement that can be brought about, by application of an inverter switching state. This will move the stator flux vector in the direction of that switching state vector at the maximum possible angular velocity of 1.0 *p.u.*

On the other hand, the possible compensation for the loss in vector displacement during the region Q can be defined as

$$|\boldsymbol{\Delta\psi}_s|_{+max} = |\boldsymbol{\Delta\psi}_s(k)|_{max} - |\boldsymbol{\Delta\psi}_s^*(k)|_{max} \tag{3.26}$$

where $|\boldsymbol{\Delta\psi}_s|_{+max}$ is the possible compensation. In order to achieve complete compensation of whatever is lost during the region P, $|\boldsymbol{\Delta\psi}_s|_{-max}$, should be compensated during the region Q. Using equations (3.25) and (3.26) we get the equality required for compensation,

$$|\boldsymbol{\Delta\psi}_s^*(k)|_{max} - 0.907|\boldsymbol{\Delta\psi}_s(k)|_{max} = |\boldsymbol{\Delta\psi}_s(k)|_{max} - |\boldsymbol{\Delta\psi}_s^*(k)|_{max} \tag{3.27}$$

$$2|\boldsymbol{\Delta\psi}_s^*(k)|_{max} = 1.907|\boldsymbol{\Delta\psi}_s(k)|_{max} \tag{3.28}$$

This gives $|\boldsymbol{\Delta\psi}_s^*(k)|_{max} = 0.9535|\boldsymbol{\Delta\psi}_s(k)|_{max}$, at which overmodulation I region ends. This corresponds to a modulation index of 0.9535 and is greater than that obtained in the schemes like [27] and [53] that all end at 0.952. In [38] performance evaluation of several overmodulation switching strategies is given. According to that analysis, Depenbrock's method [39] achieves much higher range of overmodulation, than any other method, including the one proposed here. However,

no comment is provided on the average angular velocity control of the stator flux vector.

In region P, $\tau_0 < 0$ and the zero switching state cannot be switched. The resulting switching times are

$$\tau_a(k) = |\boldsymbol{\Delta\psi}_s^*(k)| \frac{\sin(\frac{\pi}{3} - \gamma)}{\frac{\pi}{3}\sin\frac{\pi}{3}}$$
$$\tau_b(k) = \tau_s - \tau_a(k) \tag{3.29}$$

While in region Q, where $\tau_0 > 0$, the modified switching times $\tau_{a1}(k)$, $\tau_{b1}(k)$ and $\tau_{01}(k)$ are,

$$\tau_{a1}(k) = \tau_a(k) + 0.5\lambda * \tau_0(k)$$
$$\tau_{b1}(k) = \tau_b(k) + 0.5\lambda * \tau_0(k)$$
$$\tau_{01}(k) = \tau_s - (\tau_{a1}(k) + \tau_{b1}(k)) \tag{3.30}$$

where $\tau_a(k)$, $\tau_b(k)$ and $\tau_0(k)$ are the switching times calculated in the normal region and are same as, eqn. (3.20) and the compensation factor λ is given as,

$$\lambda = \frac{|\boldsymbol{\Delta\psi}_s^*(k)| - 0.907|\boldsymbol{\Delta\psi}_s(k)|_{max}}{0.9535|\boldsymbol{\Delta\psi}_s(k)|_{max} - 0.907|\boldsymbol{\Delta\psi}_s(k)|_{max}} \tag{3.31}$$

Here, λ is expressed as ratio of error in magnitude of the vector displacement to the maximum possible compensation. Though this equation is computed for every value of $\boldsymbol{\Delta\psi}_s^*(k)$, it is a simple equation when expressed in terms of constant and variables. The constants can be combined in,

$$g = \frac{0.907|\boldsymbol{\Delta\psi}_s(k)|_{max}}{0.9535|\boldsymbol{\Delta\psi}_s(k)|_{max} - 0.907|\boldsymbol{\Delta\psi}_s(k)|_{max}} \tag{3.32}$$

and

$$h = 0.9535|\boldsymbol{\Delta\psi}_s(k)|_{max} - 0.907|\boldsymbol{\Delta\psi}_s(k)|_{max} \tag{3.33}$$

Thus giving,

$$\lambda = \frac{|\boldsymbol{\Delta\psi}_s^*(k)|}{h} - g \tag{3.34}$$

Hence, estimation of λ requires just two arithmetic operations, division and subtraction. For a constant value of the angular velocity ω_s, repeated calculations of λ are not required. Therefore, the control algorithm checks for the change in operating angular velocity before proceeding to calculate a fresh value of λ. Instead of having look-up tables as in [27], [29] or solving nonlinear equations as in [28], the volt-sec loss in region P can be compensated in real time, achieving closed loop stator flux vector angle and magnitude control.

The proposed switching strategy effectively reduces the switching times of zero states while increasing those of active states. This increases the vector displacement in region Q. Since the stator flux vector stops for a smaller time, the average angular velocity is proportionately increased. The maximum value of λ is 1.0 and occurs at $\omega_s = 0.9535\ p.u.$ For this value of λ, the modified time $\tau_{01}(k)$ for switching a zero state becomes zero and no volt-sec compensation can be brought about in region Q, using the proposed overmodulation I switching strategy.

At the boundary of normal range and overmodulation I, τ_0 in region P will be zero as the circular trajectory of $\boldsymbol{\Delta\psi}_s^*$ touches the hexagonal limit. In a sector, this will happen at $\gamma = \frac{\pi}{6}$. Thus the need to compensate the angular velocity drop

in overmodulation I using equations. (3.29) can be verified by calculating the value of τ_0 for $\gamma = \frac{\pi}{6}$. Using equation (3.20),

$$\tau_0 = \tau_s - \frac{3}{\pi}\frac{|\boldsymbol{\Delta\psi}_s^*(k)|\sin(\pi/3+\gamma)}{\sin(\pi/3)} \tag{3.35}$$

and $\tau_0(\frac{\pi}{6})$ is given as,

$$\tau_0(\frac{\pi}{6}) = \tau_s - \frac{3}{\pi}\frac{|\boldsymbol{\Delta\psi}_s^*(k)|}{\sin(\pi/3)} \tag{3.36}$$

Hence if, $\tau_0(\frac{\pi}{6}) \leq 0$, overmodulation equations (3.30) will be used to compensate for the loss in angular velocity.

During overmodulation, the average angular velocity control can only be achieved in sector rather than in a sampling period. The average angular velocity of the stator flux vector in a sector can be expressed as $\omega_{sav}(sec)$ and is obtained using the following expression,

$$\omega_{s(av)}(sec) = \frac{\sum_{sec}\omega_{s(av)}(k)}{\text{No. of samples in a sector}} \tag{3.37}$$

Here, $\sum_{sec}\omega_{s(av)}$ is the sum of the average angular velocities in a sector. Though the average angular velocity $\omega_{s(av)}(k)$ varies from one sampling period to another, the angular velocity $\omega_{s(av)}(sec)$ in a sector is controlled to closely match the reference value. Result of figure 3.14 shows the stator flux vector magnitude and average angular velocity control for operation in the overmodulation I region. Switching between active states (region 'as') corresponds to the region P of figure 3.11. This results in a larger variation of stator flux vector magnitude about the reference value. The angular velocity variation is small in this region. On the other hand, switching of active and zero vectors (region 'zs') corresponds to the compensating

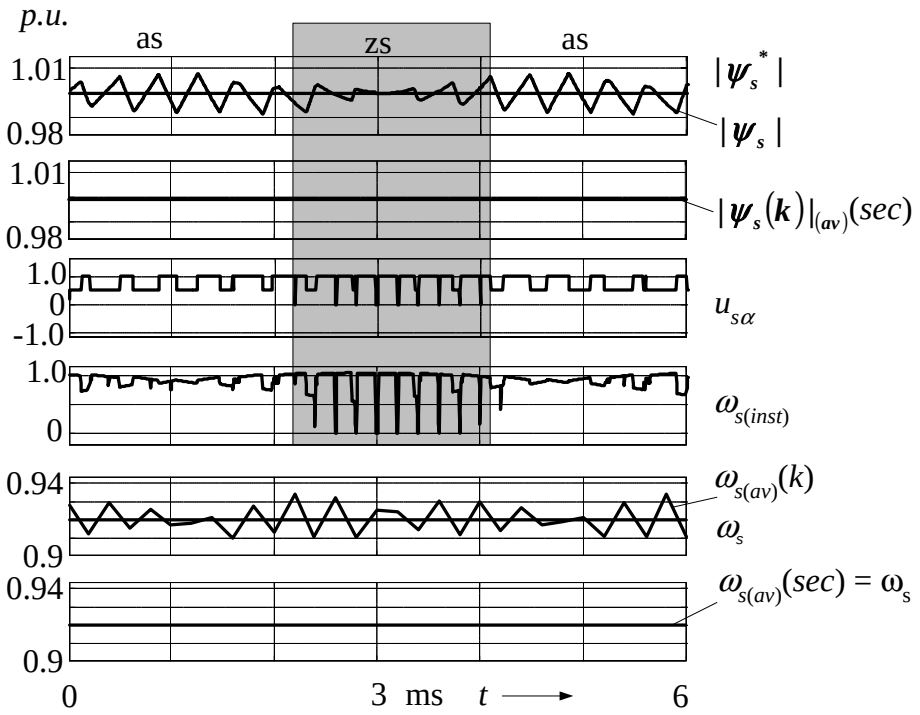

Figure 3.14: Control of stator flux vector magnitude and its average angular velocity in the overmodulation I region with the proposed switching method, ω_s is equal to 0.92 $p.u.$, Sampling time, $T_s = 400\mu s$. Here, $\omega_{s(av)}(sec)$ is the average angular velocity in a sector

region Q of figure 3.11. It makes the stator flux vector magnitude smoother. Also, the average angular velocity obtained in this region, compensates for the loss during the region 'as'. Due to the switching of zero vectors, the instantaneous angular velocity has zero values, indicating the discontinuous motion of the flux vector.

From figure 3.11 it can be observed that with the increase of ω_s, the region Q will reduce to zero. This happens at a reference angular velocity of $\omega_s = 0.9535\ p.u.$ and marks the end of the overmodulation I region. Hence no further compensation of vector displacements will be possible with the above switching strategy. Further compensation can be done by alternate holding of a single state and switching between two adjacent active states. This region of operation is called overmodulation

II.

3.5.3 Closed loop control of flux vector in overmodulation II region unto six-step

The duration for holding an active state depends upon hold angle α_h, and was first proposed by Holtz et. al, in [27]. This same idea has been presented in different forms by many researchers like in [28], [29]. The switching strategy proposed here also uses hold angle during operation in the overmodulation II region, but there are a few important differences from the approaches followed in [27], [28] and [29].

- In [27], for the duration of holding a vector, the magnitude of voltage vector increases but its angular velocity is less than the reference voltage vector. On the other hand, for the duration of hold angle, the angle of stator flux vector changes at the maximum possible rate. Hence, holding of a vector has an exactly opposite affect on the stator flux vector than on the voltage vector.

- In present work, the duration of holding the active states and switching between them in overmodulation II region is decided by the stator flux vector control requirement. This is unlike the above methods that are designed for an open loop v/f drive, purely to exploit the installed dc-link voltage. In essence, the proposed method is a feedback scheme.

- In [27], [28] and [29], the switching information for overmodulation II region is either stored in tables or it is obtained by solving non-linear equations.

The method proposed here uses a simple formula and saves the processor's memory.

3.5.4 Principle of switching

At the end of overmodulation I region, the switching times vary linearly in a sector, figure 3.15. Since zero state is not switched at all, switching times τ_a and

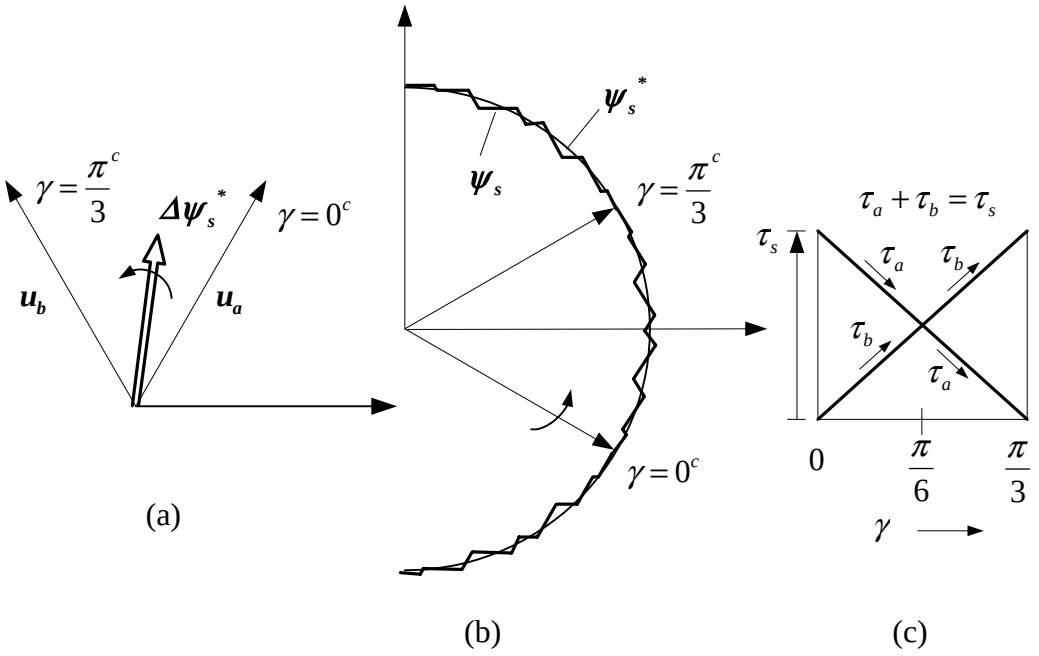

Figure 3.15: Switching state times at the end of overmodulation I

τ_b follow the relationship $\tau_a + \tau_b = \tau_s$ at every instant. Switching of active states causes the stator flux vector to follow a polygonal trajectory. The average angular velocity in a sector, $\omega_{s(av)}(sec)$ under such condition is equal to 0.9535 $p.u.$ Figure 3.15 shows the corresponding trajectories of the displacement vector $\boldsymbol{\Delta\psi}_s$ and the flux vectors, $\boldsymbol{\psi}_s^*$ and $\boldsymbol{\psi}_s$ for operation in a sector. The average magnitude of the stator flux vector is equal to the magnitude of the reference stator flux vector and

hence a constant flux vector magnitude operation is ensured.

On the other hand, in the six-step mode, the average angular velocity $\omega_{s(av)}(sec)$ is equal to 1.0 $p.u.$ This is because the time (normalized) taken by the stator flux vector to traverse the angle of $\pi/3$ radians in a sector, is equal to $\pi/3$ radians. To move the stator flux vector at this average angular velocity, vector $\boldsymbol{u}_a$ is continuously switched (or held), for values of $\gamma \leq \frac{\pi}{6}$, whereas, for $\frac{\pi}{6} < \gamma \leq \frac{\pi}{3}$ vector $\boldsymbol{u}_b$ is held, figure 3.16. The corresponding trajectories of the reference and stator flux vectors are shown in figure. The stator flux vector $\boldsymbol{\psi}_s$ follows a hexagonal trajectory while the switching state times vary as shown in figure 3.16 (c).

In order to get any average angular velocity $\omega_{s(av)}(sec) < 1.0$ $p.u.$, it is necessary to slow down the stator flux vector. This can be achieved by suitably holding a state and switching between active states $\boldsymbol{u}_a$ and $\boldsymbol{u}_b$.

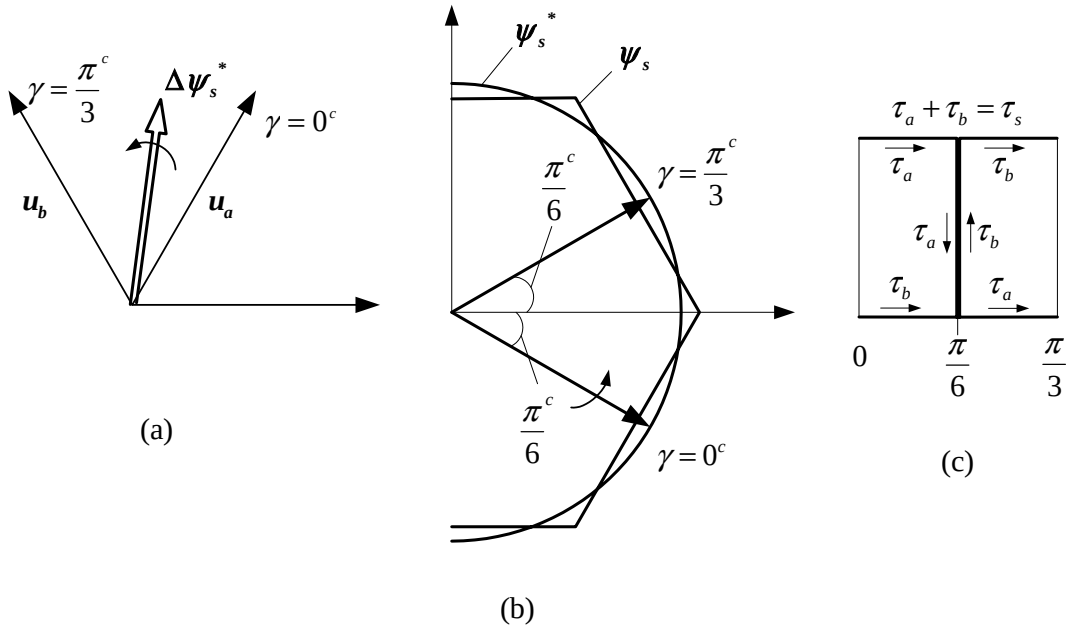

Figure 3.16: Trajectory of flux vectors and variation of switching state times during six-step

For every value of ω_s such that, $0.9535 < \omega_s < 1.0$ *p.u.*, when $\gamma < \alpha_h$ in a sector, state $\boldsymbol{u}_a$ is held. Thereafter, for $\alpha_h < \gamma < \frac{\pi}{3} - 2\alpha_h$, switching between $\boldsymbol{u}_a$ and $\boldsymbol{u}_b$ is carried out and finally for $\frac{\pi}{3} - \alpha_h < \gamma < \frac{\pi}{3}$, state $\boldsymbol{u}_b$ is held, figure 3.17.

The duration of holding an active state and that of switching the adjacent states, is decided by the angular velocity ω_s of the reference stator flux vector. For any value of ω_s, the time taken to traverse an angle of $\frac{\pi}{3}$ radians is given as, $\frac{\frac{\pi}{3}}{\omega_s}$. For the average angular velocity $\omega_{s(av)}(sec)$ of the stator flux vector to be equal to ω_s, the time taken by the stator flux vector to traverse a sector should be equal to that taken by the reference stator flux vector. A suitable combination of two possible options can achieve this. The first option is to move the stator flux vector at an average angular velocity of 0.9535 *p.u.* by switching between active vectors. This is achieved by ensuring the switching state times have a relationship as shown in figure 3.15 (c). The second available option is to move the stator flux vector at an average angular velocity of 1.0 *p.u.* by holding on to one of the two state vectors $\boldsymbol{u}_a$ and $\boldsymbol{u}_b$. Figure 3.17 illustrates the sequencing of the two options. During the total hold period of $2\alpha_h$ in a sector, the average angular velocity of the stator flux vector is equal to 1.0 *p.u.*, whereas the switching between active states in the manner as shown in figure 3.15 (c), moves it at an average angular velocity of 0.9535 *p.u.* As the total time taken by the stator flux vector $\boldsymbol{\psi}_s$ to traverse the sector should be equal to $\frac{\frac{\pi}{3}}{\omega_s}$ it can be said that,

$$\frac{\frac{\pi}{3}}{\omega_s} = \frac{2\alpha_h}{1.0} + \frac{\frac{\pi}{3} - 2\alpha_h}{0.9535} \tag{3.38}$$

The hold angle α_h is obtained using equation (3.38) and has a linear relationship

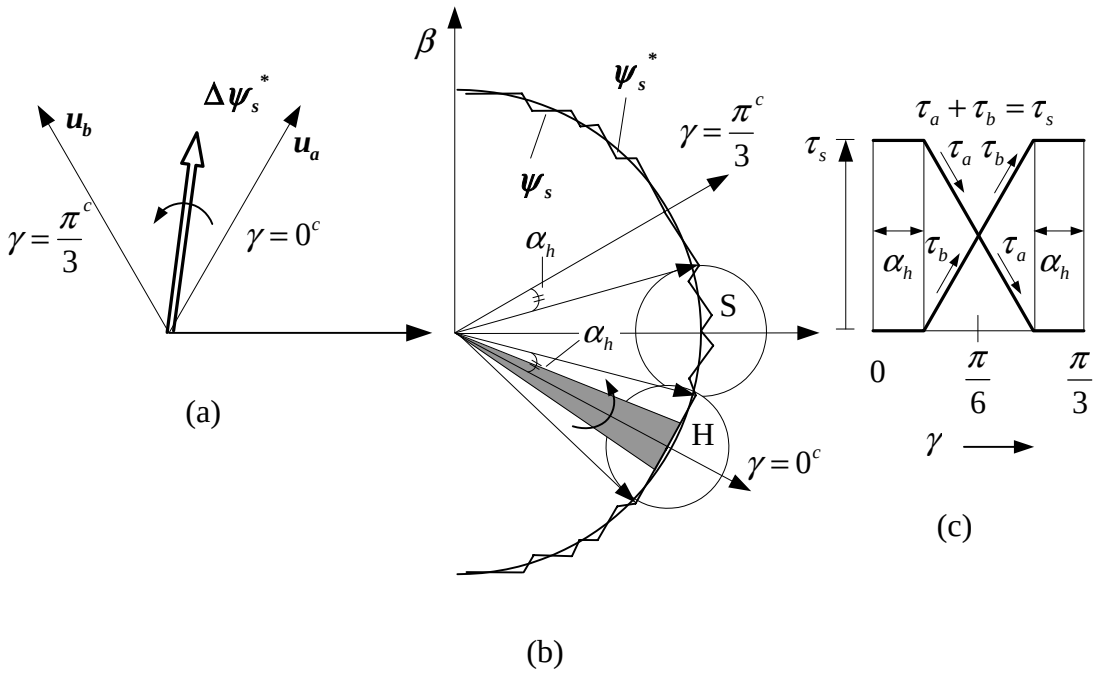

Figure 3.17: Switching state times variation in overmoduation II, here α_h is the hold angle

with the reference angular velocity. It is given as,

$$\alpha_h = 10.5(1.05 - \frac{1}{\omega_s}) \tag{3.39}$$

During the hold period (region 'H' in figure 3.17) the stator flux vector moves along the hexagon parallel to the switching state vector $\boldsymbol{u}_a$. The instantaneous angular velocity $\omega_{s(inst)}$ (and also the average angular velocity in sampling period, $\omega_{s(av)}(k)$) is determined by the angle inscribed by $\boldsymbol{\Delta\psi}_s(\boldsymbol{u}_a)$ vector (shaded area in region 'H', figure 3.17). As γ increases, the triangle formed by the vector $\boldsymbol{\Delta\psi}_s(\boldsymbol{u}_a)$ and the center 'o', is no more isosceles, figure 3.18. Hence the angle inscribed by $\boldsymbol{\Delta\psi}_s(\boldsymbol{u}_a)$ becomes more acute ($\xi_2 < \xi_1$) as γ increases from zero. The inscribed angle is maximum at $\gamma = 0$ and $\gamma = \frac{\pi}{3}$ and so is the instantaneous angular velocity $\omega_{s(inst)}$ and the average angular velocity $\omega_{s(av)}(k)$. However, as the stator flux vector trajectory is along the hexagon, its average magnitude during the hold period is less

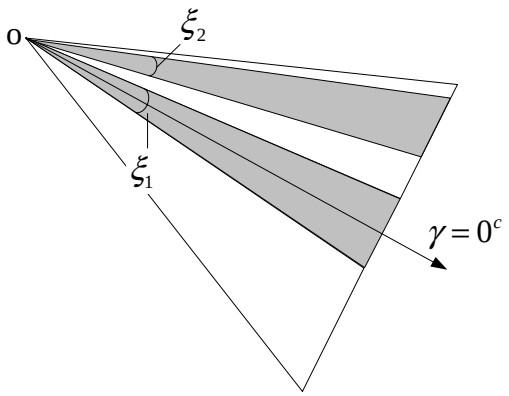

Figure 3.18: Angle inscribed at the center 'o' by two different positions of $\boldsymbol{\Delta\psi}_s(\boldsymbol{u}_a)$ during the hold period. Here $\xi_1 > \xi_2$

than the reference value. For $\gamma > \alpha_h$, active vectors are switched as per equation (3.29), (region 'S' in figure 3.17). This causes the stator flux vector magnitude to increase. However, the resulting average angular velocity drops below the reference value. The nature of switching defined by equation (3.38), controls the average angular velocity and magnitude of the stator flux vector within a sector (duration $\frac{\pi}{3}$), figure 3.19. Thus the proposed control method achieves closed loop stator flux vector control without magnitude and phase angle error.

The simulated result of variation of the average angular velocity in the over-modulation II region is given in figure 3.19 for $\omega_s = 0.985\ p.u.$ During switching between active states, the average angular velocity $\omega_{s(av)}(k)$ is reduced but the magnitude of the stator flux vector increases. On the other hand, during the holding of vectors, the stator flux vector moves along the voltage vector held, reducing its magnitude but at the same time the angular velocity increases. Figure 3.20 shows the variation of the angular velocity of the stator flux vector during six-step operation. The average angular velocity is equal to the reference value. Moreover,

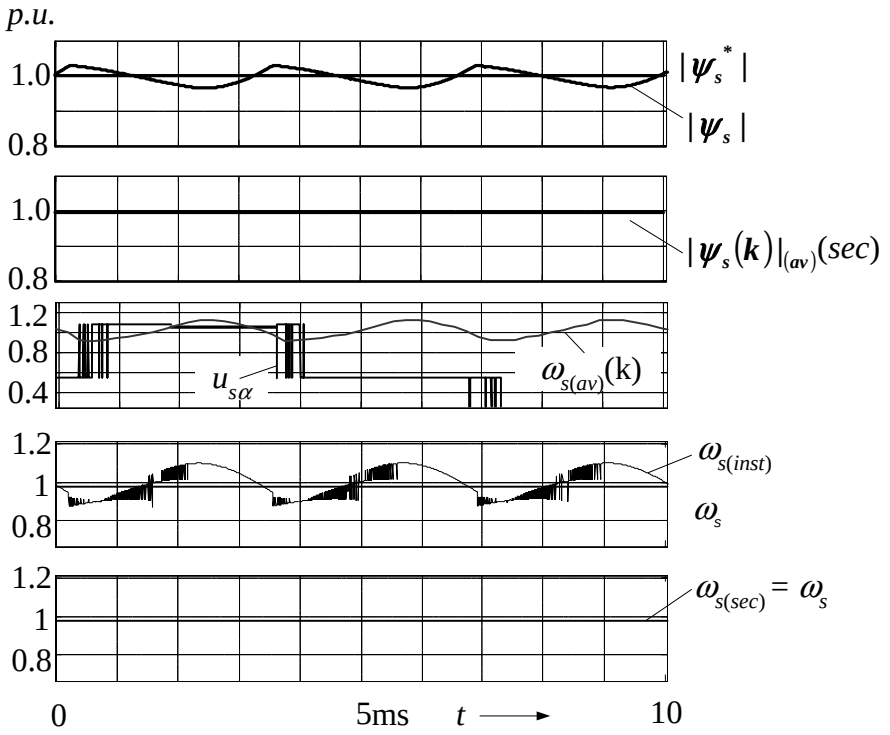

Figure 3.19: Flux vector magnitude and angular velocity control in the overmodulation II region. $\omega_s = 0.985\ p.u.$

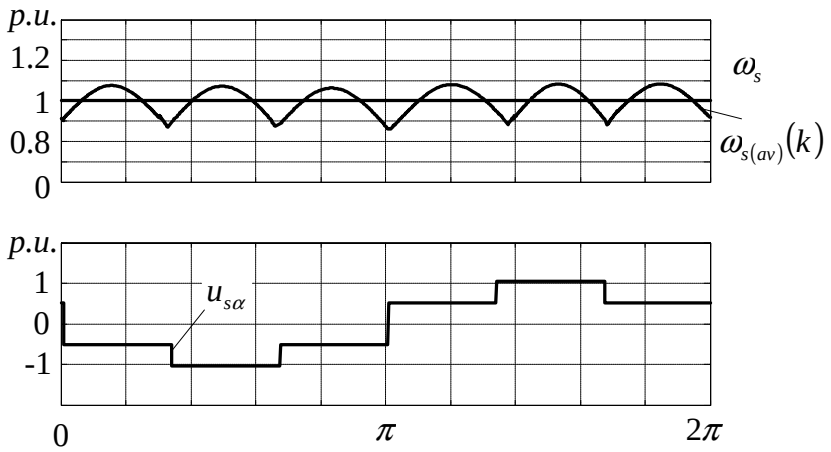

Figure 3.20: Variation of the instantaneous angular velocity during six-step operation

it is controlled in every individual sector of operation. The trajectory of the stator flux vector during overmodulation II region can be seen from figure 3.21. While the trajectory of the reference stator flux vector is circular, holding and switch-

ing regions are clearly seen in the stator flux vector. During the hold region, the magnitude of the stator flux vector gets reduced as it follows the linear trajectory along the voltage vector held. On the other hand, during the switching of adjacent states, the magnitude of the stator flux vector increases and it slows down due to a longer path. Similarly, the α-component of the reference stator flux error vector has a purely sinusoidal waveform whereas, the affect of switching and holding the active states can be observed in the α-component of the stator flux error vector waveform.

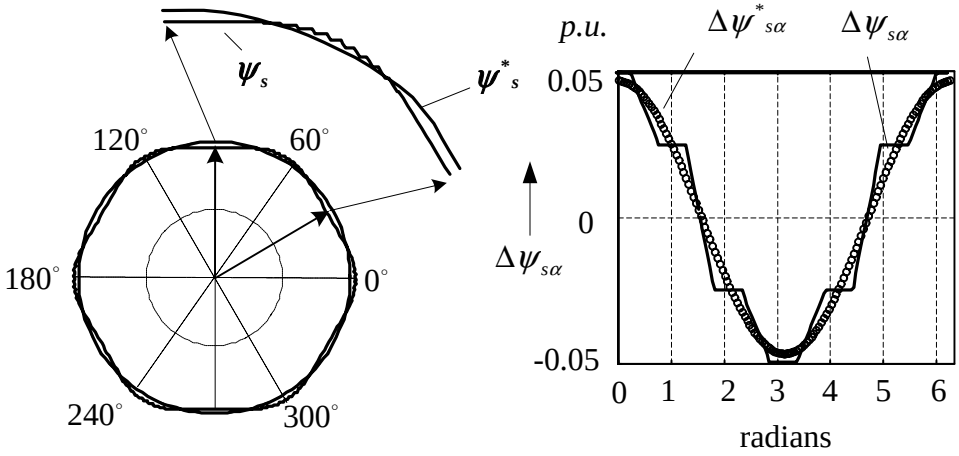

Figure 3.21: Control of phase angle of the flux vector and the trajectories of the reference and the stator flux vectors

Besides being simpler to implement in real time, the proposed switching logic in the overmodulation region achieves closed loop control of the stator flux vector phase angle and magnitude in a fundamental cycle. Pre-processors and look up tables are not required and no approximation is needed.

3.6 Comparison of modulation performance with other prominent schemes in the overmodulation region

The schemes of overmodulation considered for comparison are given in references [54] and [38]. These methods manipulate the reference voltage vector in real time, to achieve linearity of the fundamental voltage. As such, they do not require tables to store the switching information. Bolognani, [54] merges both the overmodulation zones in one and represents the manipulated reference voltage in the form of an equation. Hava, [38] on the other hand describes a "gain linearization" method that achieves voltage gain linearity. The advantage of these schemes are their easy and direct real time digital implementation, but it is not yet clear as to how these schemes fair when used for constant switching frequency direct control of torque and stator flux vector. As the linear range of modulation is common to all the PWM schemes, only the overmodulation region of operation is considered. Such a comparison will bring out the ability of the modulation to maintain a linear relationship between the reference angular velocity and the average angular velocity of the stator flux vector throughout the overmodulation region. For closed loop stator flux vector control and constant switching frequency DTC, it is important to achieve this condition as it indicates that the phase error in an operating cycle is zero. Moreover, this ensures the control of the stator flux vector magnitude in a fundamental cycle. The average angular velocity $\omega_{sav}(sec)$ in sector has been used.

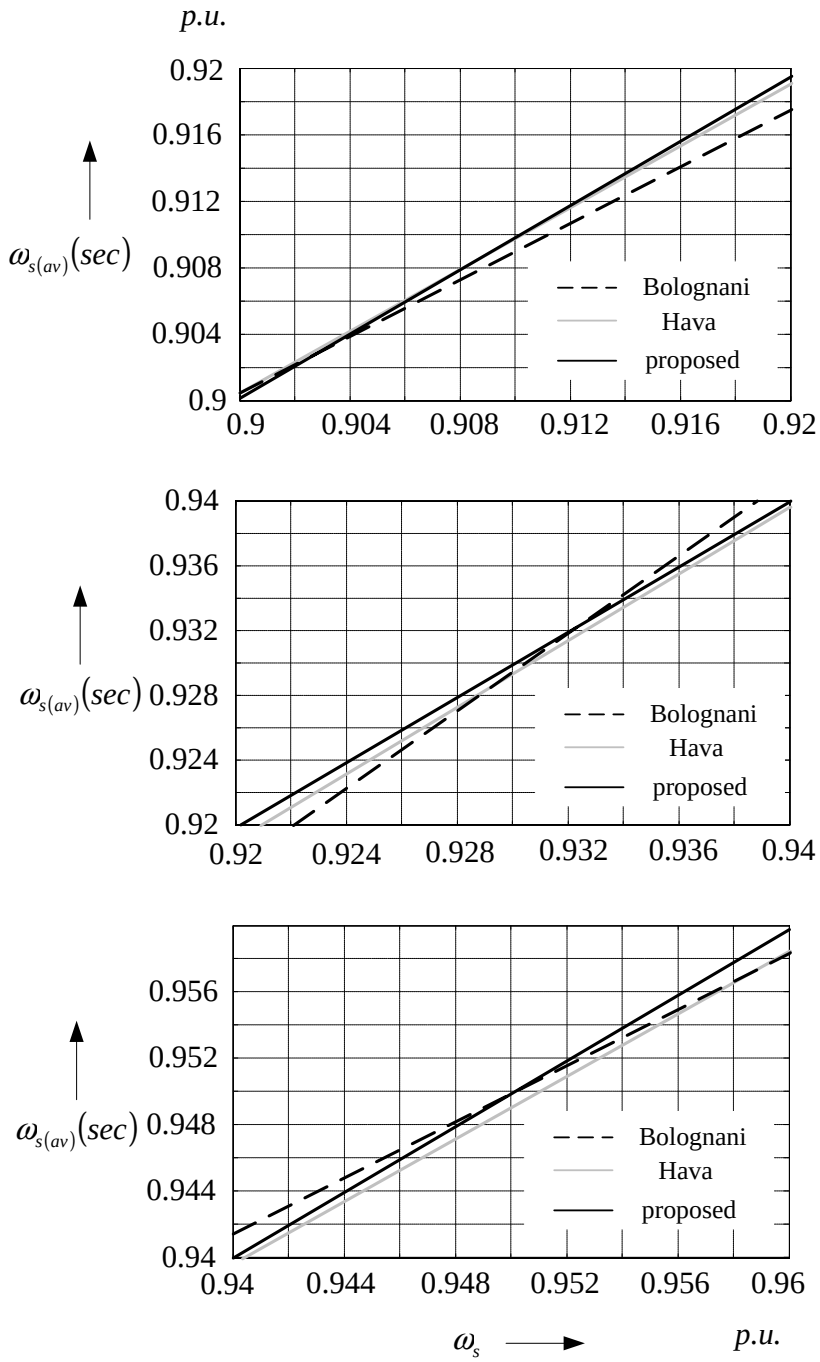

Figure 3.22: Comparison of angular velocity variation for three different methods of direct digital implementation. Range of operation from 0.9 - 0.96 *p.u.*

Figures 3.22 and 3.23 show the variation in the average angular velocity of the flux vector. Following conclusions can be drawn from these results, (a) In Bolognani's [54] method, the average angular velocity of the stator flux vector in

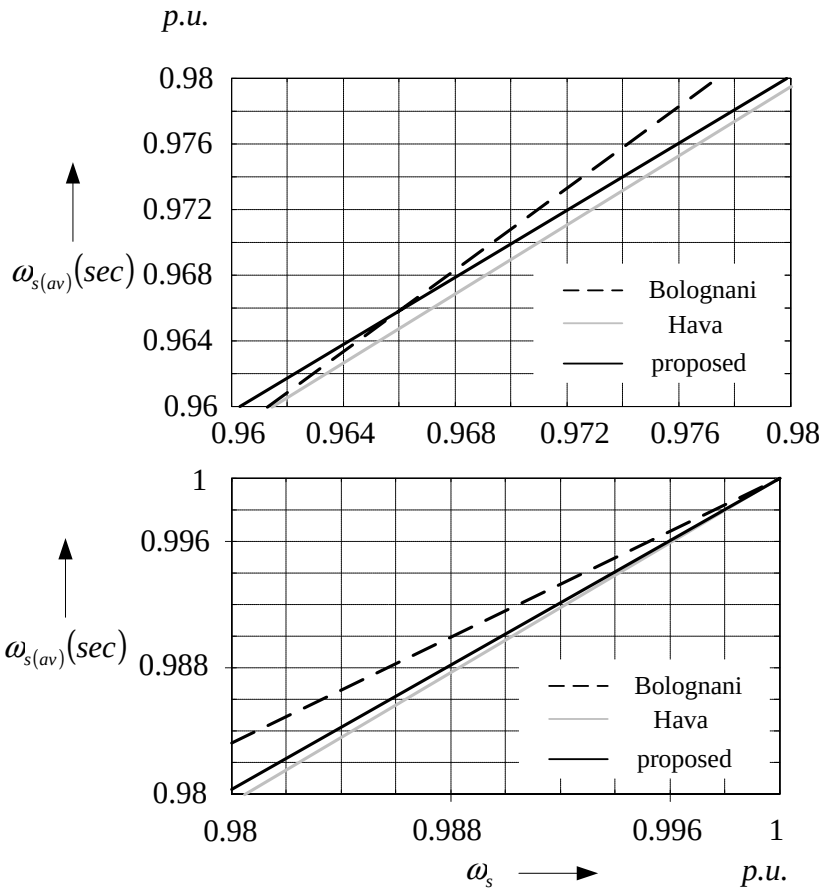

Figure 3.23: Comparison of angular velocity variation for three different methods of direct digital implementation. Range of operation from 0.96 - 1.0 *p.u.*

an operating cycle is less in overmodulation I region (as defined in the present work) or more in overmodulation II region. Hence there will be a phase error present throughout the overmodulation region of operation. (b) In Hava's [38] method, this error is always present and is consistent in the sense that the average angular velocity is always less than the reference value. (c) As the proposed method defines the switching strategy to maintain the angular velocity equality, it produces minimum average phase and magnitude error when compared with the other two methods.

3.7 Flux distortion due to the proposed method of switching

Due to switching of inverter, the trajectory of the stator flux vector is polygonal and therefore departs from the ideal circular trajectory that can be obtained from a sinusoidal supply. During overmodulation the distortion in the flux waveforms will depend upon the nature of switching, as lower order harmonics contaminate the flux waveforms. It is necessary to investigate the distortion produced in the stator flux vector, as it is indicative of the ripple in torque. The total harmonic distortion (THD) is a measure of the deviation of the flux vector trajectory from the ideal sinusoidal trajectory and is defined as,

$$\psi_{s\alpha}(thd) = \sqrt{\frac{(\psi_{s\alpha(rms)})^2 - (\psi_{s1\alpha(rms)})^2}{(\psi_{s1\alpha(rms)})^2}} \tag{3.40}$$

Here, $\psi_{s\alpha(rms)}$ is the root mean square (rms) value of the α component of the stator flux vector and $\psi_{s1\alpha(rms)}$ is the rms value of the fundamental component of it. Figure 3.24 shows the distortion in alpha component at any value of the reference angular velocity with respect to the distortion $\psi_{s\alpha}(thd)_{ss}$, during six-step operation. Two different values of switching frequencies f_{sw} are considered and a substantial increase in distortion is observed for a low switching frequency of 0.5 kHz. Figure 3.25 gives a comparison of the distortion produced due to three different switching strategies in the overmodulation region. In Bolognani's method, [54], relatively large number of harmonics in the voltage waveforms reflect as a higher value of flux waveform distortion. Hava's method [38], is close to the proposed method in

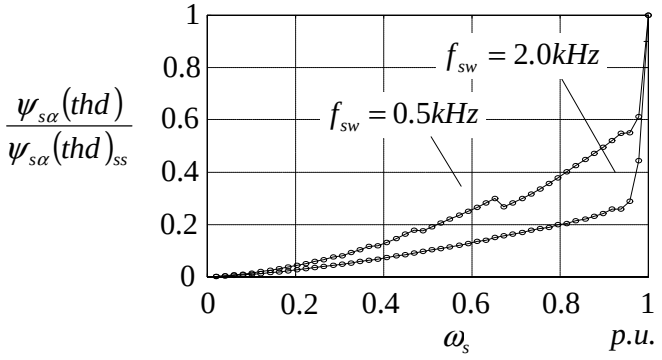

Figure 3.24: Total harmonic distortion in the α component of the stator flux vector at two different switching frequencies

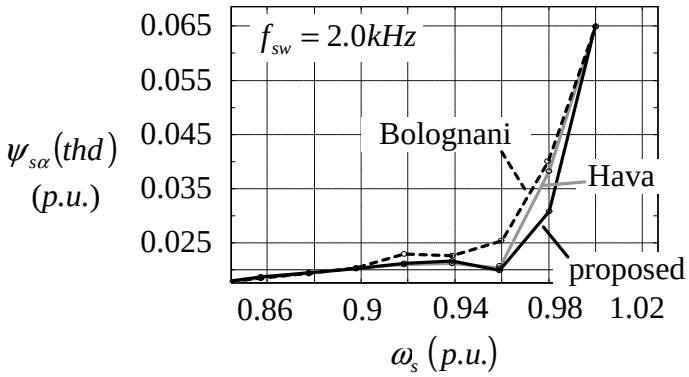

Figure 3.25: Comparison of flux distortion

terms of harmonic distortion, specially in the overmodulation I region of operation. However, the piecewise linearized and approximated relationship between the output voltage and the reference voltage vector, tends to distort the flux waveform in the overmodulation II region. The maximum deviation occurs at an operating angular velocity of 0.98 *p.u.* The proposed method however has the advantage of simple real time implementation and uses no approximations.

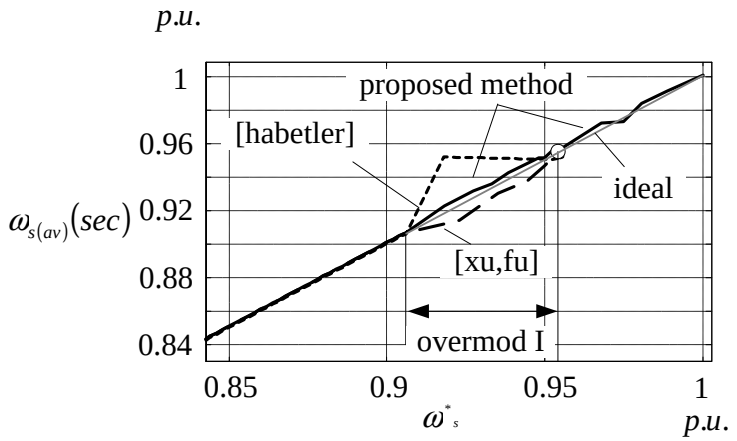

Figure 3.26: Comparison of the average angular velocities for the three methods doing closed loop control of the flux vector in overmodulation I region

3.8 Comparison with the other closed loop stator flux vector control schemes

Figure 3.26 compares the average angular velocity of the stator flux vector, obtained in overmodulation I range using the switching methods given in references [1] and [22] with that obtained using the proposed method. These methods are selected for comparison as they do closed loop torque and stator flux vector control at constant switching frequency. Although, the switching strategy adopted in these, does not have overmodulation II operation, overmodulation I switching strategy of reference [1], overcompensates the drop in angular velocity. As such, the average angular velocity of the machine is higher than the reference value. In reference [22], no compensation is implemented, hence the average angular velocity of the stator flux vector reduces with the increase in ω_s. Therefore a constant phase angle error will be present during closed loop stator flux vector control, figure 3.27. In the proposed method, as the average angular velocity of the stator flux vector is

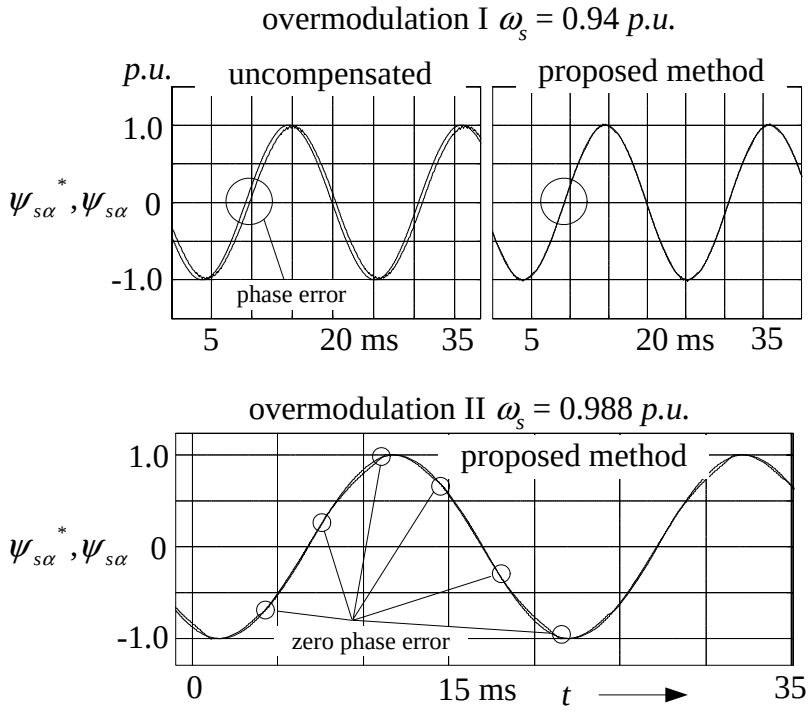

Figure 3.27: Phase error in overmodulation

very close to the angular velocity of the reference, minimum phase error is ensured. This is verified for both regions of operation by the result of figure 3.27. Presence of a phase error effects both the phase angle of the stator flux vector as well as the fundamental frequency that is obtained. Though the fundamental frequency in an operating cycle differs by a very small amount, the phase error in a fundamental cycle will accumulate and will be larger in the reference [1] than in the proposed scheme. Hence in [1], there will be a larger phase difference between the reference stator flux vector and the stator flux vector.

Complete overmodulation I range is achieved with closed loop control of stator flux vector, unlike, [54], [27], [53] and [55].

3.9 Dynamic control of the stator flux vector

Dynamic in stator flux vector implies (1) step change in the angle of the stator flux vector and (2) step change in its magnitude. Step change in the angle is needed when fast change in torque is required, while the change in magnitude is required during field weakening range of operation when an increase in speed has to be carried out under the voltage limiting conditions. Hence, dynamic operation occurs when a change in torque and/or speed is required.

During dynamics, the maximum rate of change in stator flux vector is limited by the dc-link voltage. In any sampling cycle during dynamic operation, the stator

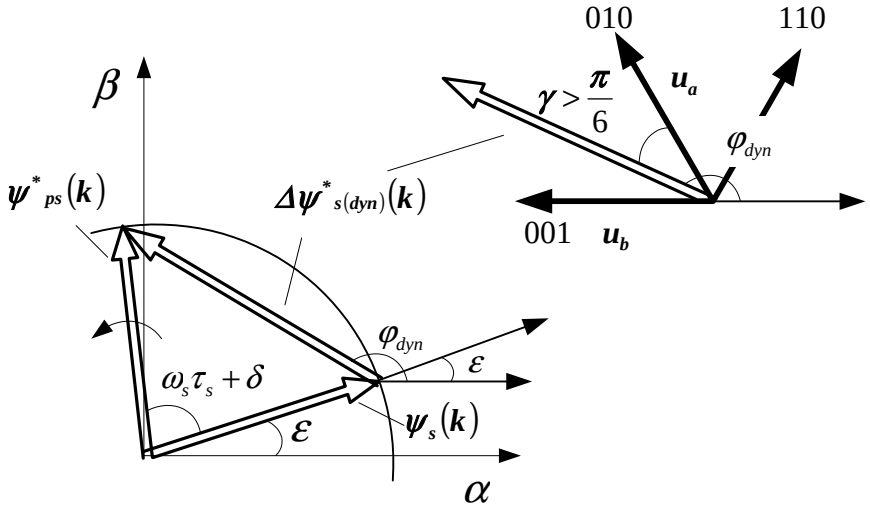

Figure 3.28: Large change in the flux vector signifies dynamic operation

flux error vector shown in figure 3.28 will have a large magnitude and angular displacement. In addition to an angular displacement equal to $\omega_s\tau_s$ (figure 3.3) in steady state, an additional displacement of δ in the dynamic state will be there that signifies the dynamic operation. The flux error vector $\boldsymbol{\Delta\psi}^*_{s(dyn)}$ under such

conditions will be appreciably larger than during steady state. Error vector angle during dynamics will be given by

$$\varphi_{dyn} = \pi/2 + \omega_s \tau_s + \epsilon + \delta \tag{3.41}$$

and will be much larger than that shown in figure 3.6 (b), (c). The flux error vector magnitude will also be large and greater than the maximum possible value of $\frac{\pi}{3}\tau_s$ in one sample. Hence, it is not possible to achieve the required stator flux vector change, $\boldsymbol{\Delta\psi}^*_{s(dyn)}$, in one sampling cycle. In the proposed scheme, during the dynamic condition when $|\boldsymbol{\Delta\psi}^*_{s(dyn)}| > |\boldsymbol{\Delta\psi}_{s(max)}|$, the algorithm selects the maximum possible switching state voltage vector close to the reference stator flux error vector $\boldsymbol{\Delta\psi}^*_{s(dyn)}$. For example in figure 3.28, the voltage vector $\boldsymbol{u}_b$ is the nearest switching state voltage vector to the flux error vector $\boldsymbol{\Delta\psi}^*_{s(dyn)}$. As such, this vector is continuously switched (or held) resulting in the fastest possible compensation of the flux error vector. This results in the fastest possible change in stator flux vector angle with minimum possible reduction in its magnitude. Under such dynamic conditions, the scheme described in [1] still uses switching that is similar to the overmodulation I region, that is, tries to achieve the required voltage vector by switching between two adjacent vectors between a sector. Similarly, [22] does not employ a separate switching mechanism for dynamic control of the stator flux vector angle. These schemes therefore will not provide the best dynamic for a large change in stator flux vector.

To summarize the switching strategy used for the closed loop stator flux vector control, a flow chart is given in the figure 3.29. The block C in figure 3.1

implements figure 3.29. Apart from the steady state control switching, this flow

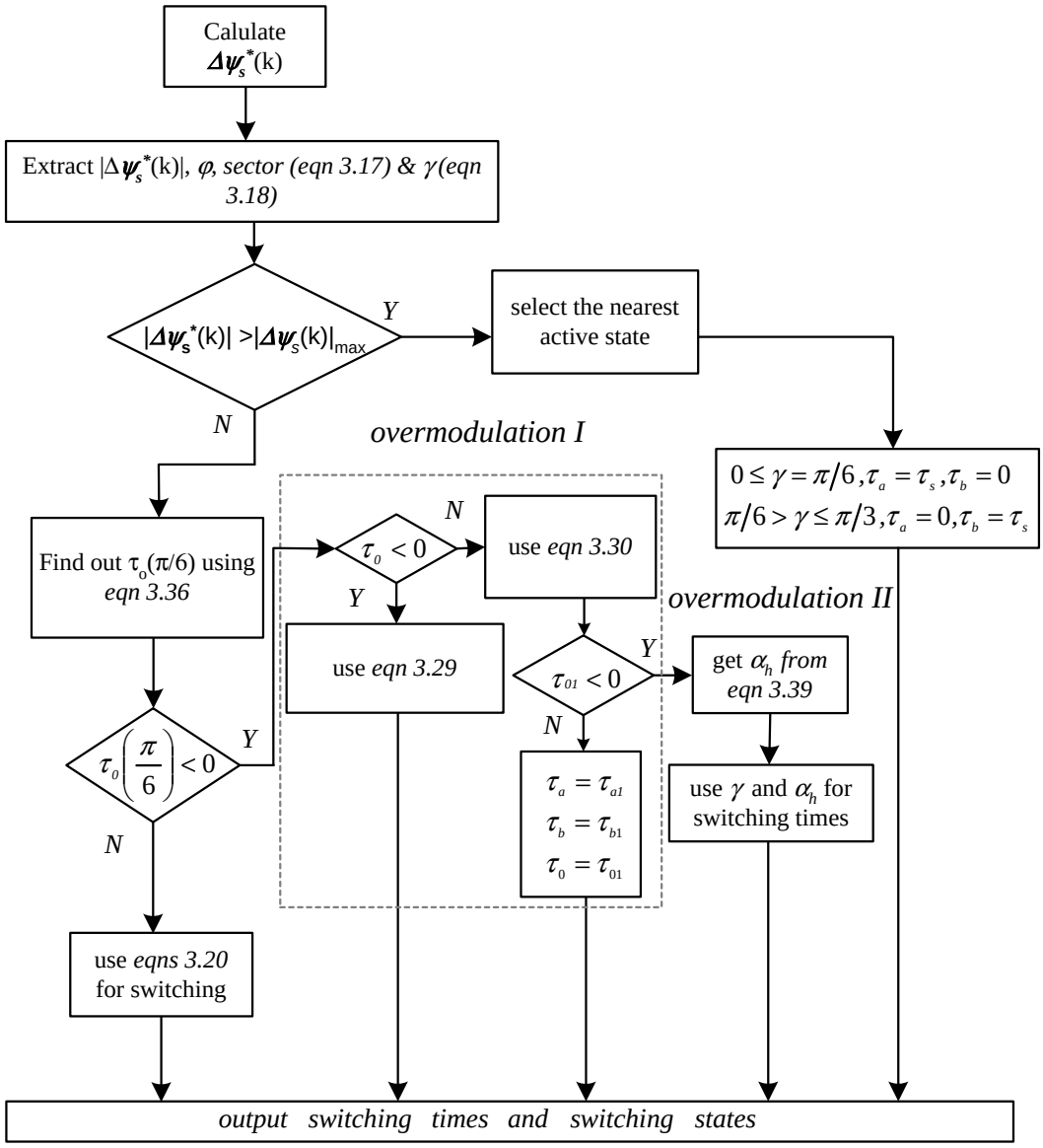

Figure 3.29: Flowchart of the proposed algorithm

chart also defines a large signal algorithm that applies a suitable maximum voltage vector to compensate for the stator flux vector error at the fastest possible rate.

The algorithm first checks the magnitude of the stator flux error vector $\boldsymbol{\Delta\psi}_s^*(k)$. If this magnitude is greater than $|\boldsymbol{\Delta\psi}_s(k)|_{max}$, the maximum that can be

obtained in a sampling interval, it indicates a dynamic condition and the appropriate switching state vector that produces the fastest possible change, is continuously switched. As the angle of $\boldsymbol{\Delta\psi}_s^*(k)$ changes, the maximum voltage vector changes as well. After every sampling time period, the status of the stator flux error vector gets updated. If $|\boldsymbol{\Delta\psi}_s^*(k)| < |\boldsymbol{\Delta\psi}_s(k)|_{max}$, the conditions for overmodulation are tested. Thus for $0.907|\boldsymbol{\Delta\psi}_s(k)|_{max} < |\boldsymbol{\Delta\psi}_s^*(k)| < 0.9535|\boldsymbol{\Delta\psi}_s(k)|_{max}$, the operation is identified to be in overmodulation I region and modified switching times as per equations (3.31), (3.29) and (3.30) are used. However if, $0.9535|\boldsymbol{\Delta\psi}_s(k)|_{max} < |\boldsymbol{\Delta\psi}_s^*(k)| < |\boldsymbol{\Delta\psi}_s(k)|_{max}$, the operation is identified to be in the overmodulation II region and equations (3.38), (3.39) are used for switching. In case none of these conditions is true, the operation is in the normal region and switching state times for the normal region are made use of.

3.10 Experimental results

Implementation of the proposed stator flux vector control scheme was carried out on a dSPACE/DS1102 controller board for rapid prototyping. The board consists of a floating point DSP TMS320C31, a DSP-microcontroller TMS320P14 based digital I/O subsystem, A/D and D/A converters and encoder interfaces. The main DSP processes the numeric intensive algorithms and the DSP microcontroller has the function of PWM generation. A "dead-time" of 2.0 μs is set between the switches of the same leg. The control algorithm of the proposed method is written in the C-programming language. Phase currents and voltages are measured using Hall

affect sensors and analog filters are used to prevent aliasing. Since the sampling rate used for control is 175 - 200μs and the algorithms are relatively simple, it can also be implemented on a fixed-point embedded DSP controller for drives application. As opposed to nonlinear control schemes, no hysteresis comparators are required, nor is the sampling rate very high (approx. 40μS in DTC). A 3 phase inverter of 2 kW, operating at 5kHz was used to drive a 0.75 kW induction motor (motor parameters are given in chapter 6).

3.10.1 Modified low pass filter for stator flux vector estimation

Voltage model, [46] has been used for estimating the stator flux vector as it is more robust against the parametric variations. To prevent integrator saturation in voltage model of stator flux vector estimation, low pass filtering is employed. For the operating angular frequencies greater than the cut off frequency of this filter, accurate results are obtained. However, at frequencies close to the filter cut off, large magnitude and phase error occur. To mitigate this problem, references [48] and [50] use inverse magnitude and phase angle gains to compensate for the error created due to low pass filtering. The poles of this modified low pass filter are made to change with respect to the angular velocity of operation. However, the extent of shifting of poles is decided by trial and error. Figure 3.30 shows the method. Compensation in the magnitude and angle of the stator flux vector is done after low pass filtering. This method is good at discarding high frequency

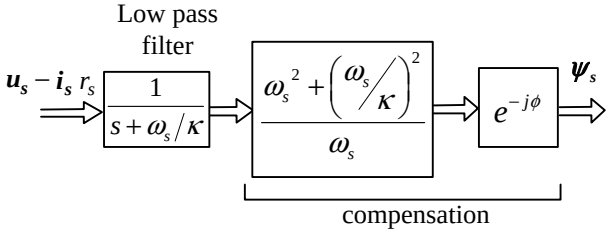

Figure 3.30: Modified voltage model for flux estimation

noise but the dc-offset still appears at the output of the filter, specially at very low operating velocities. Moreover, the closed loop operation at speeds around zero will depend upon the parameter κ which needs to be tuned by trial and error [48]. In [50] a cascaded assembly of a complex compensating gain, a high pass filter and an integrator is employed. This cascade combination effectively is once again a compensated low pass filter. Following equation is used for stator flux estimation,

$$\boldsymbol{\psi_s} = \int \{(1 - j\kappa sign(\omega_s))(\boldsymbol{u_s} - \boldsymbol{r_s i_s}) - \kappa\omega_s \boldsymbol{\psi_s}\} d\tau \tag{3.42}$$

here, ω_s is the synchronous angular velocity and κ is a tuning parameter. The poles of the resulting low pass filter will change corresponding to the operating angular velocity. This model will work well only if the following two conditions are satisfied. (a) amount of dc-offset is same for the sensed currents and (b) analog gains provided by the anti noise/aliasing filters are exactly equal. Implementation of the modified voltage model helps to deal with the problems of noise and drift. However, the estimated stator flux vector still exhibited a dc offset bias at operating frequencies around the zero value (less than 50 RPM).

For good dynamic response, κ should be very small, [50]. However, for smaller values of κ the affect of DC-bias will be more pronounced. In the method proposed

here, the detection and elimination of DC-bias is made independent of κ. Figure 3.31 illustrates the proposed algorithm. Stator flux vector locus has a displaced

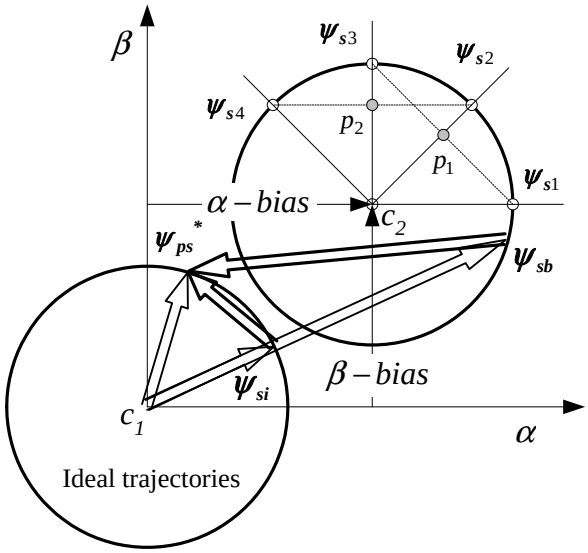

Figure 3.31: Problem due to displaced flux trajectory and detection of DC-bias

center c_2 due to the presence of a small amount of DC-bias. The locus with center c_1 is the ideal trajectory. Under ideal conditions, the stator flux vector error is given as, $\boldsymbol{\psi}^*_{ps} - \boldsymbol{\psi}^*_{si}$ and accordingly the switching states are selected. However, when the center of this circle is displaced to c_2, the error vector will be defined by $\boldsymbol{\psi}^*_{ps} - \boldsymbol{\psi}^*_{sb}$ and therefore will result in erroneous switching, producing distortion in currents (as the current is not controlled) and torque. This will make low speed operation difficult. Hence it is necessary to detect and eliminate this bias without disturbing the actual control. To this end, Slemon et. al have proposed a method in reference [56]. The authors detect the displaced center c_2 by finding out the maximum and minimum values of the α and β components in the flux vector locus. This method however, requires one complete operating cycle for detection of the bias.

3.10.2 Proposed method

$\boldsymbol{\psi}_{s1}$,(x_0, y_0) , $\boldsymbol{\psi}_{s2}$,(x_1, y_1), $\boldsymbol{\psi}_{s3}$,(x_2, y_2) and $\boldsymbol{\psi}_{s4}$,(x_3, y_3) are the stator flux vector estimates at equally separated angular positions of the non-ideal stator flux vector trajectory. Once these points are located on the locus of the stator flux vector, lines joining the points $\boldsymbol{\psi}_{s1}$, $\boldsymbol{\psi}_{s3}$ and $\boldsymbol{\psi}_{s2}$, $\boldsymbol{\psi}_{s4}$ are known. Points p_1 and p_2 divide these lines in two equal parts and the co-ordinates of these points are given as, $(x_2 + x_0)/2, (y_2 + y_0)/2$ and $(x_1 + x_3)/2, (y_1 + y_3)/2$. The lines joining p_1 and (x_1, y_1) and p_2 and (x_2, y_2) intersect each other at a point (x_c, y_c). This point is the displaced center c_2 due to biasing. Hence the bias can be detected within an operating cycle. The easiest way to eliminate the bias is to add the detected center

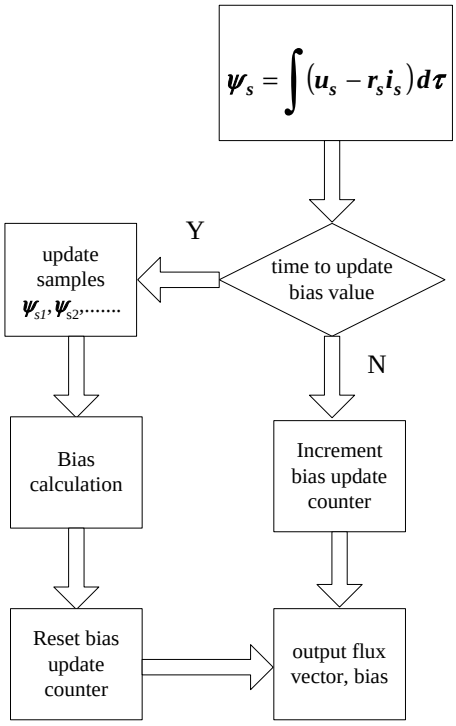

Figure 3.32: Flow Chart for bias correction

with the measured vector with appropriate sign. A flow chart showing the steps

of bias estimation and correction is shown in the figure 3.32. The affect of bias compensation can be seen from the plots of figures 3.33. The correction algorithm is initiated at $t = 0.6$s. The detected center is used for compensating the displaced flux vector trajectory. Figure 3.34 shows the locus of the stator flux vector at a rotor angular velocity of 0.025 Hz. As the operating frequency increases beyond 10% of the rated value the modified voltage model as given in equation (3.42) gives accurate estimate of the stator flux vector.

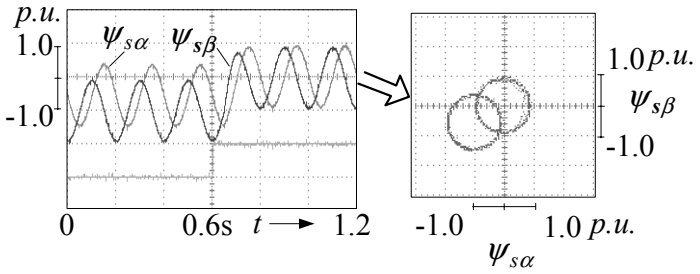

Figure 3.33: Bias correction (experimental result): Stator flux vector locus with a deliberately added bias

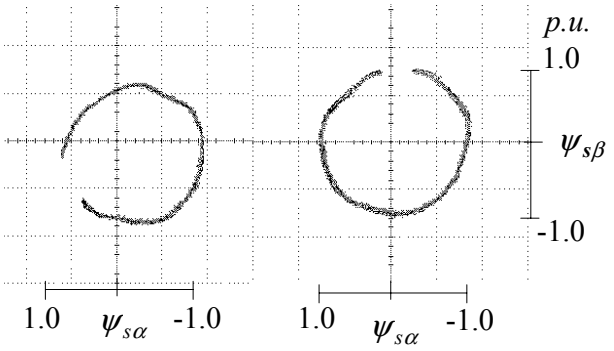

Figure 3.34: Stator flux vector locus at 0.05 Hz, without (left) and with (right) bias correction algorithm (experimental result)

3.10.3 Steady state PWM and control performance

To start the actual experiment, the stator flux vector is gradually build up along the α-axis before applying an angular velocity step. This prevents large magnetizing currents. Steady state operation in the normal region is shown in figure 3.35 for operating conditions $\omega_s = 0.5$ *p.u.* and a sampling period of $T_s = 175\mu$s. Predictive stator flux vector control ensures the elimination of phase delay, achiev-

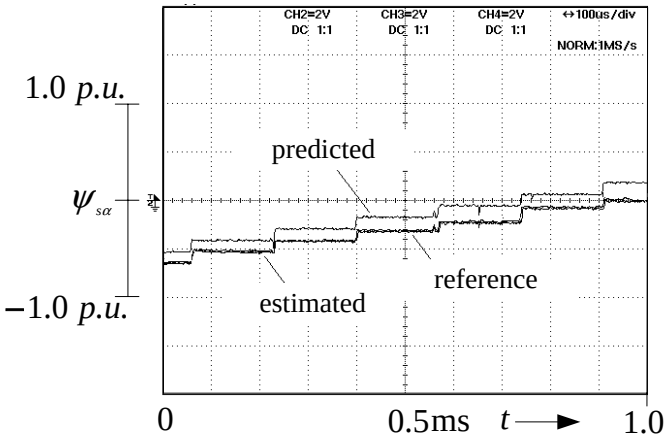

Figure 3.35: Experimental result of predictive stator flux vector control

ing accurate stator flux vector angle and magnitude control. Phase current and voltage waveforms are shown in figure 3.36, at an operating angular velocity of 0.4 *p.u.* These steady state waveforms are similar to those obtained for a conventional SVM method. Hence the SVM using the flux error vector is similar in performance to the conventional SVM using a voltage vector as reference. This has advantages during torque control as it results in a smooth current and low torque ripple. The modulation performance of the proposed algorithm with closed loop stator flux vector control can be seen from figure 3.37 that gives the nature of switching

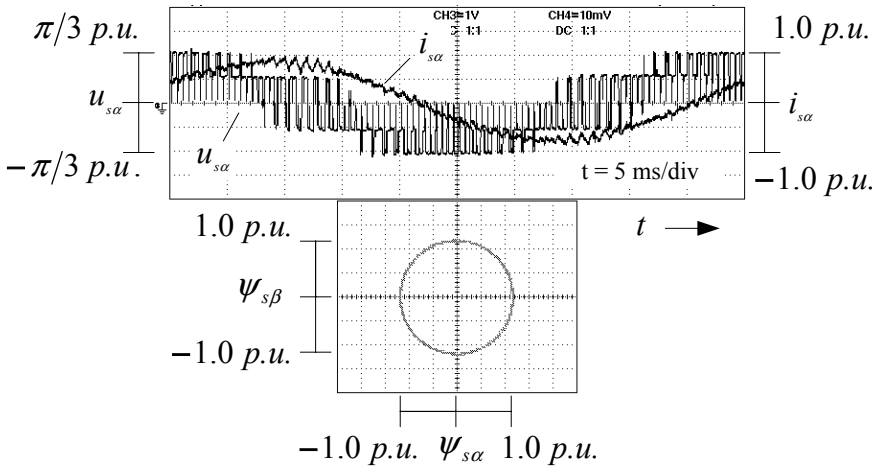

Figure 3.36: Phase voltage, current and the stator flux vector in the normal range of operation

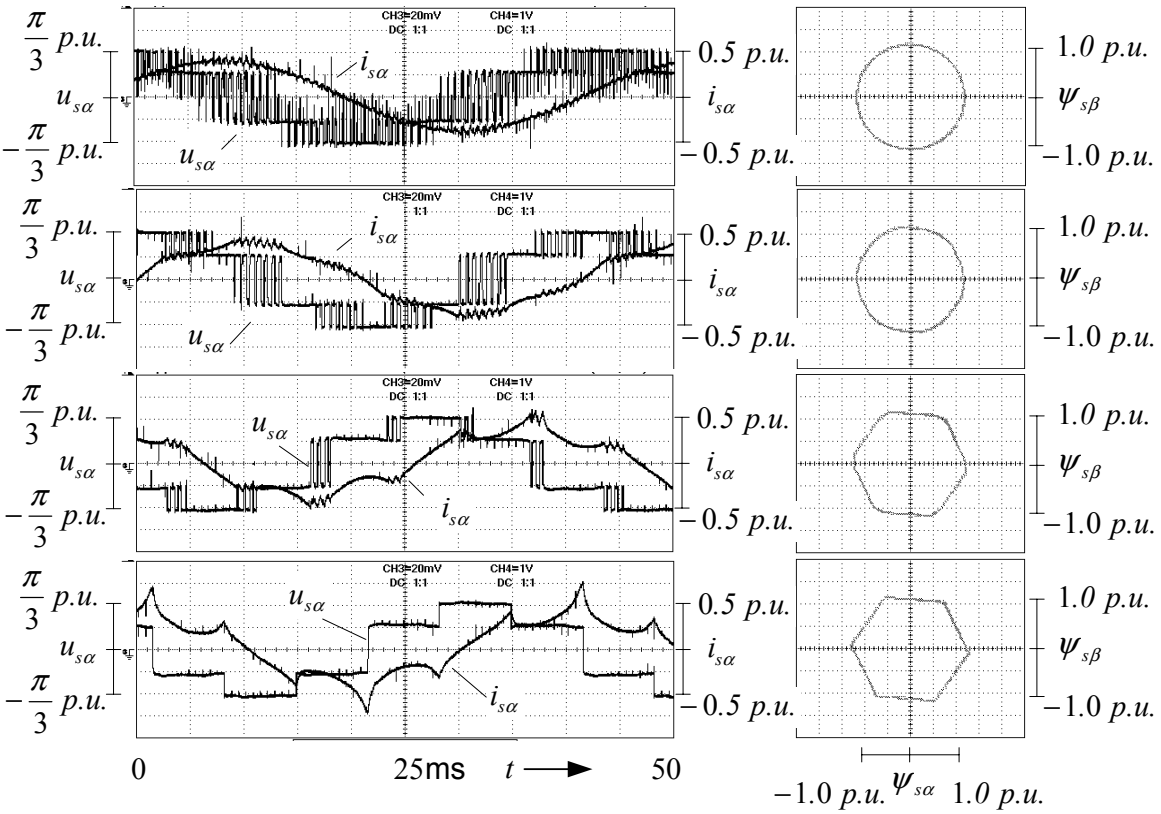

Figure 3.37: Test results showing phase voltage and current waveforms for increasing angular velocity, switching frequency = 1.5 kHz. From top to bottom, the results are for $\omega_s = 0.906$, 0.94, 0.985 and 1.0 *p.u.*

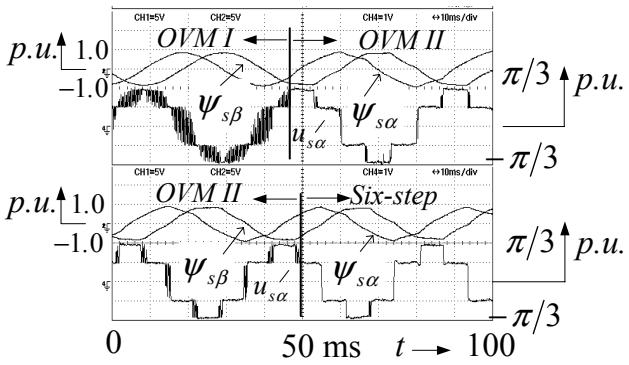

Figure 3.38: Transition of operation from overmodulation I region to to overmodulation II region (figure on top) and from overmodulation II region to six-step operation (bottom figure)

for the entire overmodulation range until six-step during steady state. Continuous closed loop stator flux vector control in the overmodulation region removes all the current control problems of the FOC method.

Figure 3.38 shows smooth transitions between the overmodulation regions and to the six-step operation. Switching and holding regions can be clearly seen in the voltage waveforms. Hence accurate steady state stator flux vector control is achieved without complicated overmodulation algorithms.

3.10.4 Dynamic performance

Dynamic conditions of stator flux vector can be brought about, by a step change in either its magnitude or angle. Both these conditions have distinct significance. More frequent dynamic operation is when the motor has to be accelerated or decelerated at a fast rate and hence requiring large accelerating/decelerating torques. This necessitates fast change in the stator flux vector angle. The response

of the proposed method to such a dynamic change in the stator flux vector angle can be studied from the figure 3.39. A change in the stator flux vector angle has been brought about, by a step change in the commanded angular velocity ω_s of the reference stator flux vector. This figure demonstrates the switching of the best possible state to change the stator flux vector angle at its maximum rate. The decision of the switching state to be selected is taken by the magnitude and angle of the flux error vector. As long as the magnitude of the error vector is greater

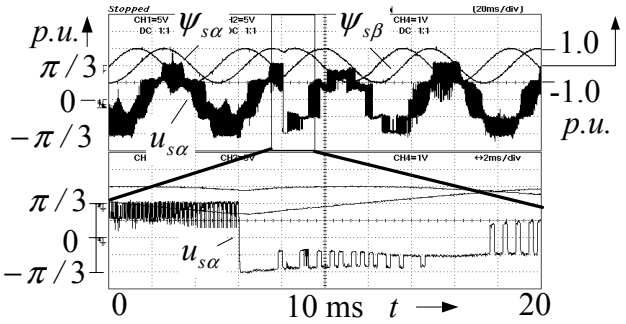

Figure 3.39: Angular velocity reversal showing maximum voltage vector switching during dynamic

than or equal to the maximum value permitted by the inverter voltage limit, single state is switched for the entire sampling period. The status of this state gets updated after every sampling period. In figure 3.40, a step change in the angular velocity command is given from a small value of 0.2 *p.u.* to a large value of 0.9 *p.u.* This change is within the normal range but the transition between two steady state values of operation is through the six-step mode making the transition very quick. It is evident from the result that for the dynamic operation the flux trajectory is along the hexagon which is possible only when the active vectors are switched without any modulation.

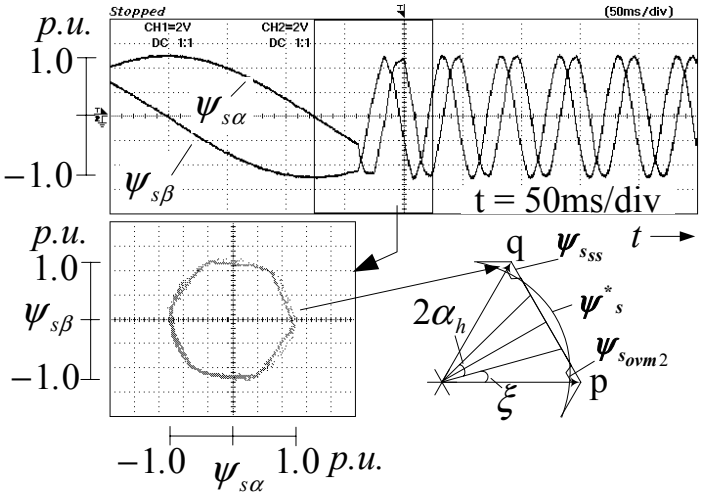

Figure 3.40: An angular velocity step in normal range with closed loop stator flux vector control

The other dynamic condition occurs when a step change of the stator flux vector magnitude is demanded. For a step change of magnitude (reduction of magnitude) the fastest possible response is ensured as a single vector is switched during the transition from one level to the other. This can be observed from figure 3.41. Both results show how the proposed stator flux vector control scheme is

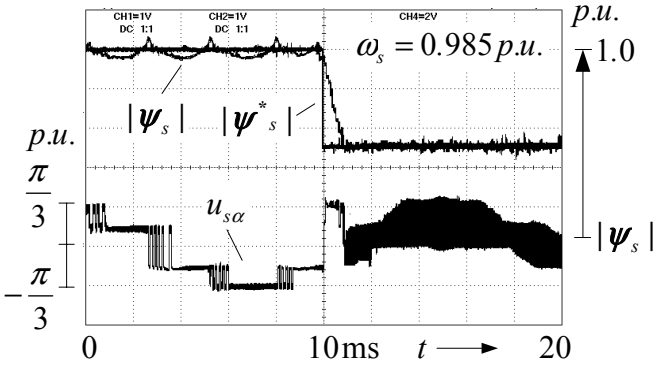

Figure 3.41: Control of flux vector magnitude for a step change of 0.5 *p.u.* during operation in the overmodulation II region

able to achieve the dynamic response that is similar to that of DTC in which the nonlinear controllers apply the single largest voltage vector to achieve the fastest

response.

Closed loop steady state control during the overmodulation region has been a major problem of the current regulated AC drives. Figure 3.42 shows the control of angle of the flux vector during a transition from overmodulation II region to overmodulation I region with closed loop stator flux vector control. This transition is brought about by a step change in the angular velocity ω_s of the reference stator flux vector. Another transition is shown in figure 3.43 from the overmodulation I

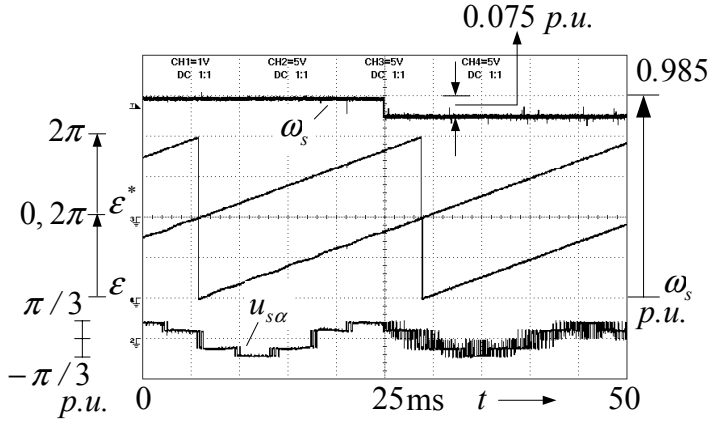

Figure 3.42: Control of stator flux vector angle for a transition from overmodulation II region to overmodulation I region. Here, ϵ^* and ϵ are angles of the reference and the stator flux vectors

region to the six-step mode. The effect of changing the stator flux vector angle on current is seen from this figure. Continuous control of the stator flux vector angle and magnitude, from six-step operation in one direction to the six-step operation in the other direction is depicted in figure 3.44. Steady state and dynamic control of the stator flux vector in the six-step range is shown in figures 3.45 and 3.46. Above base speeds, the magnitude of the reference stator flux vector has been reduced such that it varies as an inverse proportionality with the reference angular velocity

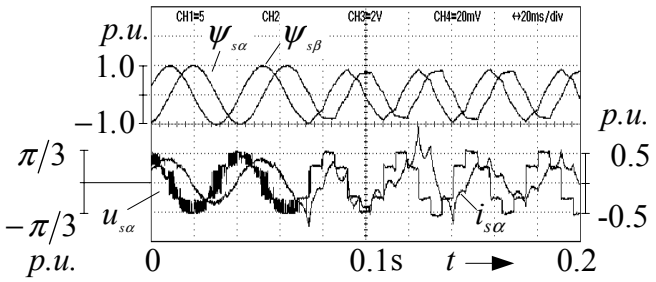

Figure 3.43: Angular velocity step from overmodulation I range, 0.92 $p.u.$ to six-step operation

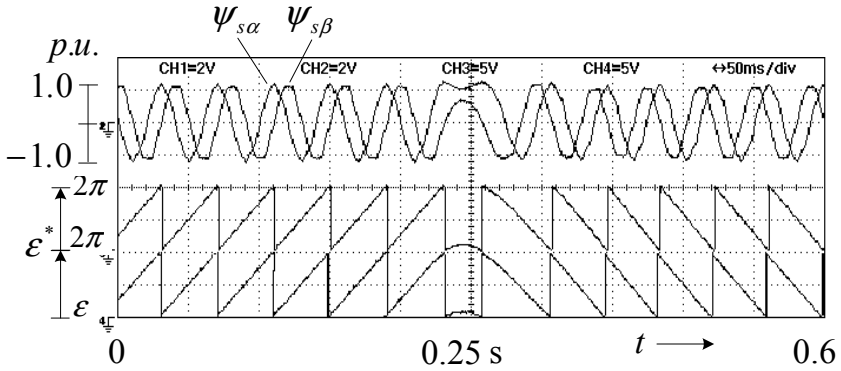

Figure 3.44: Control of stator flux vector with speed reversal from six-step to six-step

ω_s. Fig. 3.45 gives a result showing the stator flux vector dynamic during six-step

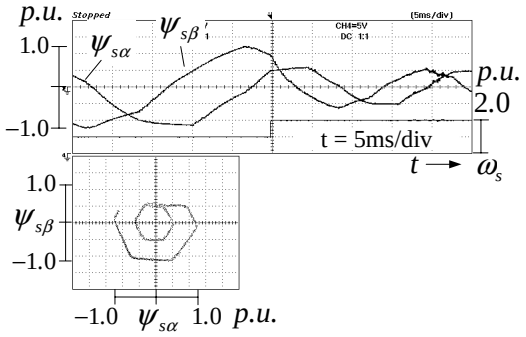

Figure 3.45: Trajectory of the stator flux vector for a step change in the angular velocity ω_s with six-step operation

operation. Control of the angle is achieved both during steady state and during the dynamic in the field-weakening region.

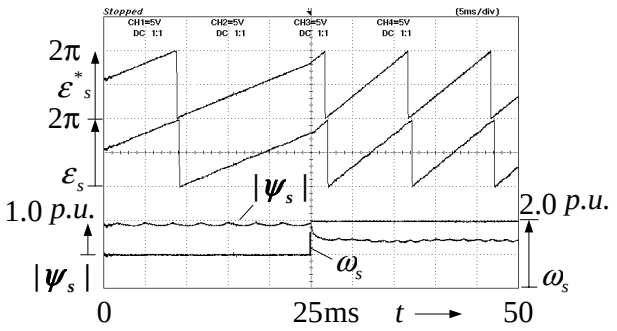

Figure 3.46: Result showing the control of the stator flux vector angle (ε_s) during steady state and dynamic conditions in the six-step region

3.10.5 A simple speed control drive with slip speed compensation

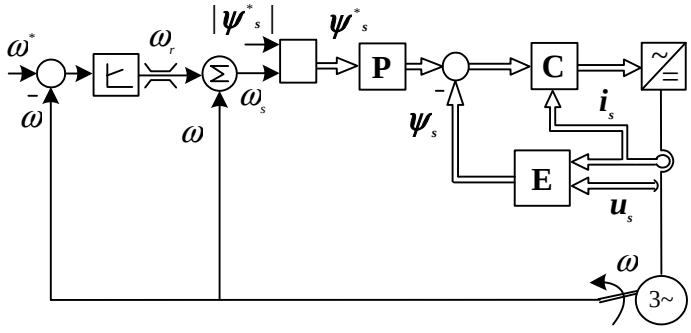

Figure 3.47: Speed control based upon predictive dead-beat stator flux vector control

Scheme of figure 3.47 uses the predictive flux vector control described in this chapter, to implement a simple method of speed control without precise control of torque. The speed controller produces the rotor angular frequency ω_r which is limited to the maximum value to prevent pull out. Such a drive can be employed as a substitute to all those applications in which a conventional v/f drive is used. A distinct advantage of this scheme over the conventional v/f drives, is the range of operation of the drive with the best possible utilization of the inverter DC-link voltage dynamic response that can be achieved using such a control method.

This is due to the ability of the switching strategy to appropriately select the maximum voltage vector during transients of the magnitude and angular velocity of the reference stator flux vector. Another advantage is its inherent current control feature in spite of the fact that there is no deliberate control of current. This feature will be elaborated in chapter 4.

The reference stator flux vector, is defined by the outer speed control loop. Output of the speed controller is the rotor angular frequency ω_r which when added with the rotor speed, defines ω_s. Figure 3.48 shows the control of rotor angular

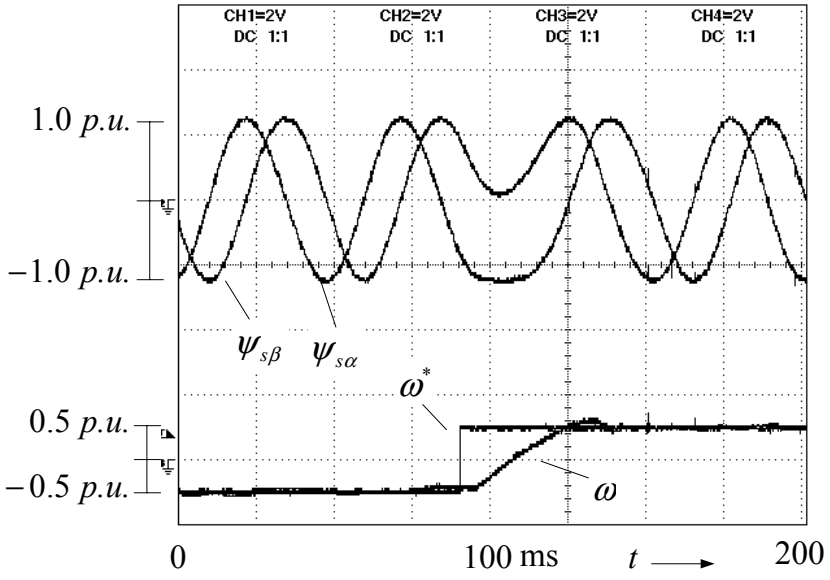

Figure 3.48: Speed reversal using the control scheme of figure 3.47

velocity from one direction to the other with the scheme proposed in figure 3.47. The current control feature can be observed from figure 3.49 that shows the phase current and voltage waveforms for a step change in the speed command from 0.25 *p.u.* to 1.0 *p.u.*

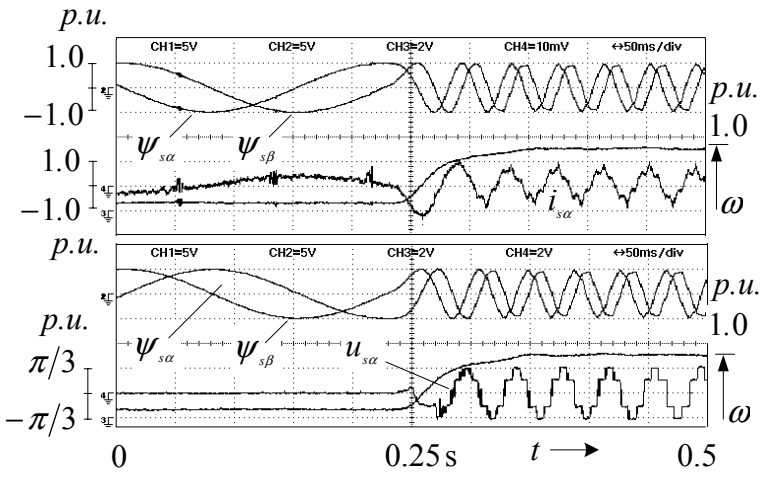

Figure 3.49: Phase current and voltage for a step change in speed command

3.11 Effect of change in stator resistance

Stator resistance influences the stator flux vector estimation and can cause unstable operation at low angular frequencies [57]. However at higher frequencies, as no coordinate transforms are used, the proposed method is relatively more robust than an FOC scheme. To test the robustness of the flux vector estimation, low speed operation with a full load torque was carried out. The control is not affected by

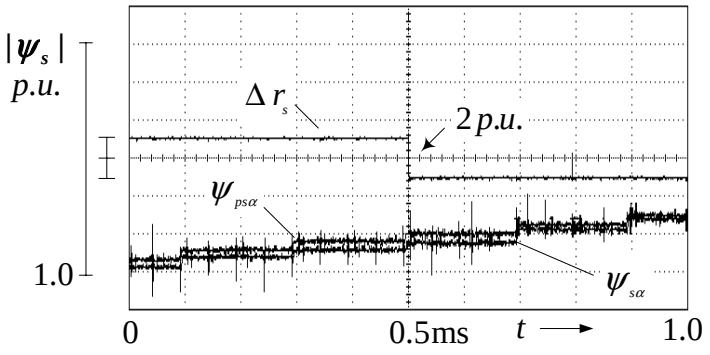

Figure 3.50: Step change in resistance at low speeds

the change in stator resistance caused due to rise in temperature of the windings.

A stable control of stator flux vector was observed at very low frequencies of 0.05 Hz and at full load for a step reduction in model resistance of 2 *p.u.*, figure 3.50.

3.12 Summary

This chapter has presented a closed loop stator flux vector control method that can be used for direct control of torque. In the proposed scheme, a simple method of prediction achieves control of the stator flux vector angle and magnitude during normal range. Since the switching states of the inverter are decided by closed loop control of stator flux vector, the proposed method falls under the category of feedback PWM. In the overmodulation range, the proposed compensation technique achieves control of the stator flux vector despite of the voltage vector limit. In so doing, it solves the current control problem in overmodulation and six-step range. The control of average angular velocity results in smaller phase angle error between the stator flux vector and the reference stator flux vector than the other schemes of overmodulation. While achieving constant switching frequency operation in steady state, it is able to achieve fast dynamic change in stator flux vector during the flux vector angle and magnitude transients. Since it is based on space vector modulation and simple control algorithms, this control scheme can be easily implemented on available embedded DSP controllers for drive applications. The usefulness of predictive stator flux vector control in direct control of torque is explored in the next chapter.

Chapter 4

Direct Torque Control at constant switching frequency

4.1 Introduction

In a DTC scheme, torque control is achieved by controlling the magnitude and phase angle of the stator flux vector. Proposed constant switching frequency DTC is described in this chapter. The method exploits closed loop stator flux vector control developed in the previous chapter to achieve torque control. Following features pertaining to the steady state and dynamic control of torque are discussed here,

- Principle of the proposed torque control method is introduced. Steady state and dynamic control of torque is described for all operating angular velocities. The affect of voltage limit on steady state control of torque using the proposed DTC-SVM scheme is studied. It is shown that the inability of a control

scheme to exploit the installed DC link voltage reduces the average torque. A solution is described to mitigate this problem. A large signal algorithm is proposed for operation during a torque dynamic. Based on this, a switching strategy is formulated. Dynamic response obtained is compared with other DTC schemes.

- Analysis of the steady state torque quality of a constant switching frequency DTC scheme is carried out for the complete operating range. Causes of torque ripple and torque pulsations are investigated.

- In FOC method, the stator flux vector is indirectly controlled by controlling the stator current vector. One advantage of this approach is that it keeps the currents within the drive specifications while controlling the torque. In a DTC scheme, deliberate control of the current vector is not done. Therefore it becomes important to study the current vector dynamics specially when torque and stator flux vector dynamics are taking place. An analytical proof of inherent current control is given that establishes the redundancy of current controllers.

- Qualitative evaluation of the steady state and dynamic response is carried out by comparing the performance of the proposed method with some of the other DTC methods.

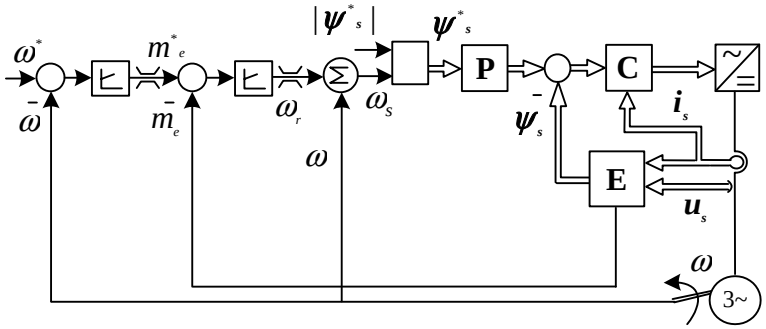

Figure 4.1: Block diagram of the control scheme

4.2 Control Scheme

The innermost stator flux vector control loop of the control scheme shown in figure 4.1 has been discussed in detail in the previous chapter. There, the angular velocity ω_s of the reference stator flux vector was an independent variable. However when the stator flux vector control loop is embedded in the torque control structure, ω_s will be decided on the basis of the torque control requirement. The torque controller produces a slip angular frequency ω_r depending upon the error Δm_e between the commanded torque m_e^* and the estimated value m_e. The reference torque and the slip angular frequency are limited to their respective pull out magnitudes. The synchronous angular velocity ω_s of the reference stator flux vector $\boldsymbol{\psi}_s^*$ is obtained by summing up the rotor angular velocity ω and the slip angular frequency ω_r. This defines the position of the reference stator flux vector $\boldsymbol{\psi}_s^*$. Using the error between the reference stator flux vector and the stator flux vector, the switching states required for torque and stator flux vector control are obtained.

4.3 Torque control: Principle of operation

Electromagnetic torque in a sinusoidally excited machine is given as [52],

$$m_e = -\frac{k_r}{\sigma l_s}\boldsymbol{\psi}_s \times \boldsymbol{\psi}_r \tag{4.1}$$

The trajectories of $\boldsymbol{\psi}_s$ and $\boldsymbol{\psi}_r$ are circular and they rotate at a uniform angular velocity of ω_s, producing a smooth torque. However in inverter fed machines, switching of zero and active states results in a change of the instantaneous value of torque. This change in instantaneous torque will be referred to, as torque ripple. Assuming that the switching has negligible affect on the rotor flux vector, a zero switching state will decelerate the stator flux vector (due to the drop in the stator resistance) causing a reduction in instantaneous torque while an active switching state will accelerate the stator flux vector causing an increase in instantaneous torque. Steady state torque quality depends upon the torque ripple $m_{e(rip)}$ which can be expressed as,

$$m_{e(rip)} = \frac{m_{e(max)} - m_{e(min)}}{m_{e(R)}} \tag{4.2}$$

here, $m_{e(max)}$ and $m_{e(min)}$ are the minimum and maximum steady state values of

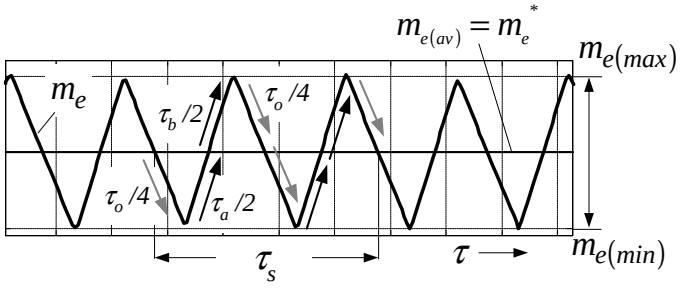

Figure 4.2: Torque ripple

torque as shown in figure 4.2 and $m_{e(R)}$ is the rated torque of machine. Figure 4.2 shows the variation in instantaneous torque, when the conventional SVM switching sequence is employed. Grey arrows indicate the affect of the zero vector switching while the black arrows indicate that an active voltage vector has been switched. The conventional SVM with split zero vector switching produces a torque ripple which is similar to DTC/DSC. Magnitude of torque ripple depends upon the switching frequency $f_{sw} = \frac{1}{\tau_s}$ and also upon the operating angular velocity ω_s. It can be observed from figure 4.2 that for lower switching frequencies, torque ripple produced will be larger. However, the affect of operating angular velocity on torque ripple is not so apparent and hence requires detailed investigation.

Figure 4.2 also indicates that, to achieve control, the average value $m_{e(av)}$ of torque should be equal to the reference torque m_e^*. Hence in steady state, in every sampling period, the condition, $\Delta m_{e(av)}(k) = 0$ should hold. Here, $\Delta m_{e(av)}(k)$ is the change in average torque at the k^{th} sampling instant. If this condition is not satisfied, there will be an error in average value of torque. To achieve zero average torque error, it is necessary to ensure that the acceleration and deceleration of the stator flux vector $\boldsymbol{\psi}_s$ in every sampling period is equal. To this end, it is essential to maintain the average angular velocities of the stator flux vector and rotor flux vector constant and equal to the reference value. This is achieved using predictive control of the stator flux vector as described in the previous chapter. In so doing, the equality $\boldsymbol{\psi}_s(k) = \boldsymbol{\psi}_s^*(k)$ is ensured. Here $\boldsymbol{\psi}_s^*(k)$ is the reference stator flux vector at the k^{th} sampling instant. In figure 4.3 at the k^{th} sample,

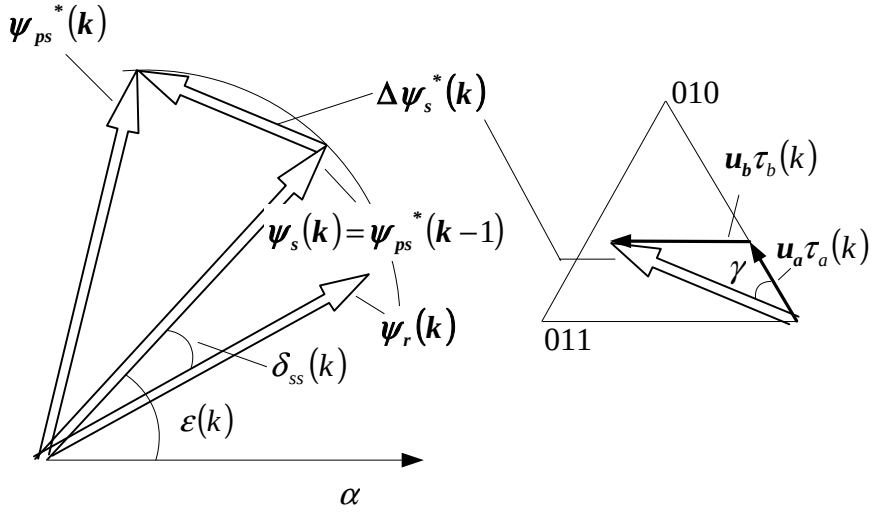

Figure 4.3: Principle of torque control using the proposed method

$\boldsymbol{\psi}_s(k) = \boldsymbol{\psi}_{ps}^*(k-1)$. However, the predicted reference $\boldsymbol{\psi}_{ps}^*(k)$ will be at a new location producing a reference stator flux error vector, $\boldsymbol{\Delta\psi}_s^*(k)$. In order to achieve this vector displacement of stator flux vector, the switching states of the inverter are controlled such that,

$$\boldsymbol{\Delta\psi}_s^*(k) = \boldsymbol{u}_a\tau_a(k) + \boldsymbol{u}_b\tau_b(k) \tag{4.3}$$

This will move the stator flux vector such that at the beginning of the $(k+1)^{th}$ interval,

$$\boldsymbol{\psi}_s(k+1) = \boldsymbol{\psi}_s^*(k+1) = \boldsymbol{\psi}_{ps}^*(k) \tag{4.4}$$

achieving stator flux vector control without a phase error. Thus the required average angular velocity of the stator flux vector can be obtained. The instantaneous torque will depend upon the trajectory followed by the stator flux vector and is therefore decided by the switching sequence.

4.4 Analysis of steady state torque control for the conventional SVM switching sequence

The switching pattern and times that satisfy equation (4.3) are calculated using space vector modulation and have been derived in Chapter 3. Switching times obtained are,

$$\begin{aligned} \tau_a(k) &= \frac{3}{\pi}\frac{|\boldsymbol{\Delta\psi}_s^*(k)|\sin(\pi/3-\gamma)}{\sin(\pi/3)} \\ \tau_b(k) &= \frac{3}{\pi}\frac{|\boldsymbol{\Delta\psi}_s^*(k)|\sin(\gamma)}{\sin(\pi/3)} \\ \tau_0(k) &= \tau_s - \tau_a(k) - \tau_b(k) \end{aligned} \tag{4.5}$$

During steady state operation, the reference torque is of constant value. However, the switching of active and zero states makes the stator flux vector trajectory look like a polygon and this creates ripples in the developed torque. The difference between the reference and actual torque after a time $\frac{\tau_0}{2}$, will be called torque ripple $m_{e(rip)}(0)$ because of switching of the zero vector. This ripple is generated due to the difference between the stator flux vector $\boldsymbol{\psi}_s$ and the reference stator flux vector $\boldsymbol{\psi}_s^*$ after a time interval $\frac{\tau_0}{2}$. This vector difference will be called flux ripple vector $\boldsymbol{\psi}_{s(rip)}(0)$, to distinguish it from $\boldsymbol{\Delta\psi}_s^*(k)$ which is the stator flux vector displacement required in a sampling period for torque and stator flux vector control. Similarly, for switching of active states, $\boldsymbol{u}_a$ and $\boldsymbol{u}_b$, the corresponding flux ripple vectors $\boldsymbol{\psi}_{s(rip)}(a)$ and $\boldsymbol{\psi}_{s(rip)}(b)$ can be defined.

Flux ripple vectors were used to compare the total harmonic distortion of machine currents due to different PWM switching sequences in the reference [58].

The authors have used a rigorous mathematical approach for analysis. However in the present work, the focus will be to study the quality of torque produced as a result of the conventional SVM switching sequence. This will be carried out by analyzing the interaction of the flux ripple vectors with the rotor flux vector. The problem of analytically obtaining torque ripple, will be broken down in two steps. Firstly, the affect of SVM switching on the stator flux vector $\boldsymbol{\psi}_s$ will be estimated by calculating the respective flux ripple vectors and subsequently, the interaction of these flux ripple vectors with the rotor flux vector $\boldsymbol{\psi}_r$, will be observed. This will define the torque ripple produced due to switching.

4.4.1 Step 1: Flux ripple vectors

Due to SVM, the stator flux vector trajectory is polygonal as shown in the simulated result of figure 4.4. In discrete time, the position of the reference stator flux vector $\boldsymbol{\psi}_s^*$ at two consecutive sampling instants is given by the points p and v. In between the sampling instants, switching of zero and active states causes the stator flux vector, $\boldsymbol{\psi}_s$ to move along p-q-r-s-v. Assuming that the stator resistance voltage drop is negligibly small (the affect of this drop will be analyzed in a later section), when the zero state is switched for time $\frac{\tau_0}{2}$, the stator flux vector $\boldsymbol{\psi}_s$ stays at point p. During this time interval, the reference stator flux vector $\boldsymbol{\psi}_s^*$ moves along the circle reaching $\boldsymbol{\psi}_s^*(\tau_1)$ at the end of $\frac{\tau_0}{2}$ (shown as a cross). This defines the flux ripple vector $\boldsymbol{\psi}_{srip}(0_1)$, see figure 4.5. In figure 4.4, when the voltage vector $\boldsymbol{u}_a$ is applied for time τ_a the vector $\boldsymbol{\psi}_s$ moves along $p-q$ and reaches q at the end

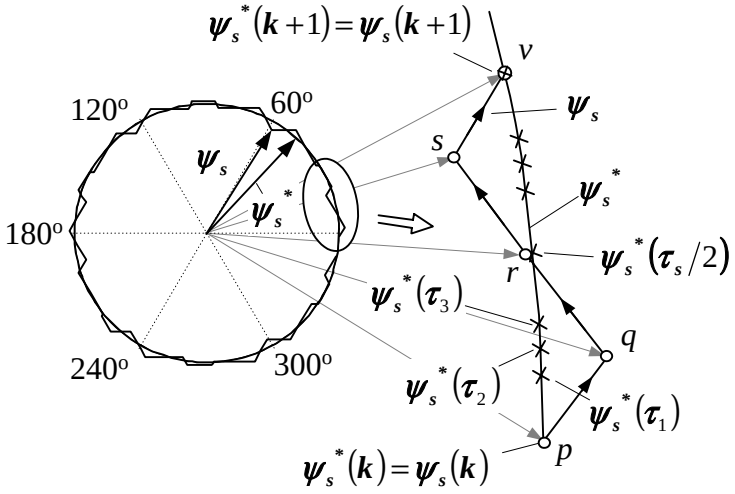

Figure 4.4: Reference stator flux vector ψ_s^* and the stator flux vector ψ_s. Deviation in the two vectors results in torque ripple

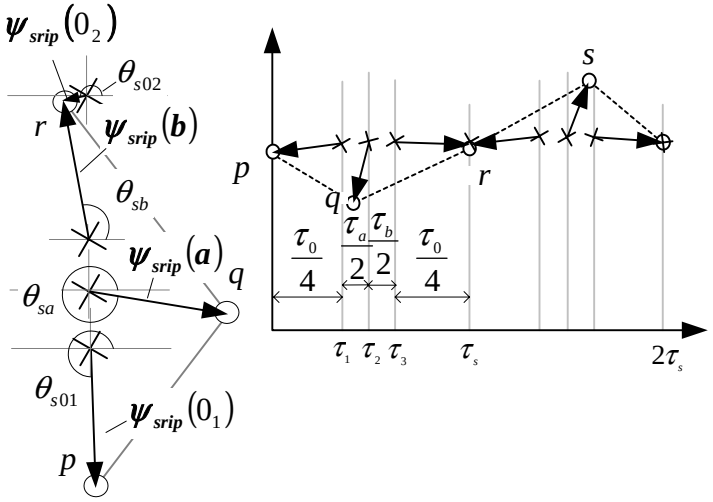

Figure 4.5: Ripple vectors in a sub-cycle(left) and in time domain (right)

of the switching instant. The reference stator flux vector attains a value $\psi_s^*(\tau_2)$ creating the ripple vector $\psi_{srip}(a)$, (figures 4.4, 4.5).

The sub-cycle ends with the zero switching state, defining $\psi_{srip}(0_2)$ which is the difference of the reference stator flux vector ψ_s^* and the stator flux vector ψ_s after the sub-cycle time interval $\tau_s/2$. For every switching instant in a sub-cycle

$\tau_s/2$, the ripple vectors are given as (see figures 4.4 and 4.5),

$$\boldsymbol{\psi}_{s(rip)}(0_1) = |\boldsymbol{\psi}_s^*|\angle\omega_s\tau_1 - |\boldsymbol{\psi}_s|\angle 0^\circ = |\boldsymbol{\psi}_{s(rip)}(0_1)|\varepsilon^{j\theta_{s0_1}} \tag{4.6}$$

$$\boldsymbol{\psi}_{s(rip)}(a) = |\boldsymbol{\psi}_s^*|\angle\omega_s\tau_2 - (|\boldsymbol{\psi}_s|\angle 0^\circ + \boldsymbol{u}_a\tau_a/2) = |\boldsymbol{\psi}_{s(rip)}(a)|\varepsilon^{j\theta_{sa}} \tag{4.7}$$

$$\boldsymbol{\psi}_{s(rip)}(b) = |\boldsymbol{\psi}_s^*|\angle\omega_s\tau_3 - (|\boldsymbol{\psi}_s|\angle 0^\circ + \boldsymbol{u}_a\tau_a/2 + \boldsymbol{u}_b\tau_b/2) = |\boldsymbol{\psi}_{s(rip)}(b)|\varepsilon^{j\theta_{sb}} \tag{4.8}$$

$$\begin{aligned}\boldsymbol{\psi}_{s(rip)}(0_2) = |\boldsymbol{\psi}_s^*|\angle\omega_s\tau_s/2 - (|\boldsymbol{\psi}_s|\angle 0^\circ + \boldsymbol{u}_a\tau_a/2 + \boldsymbol{u}_b\tau_b/2 + \boldsymbol{u}_0\frac{\tau_0}{4}) \\ = |\boldsymbol{\psi}_{s(rip)}(0_2)|\varepsilon^{j\theta_{s0_2}}\end{aligned} \tag{4.9}$$

The next step is to see the interaction of the flux ripple vectors with the rotor flux vector and hence to obtain torque ripple.

4.4.2 Step 2: Torque ripple

The instantaneous torque equation can be expressed in terms of torque ripple and flux ripple vector as,

$$m_e + m_{e(rip)} = -\frac{k_r}{\sigma l_s}(\boldsymbol{\psi}_s + \boldsymbol{\psi}_{s(rip)}) \times \boldsymbol{\psi}_r \tag{4.10}$$

This gives,

$$m_{e(rip)} = -\frac{k_r}{\sigma l_s}\boldsymbol{\psi}_{s(rip)} \times \boldsymbol{\psi}_r \tag{4.11}$$

and therefore the magnitude of torque ripple is,

$$|m_{e(rip)}| = \frac{k_r}{\sigma l_s}|\boldsymbol{\psi}_r|(|\boldsymbol{\psi}_{s(rip)}|\sin(\vartheta + \delta)) \tag{4.12}$$

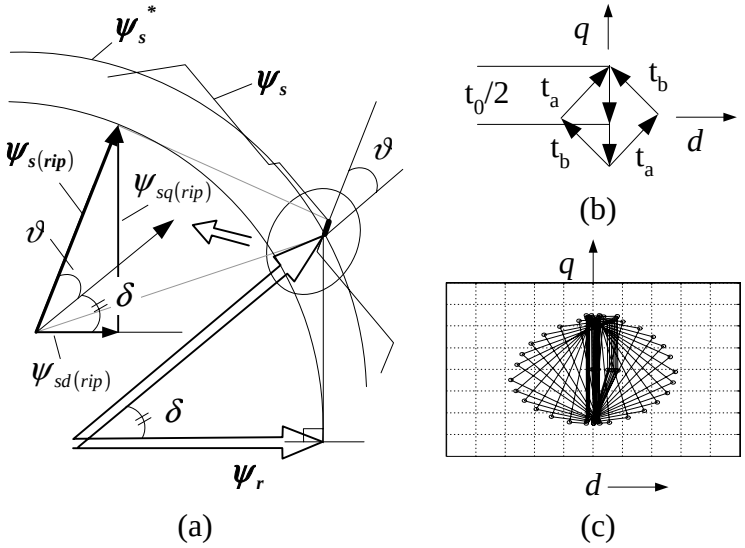

Figure 4.6: (a) Instantaneous flux ripple vector due to switching. (b) Effect of SVM switching on the flux ripple vector for one switching cycle (c) Ripple vector $\boldsymbol{\psi}_{s(rip)}$ variation in a sector

where the angle δ is torque angle and ϑ is the angle of the flux ripple vector, $\boldsymbol{\psi}_{s(rip)}$ with respect to the reference stator flux vector $\boldsymbol{\psi}_s^*$, as shown in the figure 4.6 (a). This figure shows the circular trajectories of the reference stator flux vector $\boldsymbol{\psi}_s^*$ and the rotor flux vector $\boldsymbol{\psi}_r$ and the switched trajectory of the stator flux vector $\boldsymbol{\psi}_s$. The flux ripple vector and its d and q axis components can be seen in the zoomed portion of the figure. Here, the component $\psi_{sq(rip)}$ that is perpendicular to the rotor flux vector, produces ripple in torque. The d-q system of co-ordinates is used only for the sake of analysis and explanation and is not used in the actual control. The focus will be on the q-component $\psi_{sq(rip)}$, to study torque ripple.

The ripple in torque will be estimated for one complete switching cycle. For ease of understanding, the torque ripple at no load will be considered. This gives, $\delta = 0$ and hence $\boldsymbol{\psi}_s^*$ and $\boldsymbol{\psi}_r$ are aligned to the d-axis. The affect of switching zero and active states for one switching cycle can be seen from figure 4.6 (b). Two

important conclusions can be drawn from this figure. (1) Switching of zero state contributes only to the q-component of the flux ripple vector, while switching of an active state contributes to both d- and q-components. (2) The total magnitude of the q-component of the flux ripple produced by the switching of active states, is exactly equal to that produced by the switching of zero states. Result of figure 4.6(c) shows that the q-component of the flux ripple vector is fairly constant for all the samples taken in a sector.

Hence the total deceleration in $\boldsymbol{\psi}_s$ produced by the switching of zero states, is compensated by the resultant acceleration produced by the switching of active states. This means that the average angular velocity of the stator flux vector $\boldsymbol{\psi}_s$ in a sampling period, is equal to that of $\boldsymbol{\psi}_r$ and the reference stator flux vector $\boldsymbol{\psi}_s^*$, thus maintaining a constant average torque angle δ and hence the average torque. This proves that the average torque error $\Delta m_{e(av)}(k)$ is equal to zero and torque control without torque pulsation can be achieved.

4.4.3 Effect of operating angular velocity on torque ripple: Normal range operation

In normal region, switching of a zero vector reduces torque while switching of active vectors increases it. Using conventional SVM switching, the decrease in torque in a sampling period, is compensated by the total increase due to switching of active vectors, figure 4.7 (a). Hence, to analyze the ripple in torque, it is sufficient to focus on the affect of switching a zero vector. When the switching frequency

is constant, two variables affect the switching times of these vectors. (1) The operating angular velocity and (2) Position γ of the error vector $\boldsymbol{\Delta\psi}_s^*$ in a sector. The switching state time τ_0 can be written using equation (4.5) as,

$$\tau_0(k) = \tau_s(1 - \frac{|\boldsymbol{\psi}_s^*(k)|\omega_s \sin(\frac{\pi}{3} + \gamma)}{\frac{\pi}{3}\sin\frac{\pi}{3}}) \tag{4.13}$$

or for 1.0 *p.u.* magnitude of the reference stator flux vector,

$$\tau_0(k) = \tau_s(1 - \frac{\omega_s \sin(\frac{\pi}{3} + \gamma)}{\frac{\pi}{3}\sin\frac{\pi}{3}}) \tag{4.14}$$

While the stator flux vector stops for this time in a sampling period, the angle

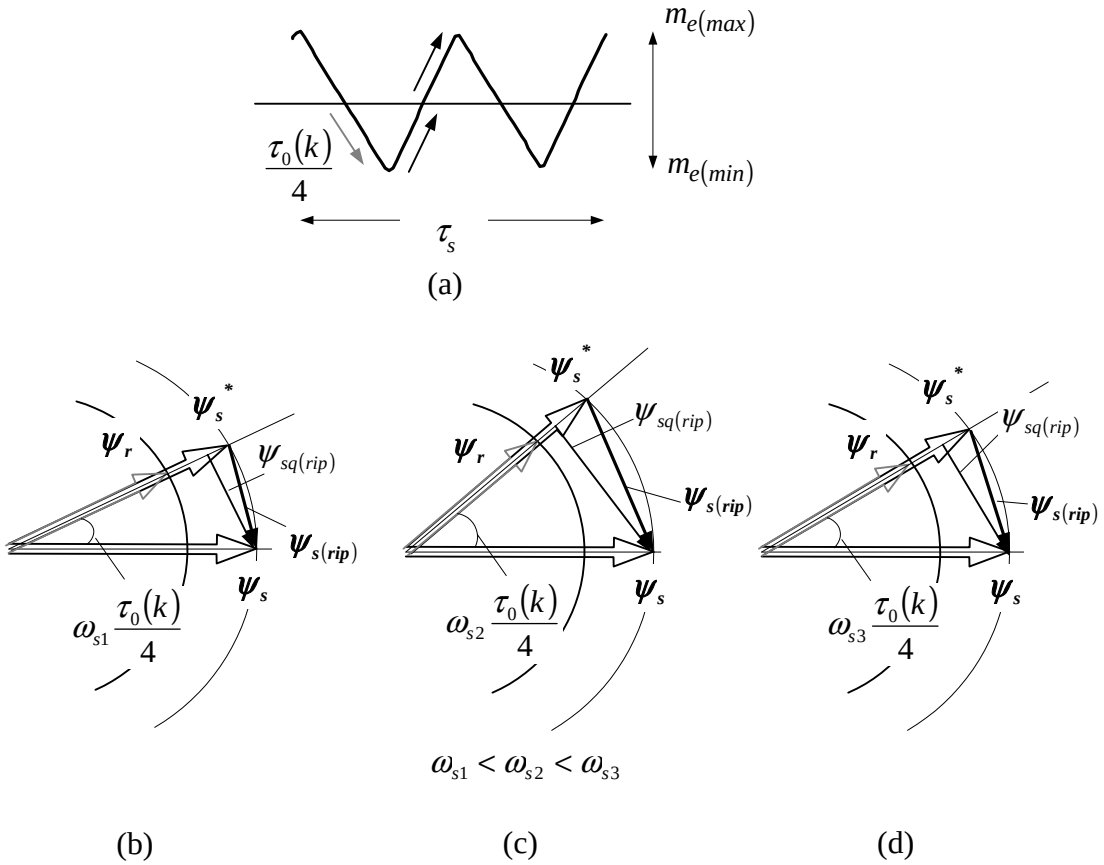

Figure 4.7: Understanding torque ripple variation with respect to the angular velocity, using flux ripple vectors

covered by the reference stator flux vector and the rotor flux vectors, figure 4.7 (a),

(b), (c) is given as,

$$\omega_s \frac{\tau_0(k)}{4} = \omega_s \frac{\tau_s}{4}(1 - \frac{\omega_s \sin(\frac{\pi}{3} + \gamma)}{\frac{\pi}{3} \sin \frac{\pi}{3}}) \tag{4.15}$$

It can be observed from the figure 4.7 that the angle $\omega_s \frac{\tau_0(k)}{4}$ has a direct influence on the q-component $\psi_{sq(rip)}$ of the flux ripple vector, which is proportional to torque ripple, equation (4.12). For a constant value of τ_s and taking $\gamma = 0$, the angle

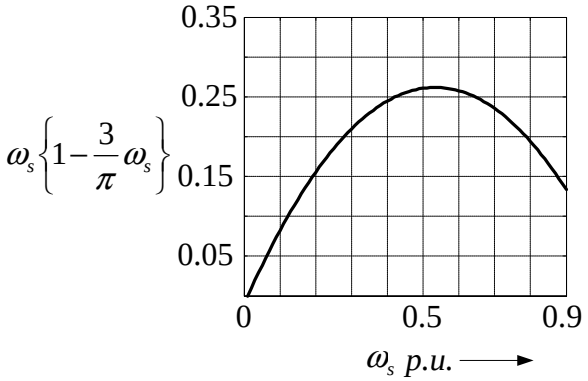

Figure 4.8: Variation of the angle $\omega_s \frac{\tau_0(k)}{4}$ with respect to ω_s: $\omega_s \frac{\tau_0(k)}{4}$ is proportional to torque ripple

$\omega_s \frac{\tau_0(k)}{4}$ will be determined by the term $\omega_s\{1 - \frac{3}{\pi}\omega_s\}$, equation (4.15). Variation of this term with the angular velocity is shown in figure 4.8. When the angular velocity ω_s is small, $\tau_0(k)$ is large (equation 4.14) but the angle $\omega_{s1} \frac{\tau_0(k)}{4}$ is small, figure 4.7 (a). This results in a small value of $\psi_{sq(rip)}$ and hence lower torque ripple. Factor $\omega_s \frac{\tau_s}{4}$ on the right hand side (RHS) in equation (4.15) is predominant until around $\omega_s = 0.5$ *p.u.* resulting in an increasing q-component of the ripple vector, figures 4.7 (c) and 4.8. Thereafter, the second factor on the RHS, starts increasing and the ripple reduces again, figures 4.7 (d), 4.8.

The influence of γ can be understood using equation (4.15). Factor $\sin(\frac{\pi}{3} + \gamma)$ in equation (4.15) varies by 13% in a sector (as γ changes from 0 to $\pi/6$) but the

affect of angular velocity ω_s dominates over any change in γ. Hence for small values of angular velocity, the change of $m_{e(min)}$, within a sector is very small and therefore the torque ripple is not effected by it. However for larger angular velocities, the ripple will vary within a sector as well, though this variation is still very small. Thus for example, the maximum and minimum values of $|m_{e(min)}|$ in a sector will differ by about 1% for an angular velocity of 0.5 *p.u.* whereas for an operating angular velocity of 0.9 *p.u.*, these will differ by around 3%.

4.4.4 Effect of stator resistance drop on torque ripple

If stator resistance drop is neglected, the stator flux vector will stop when a zero voltage vector is switched. However in actual practice, when a zero voltage vector is switched, the flux vector moves in a direction which is aligned to the vector $-\boldsymbol{i}_s r_s$. This results in a larger magnitude of $m_{e(min)}$ (figure 4.7) compared to the ideal case of zero resistance.

A simulation study was done to observe the affect of the resistive drop on torque ripple. Loading conditions are considered such that the motor is operating at the pull out slip. Thus at zero rotor angular velocity, the affect of the resistive drop will be maximum and it will gradually reduce with the increase in ω_s as the time τ_0 for switching a zero state reduces. Figure 4.9 gives a comparison of torque ripple variation for two cases. (a) When the stator resistance drop is considered negligible and (b) When it is included for calculation of the ripple. The experimental lab machine (parameters given in chapter 6) is used for this study.

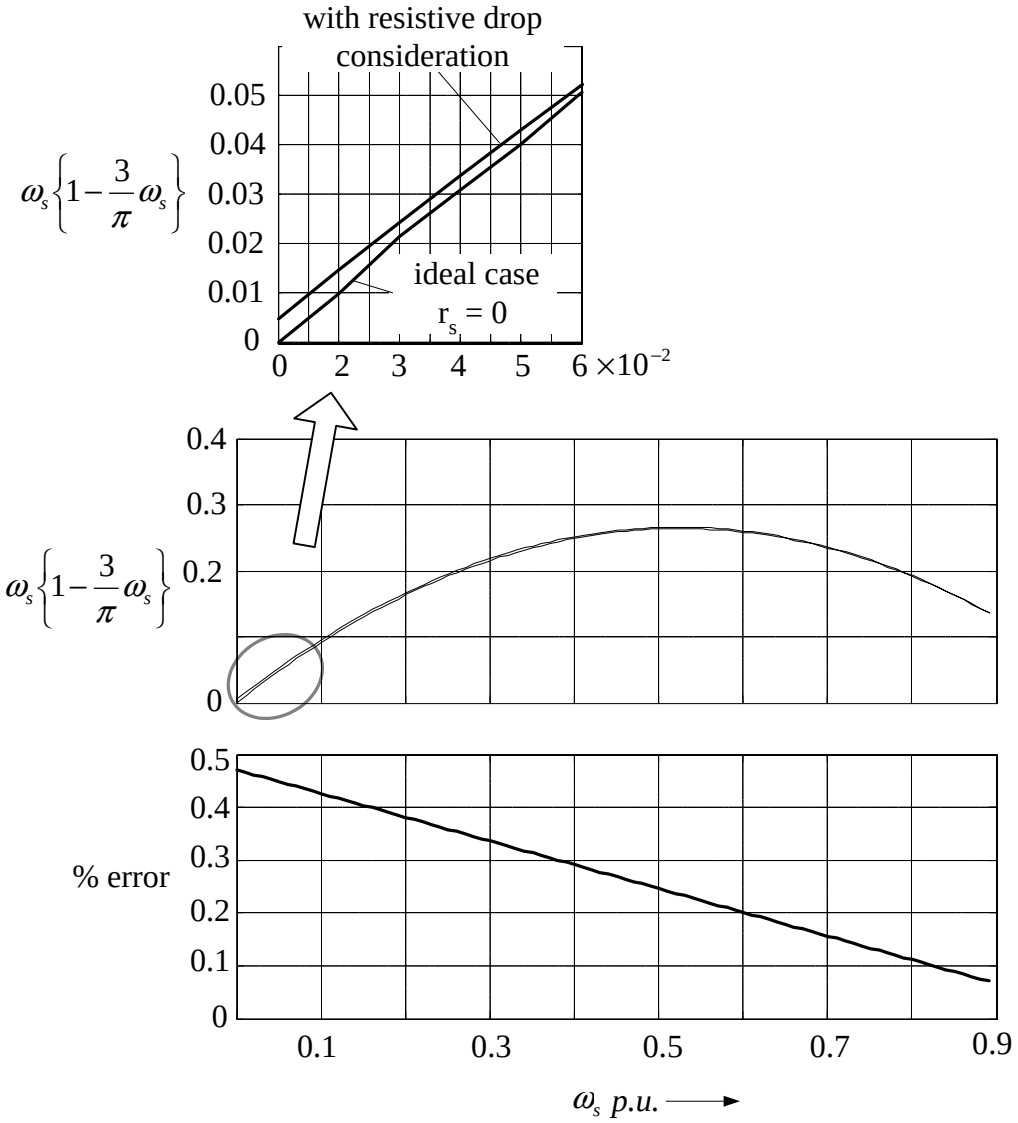

Figure 4.9: Torque ripple with and without consideration of the resistive drop

The results of this figure show a very small difference between the two cases. As the error is very small (the maximum is less than 1%), zero stator resistance can be safely considered, for the purpose of analysis. However, in actual control the resistive drop compensation has been considered.

4.4.5 Analysis of ripple at three different operating angular velocities

Figure 4.10 shows the simulated machine torque for three different steady state values of angular velocities and at a constant switching frequency of 5 kHz. The first steady state is at $\omega_s = 0.1$ *p.u.* and the second and third steady state values are for $\omega_s = 0.5$ *p.u.* and $\omega_s = 0.907$ *p.u.* respectively. The steady state torque at these angular velocities are highlighted by small squares labelled 'a','b' and 'c'. Regions 'a', 'b' and 'c' of figure 4.10 are expanded as figures 4.11 (a), 4.11

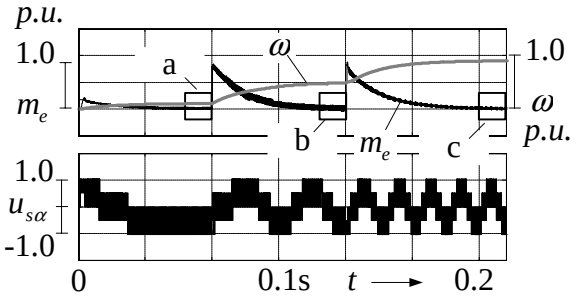

Figure 4.10: Steady state torque control at three different angular velocities

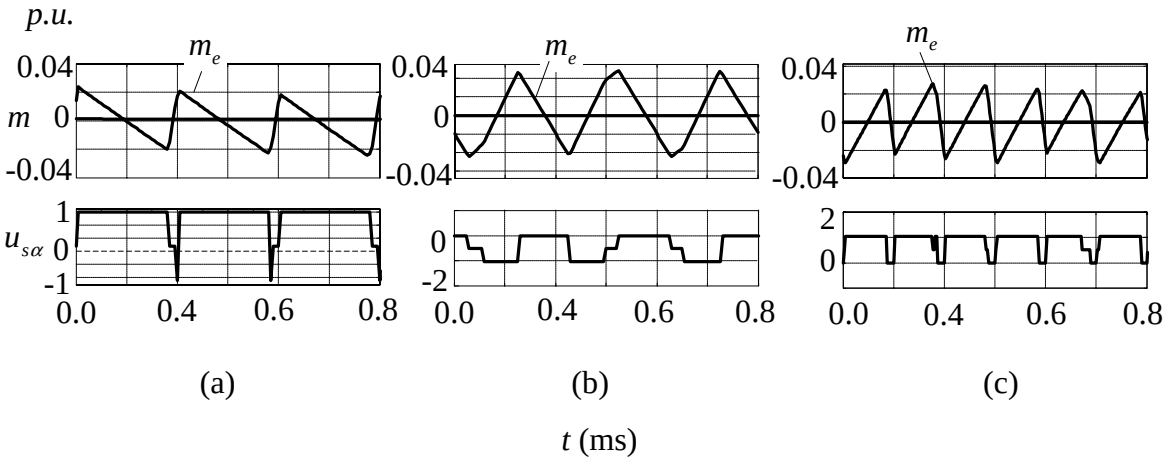

Figure 4.11: Simulated torque ripple at three different angular velocities

(b) and 4.11 (c) respectively. As predicted using analysis, the ripple in torque rises

with the increase in angular velocity and then reduces. The affect of switching zero and active vectors can be observed. Switching times of zero and active states decide the negative and positive slopes of the torque. Hence, at lower angular velocity, the positive slope is much steeper than at very high angular velocities. At around 0.5 *p.u.* both the negative and positive slopes are equal. Simulated result of figure

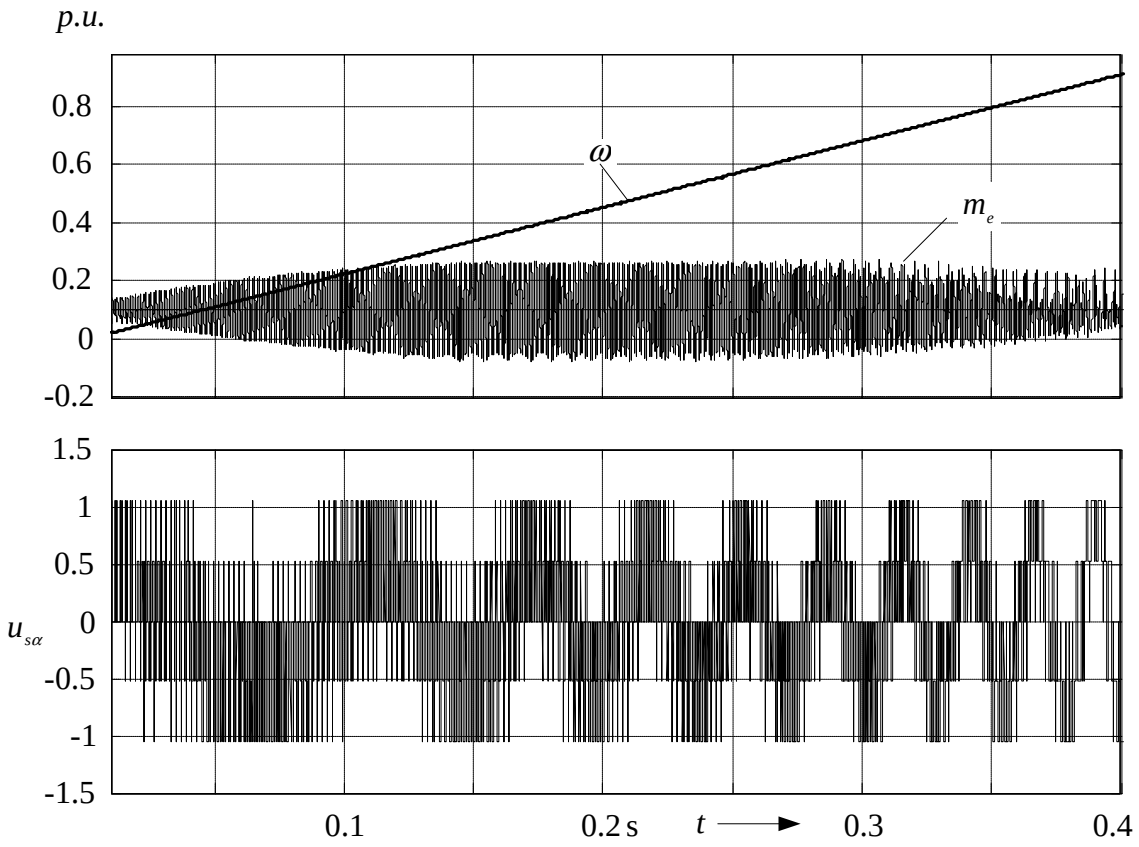

Figure 4.12: Change of torque ripple with the operating angular velocity, $f_{sw} = 0.5kHz$

4.12 shows the affect of increasing angular velocity on torque ripple at a very low switching frequency of 0.5 kHz. This result was obtained by applying a reference torque of 0.1 *p.u.* and letting the machine accelerate unto the rated value.

4.5 Comparison of the proposed method of torque control with conventional DTC: steady state operation

For sampling rates greater than 25 kHz, the conventional DTC maintains a constant torque ripple. Constant torque ripple however results in a variable switching frequency. The variation of the switching frequency can be understood using equation (4.15). For constant ripple, the left hand side of the equation should be a constant. This implies, a constant magnitude K of the q-component of the ripple vector. Hence for $\gamma = 0$,

$$K = \omega_s \frac{\tau_s}{4}(1 - \frac{\omega_s \sin(\frac{\pi}{3})}{\frac{\pi}{3}\sin\frac{\pi}{3}}) \tag{4.16}$$

or,

$$\tau_s = \frac{4K}{\omega_s\{1 - \frac{3}{\pi}\omega_s\}} \tag{4.17}$$

This gives,

$$f_{sw} = \frac{\omega_s\{1 - \frac{3}{\pi}\omega_s\}}{4K} \tag{4.18}$$

The switching frequency f_{sw} will vary in a manner given by equation 4.18 and hence similar to figure 4.8. In other words, the switching frequency will be maximum at around 0.5 *p.u.* This has been a major drawback of the conventional DTC scheme. For a large portion of the operating region, the switching capability of the inverter is not utilized. The currents are distorted, resulting in a smaller overall efficiency.

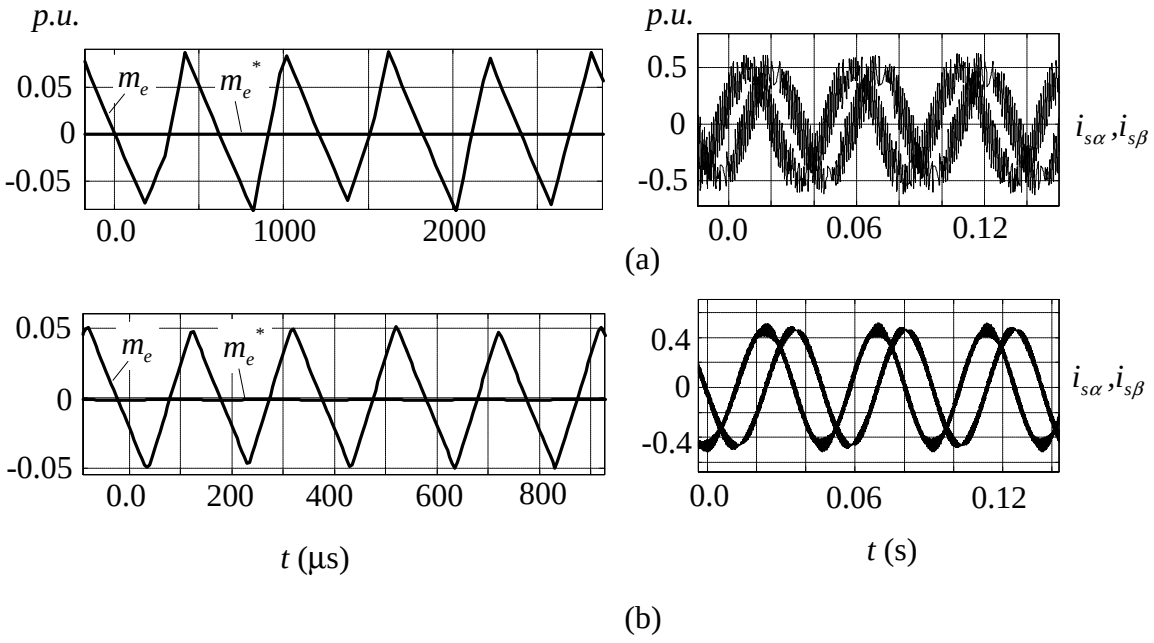

Figure 4.13: Comparison of the ripple due to the switching in the proposed method (b) with DTC (a)

Figure 4.13 gives a comparison of the ripple in torque due to the proposed method with that obtained using the conventional DTC scheme, at an operating angular velocity of 0.5 *p.u.* The torque and flux magnitude hysteresis bands are ±5% of the respective base values while the sampling period is 75 μs. The ripple in torque in case of conventional DTC is shown in part (a) of the figure. Machine currents under these conditions are also plotted. The proposed method of torque control produces a torque ripple as shown in part (b) of the figure. It can be observed that the ripple using the conventional SVM switching pattern, is more consistent even at a higher sampling period of 200 μs. Steady state currents are smoother, than in DTC.

The method of torque ripple estimation proposed in this section provides an easy tool to understand the principle of torque ripple generation due to SVM

switching. Such an analysis has not been done for constant switching frequency DTC methods of references [1], [20] and [22]. As during the normal range of operation, all constant switching frequency DTC schemes use conventional SVM switching, they should exhibit similar steady state torque control performance, as explained here.

4.6 Steady state torque control in the overmodulation region

Overmodulation region has been defined in the previous chapter as a region where the required average angular velocity of the stator flux vector cannot be achieved in every sampling period of SVM. However, in normal range, the switching state vectors required to achieve stator flux vector control and zero average torque error in a sampling time period are readily available. With an increase in the operating angular velocity beyond 0.907 *p.u.*, the vector displacement $\boldsymbol{\Delta\psi}_s^*(k)$ required for torque and stator flux vector control cannot always be compensated in a switching cycle. Under these conditions, the basic requirement of predictive stator flux vector control, ie. $\boldsymbol{\psi}_s(k) = \boldsymbol{\psi}_s^*(k)$ and torque control, $\Delta m_{e(av)}(k) = 0$ cannot always be met, by any combination of switching states of the conventional SVM switching.

The problem due to loss in angular velocity and magnitude of the stator flux vector was discussed in the previous chapter, using the geometry of figure 4.14.

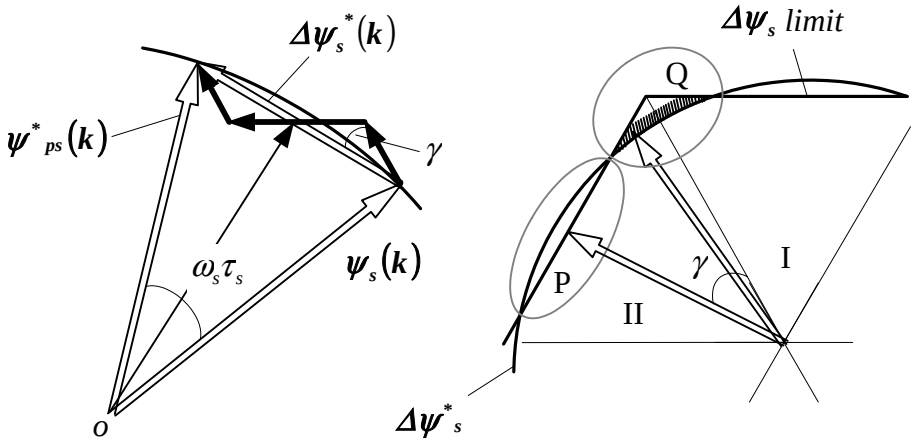

Figure 4.14: Effect of voltage vector limit on torque control during overmodulation

While it is easy to visualize that the reduction in stator flux vector magnitude reduces the average torque, the affect of reduction of average angular velocity is not very obvious. At a certain rotor angular velocity ω, the reference angular velocity ω_s defines a slip angular frequency ω_r for torque control. However, if the average angular velocity is less than the reference, the actual slip frequency will be less than that is required. This reduces the average torque in a sector. Region P is the one in which this loss occurs and it is compensated using the available volt-sec margin in region Q. However, the switching strategy that achieves this compensation results in a non-zero value of $\Delta m_{e(av)}(k)$, after every sampling period. Therefore, the average torque in a sampling period, pulsates around the reference value. Here it is important to clearly distinguish between the ripple in torque with the pulsation in torque. Torque ripple is purely dependent upon the switching of inverter states and hence is determined by the switching frequency and the switching sequence adopted. On the other hand, torque pulsations depend upon the volt-sec compensation method used in overmodulation. While it is not

possible to avoid the reduction in torque in region P, the switching strategy used in overmodulation should compensate for this loss in a sector. The proposed average angular velocity control achieves an average torque pulsation, that is equal to the reference value, figure 4.15. The average torque pulsation in a sector, $m_{e(av)}(s)$ is calculated as,

$$m_{e(av)}(sec) = \frac{\sum_{sector} m_{e(av)}(k)}{\text{number of samples in the sector}} \tag{4.19}$$

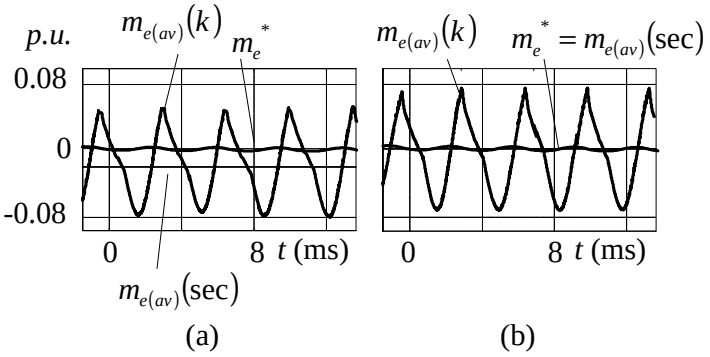

Figure 4.15: Torque control in overmodultion I region without compensation (a), using the proposed compensation (b), $f_{sw} = 5kHz$

The magnitude of torque pulsations are slightly higher than the uncompensated case. While the torque quality in the normal range of operation is given by the ripple caused by switching, the magnitude of the pulsation is a measure of torque quality in the overmodulation region. Therefore, torque pulsation in a sector, rather than torque ripple in a sample will be used to define the torque quality in overmodulation region. The average magnitude of torque pulsation in a sector is calculated by summing up the magnitudes of torque ripple values obtained for every sample in a sector and dividing this sum with the total number of samples.

Hence,

$$\Delta m_{e(ovm)} = \frac{\sum_{sector} m_{e(rip)}(k)}{\text{number of samples in a sector}} \tag{4.20}$$

where $m_{e(rip)}(k)$ is given by equation (4.6-4.9) and (4.12) and $\Delta m_{e(ovm)}$ is the average magnitude of the torque pulsation in a sector. Figure 4.16 gives a simulated

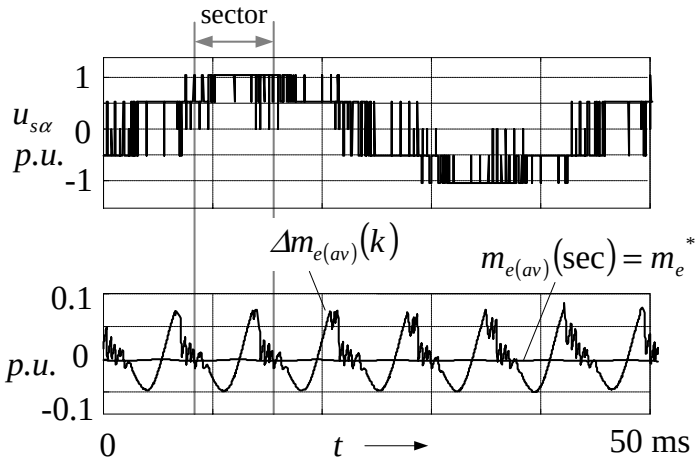

Figure 4.16: Torque control in overmodultion I region at an operating angular velocity ω_s of 0.93 *p.u.*

result for operation in the overmodulation I region and at an angular velocity ω_s of 0.93 *p.u.* Two distinct regions can be seen in a sector of switching, (1) the region where zero states are switched and (2) the region in which only the active states are switched. The average torque pulsation $m_{e(av)}(sec)$ in a sector closely matches the reference value.

Beyond $\omega_s = 0.9535$ *p.u.*, the loss of vector displacement and hence the loss of average angular velocity of $\boldsymbol{\psi}_s$ can only be compensated by adopting overmodulation II switching, as introduced in the previous chapter. During the hold period, the stator flux vector $\boldsymbol{\psi}_s$ moves along the switching state held. The angular velocity of the stator flux vector is maximum at $\gamma = 0$ and $\gamma = \pi/3$ and is less at

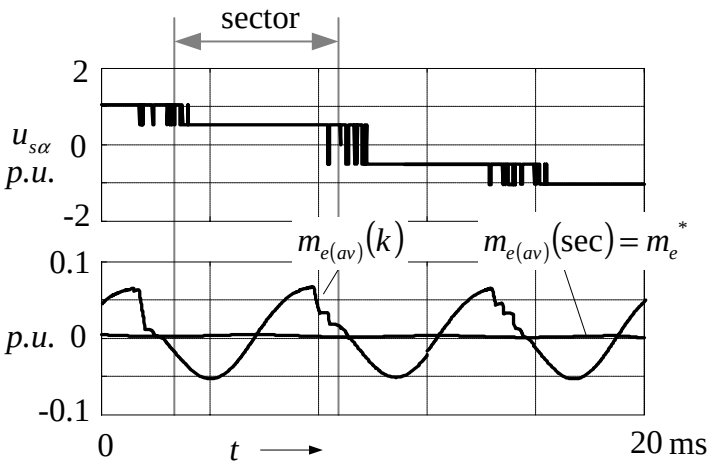

Figure 4.17: Torque ripple during overmodulation II region with the proposed switching strategy

$\gamma = \pi/6$. This causes identical variation in torque, figure 4.17, ie., the rise of torque is not linear during the hold period. On the other hand, switching between active states, reduces the angular velocity of the stator flux vector below the reference value, causing a reduction in torque. Due to average angular velocity control, the average torque in a sector is maintained equal to the reference value. The result of figure 4.17 is obtained for an operating angular velocity of 0.985 $p.u.$

A gradual change in the nature of flux ripple vectors during the overmodulation region can be seen from figure 4.18. Similar to the normal range, these vectors

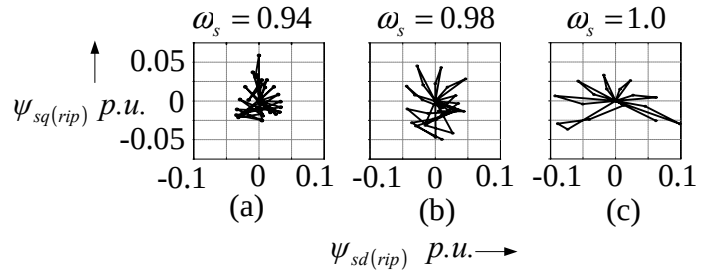

Figure 4.18: Nature of the flux ripple vector for switching in a sector at different operating angular velocities in the overmodulation range. (a) Overmodulation I (b) Overmodulation II and (c) Six-step region

are symmetrical about the q-axis but unlike the normal range, the d-component has larger variation. This is expected as the average stator flux vector magnitude also varies as the modulation voltage limit is reached.

During the entire overmodulation range, the torque pulsates at six times the operating angular velocity in a fundamental cycle. A high gain torque controller tries to control these pulsations. However, this does not work against overmodulation because during steady state the affect of torque controller output (ω_r) at very high operating angular velocities is not very significant. On the other hand, during six-step operation and under dynamic operating conditions, the switching is based upon a large signal algorithm which is explained in the following section.

4.7 Dynamic operation

The vector diagram of figure 4.19, can be used to understand the principle of control during a torque dynamic. A step in the reference value of torque creates a large angle between the reference stator flux vector and the estimated stator flux vector (points p and v in figure 4.4 get separated by a very large angle). This results in a large value of the error $\boldsymbol{\Delta\psi}_s^*(k) = \boldsymbol{\Delta\psi}_s^*(k)_{dyn}$ as shown in the figure 4.19. However, the maximum magnitude of vector displacement that can be achieved in a sample cannot be more than $\frac{\pi}{3}\tau_s$. This is an indication of a transient condition in torque or stator flux vector and it triggers the large signal algorithm shown in the figure. The switching state nearest to the error vector $\boldsymbol{\Delta\psi}_s^*(k)_{dyn}$

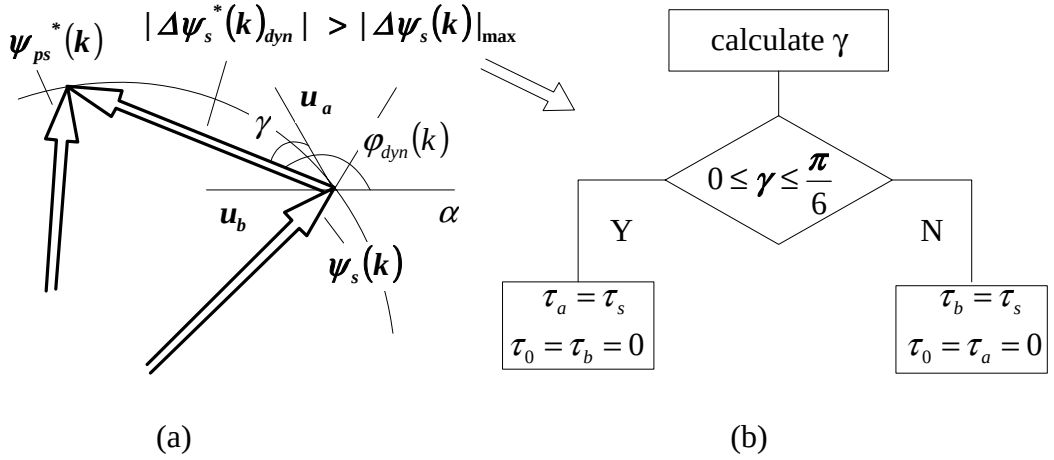

Figure 4.19: (a) Principle of dynamic control of torque, dynamic condition is defined as, $|\boldsymbol{\Delta\psi}_s(k)| > |\boldsymbol{\Delta\psi}_s(k)|_{max}$ (b) Large signal algorithm during dynamic operation

is the one that can bring about the maximum change $\boldsymbol{\Delta\psi}_s(k)$. This state is continuously switched. As a result fastest possible dynamic response, similar to DSC, is achieved. The status of the maximum switching state is updated after every sample of operation. As only a single state is switched, the trajectory of the stator flux vector gets aligned with the switching state vector. Thus during dynamic conditions, fast angular acceleration of the stator flux vector is obtained. Figure 4.20 gives a comparison of the dynamic performance of the proposed method with the constant switching frequency torque control method suggested in reference [22] and the conventional DTC [12]. These methods are selected because they are simple to implement in real time. Selection of the maximum voltage vector during a torque transient makes the dynamic response of the proposed method equivalent to that obtained from conventional DTC. However, as [22] does not exploit the installed voltage capability of the inverter, the rate of change of the stator flux vector angle is slower, resulting in a slower torque dynamic.

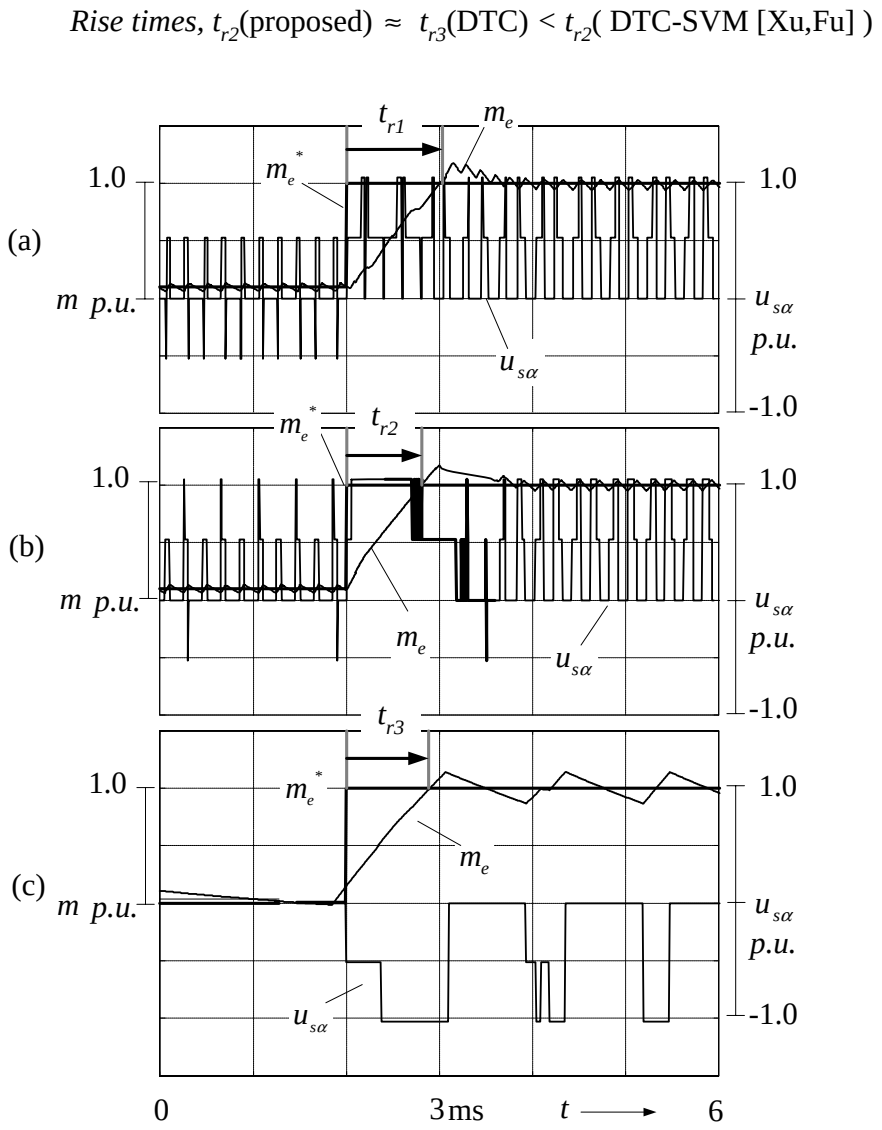

Figure 4.20: Comparison of dynamic torque response of three methods

4.8 Experimental results of steady state and dynamic control of torque

4.8.1 Steady state torque control

The experimental set-up used to implement the proposed constant switching frequency torque and stator flux vector control method, has been briefly described

in the previous chapter and will be further elaborated in chapter 6. Two main aspects of steady state torque control have been focussed in this dissertation. (1) Torque ripple analysis in the normal range of operation and (2) Analysis of torque pulsations in the overmodulation range. Further, the ripple in torque was shown to be dependant upon both the switching frequency selected and the operating angular velocity. Figure 4.21 shows steady state control of torque for two different switching frequencies. These results are obtained with a sampling frequency of 5

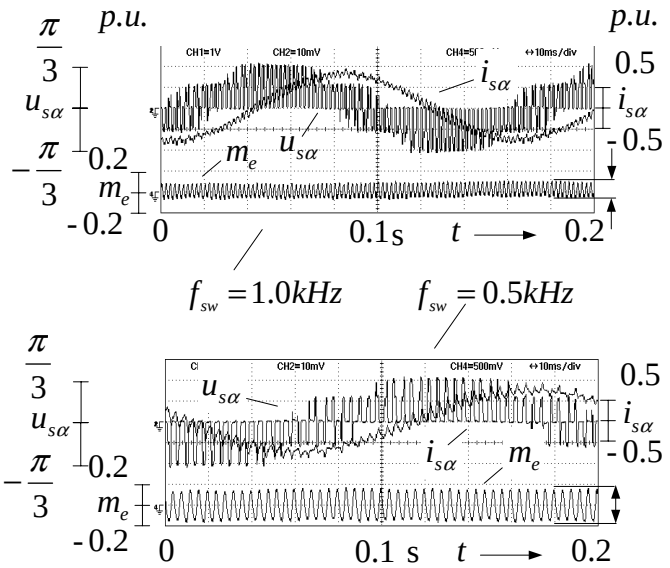

Figure 4.21: Torque ripple in the normal range for two values of switching frequency (f_{sw})

kHz. The operating angular velocity is constant and is equal 0.1 $p.u$. Variations in the instantaneous torque are purely due to the switching of zero and active states and hence this indicates ripple in torque. As the switching frequency is lowered, to 500 Hz, the ripple increases as expected.

Figure 4.22 shows a gradual reduction in the ripple with the increase in switching frequency. The ripple at a switching frequency of 5 kHz is difficult to measure

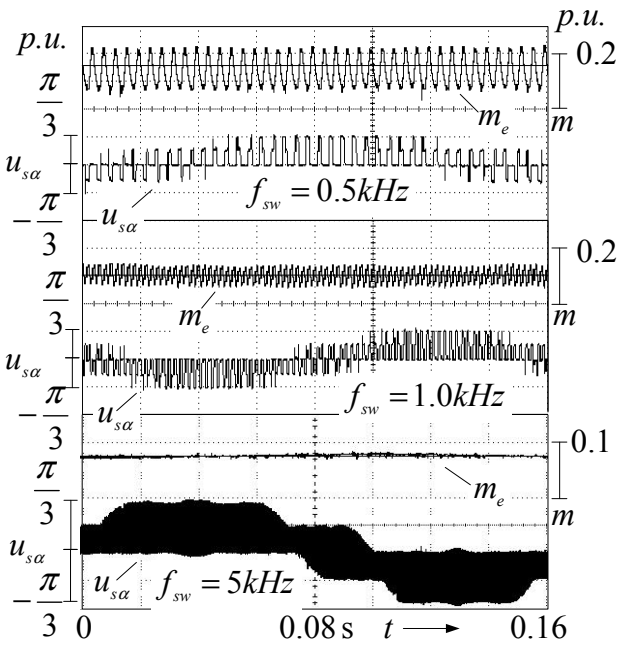

Figure 4.22: Torque ripple in the normal range for three values of switching frequency (f_{sw})

due to limitations on the value of sampling frequency.

Unlike normal range, the variation in instantaneous torque is not just a function of zero and active states switching, but is also dependant upon the switching strategy adopted, during overmodulation. Due to voltage limit, the average error in torque cannot be made zero in every sampling period. As a result, torque pulsations are produced. Using the proposed switching strategy zero average torque pulsation in every sector is achieved. This is evident in the result of figure 4.23 in which steady state torque control during overmodulation I region is shown. Switching ripples can also be observed. The torque pulsates at a frequency that is 6 times the operating angular velocity ω_s.

As the operation shifts in the overmodulation II region, the slope of torque

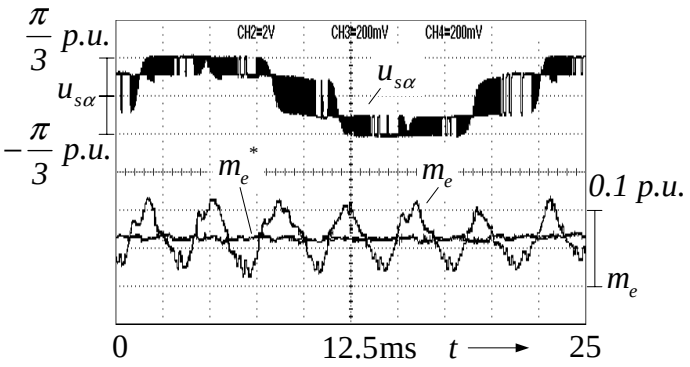

Figure 4.23: Torque control in overmodultion I region at an operating angular velocity of 0.93 *p.u.*

pulsation is defined by the switching and holding of the active voltage vectors. Hence in figure 4.24, when a voltage vector is held, the slope of torque pulsation has a positive value because the average angular velocity of the stator flux vector $\boldsymbol{\psi}_s$ increases above the reference value.

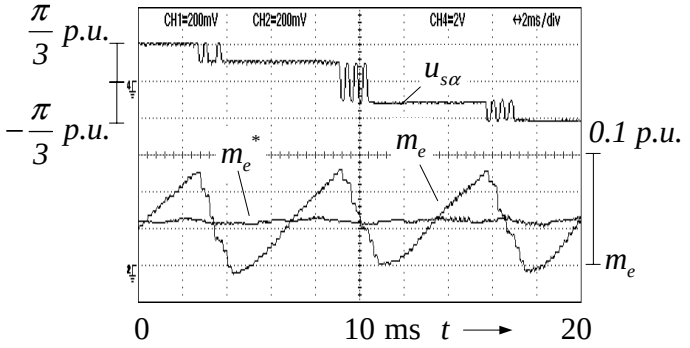

Figure 4.24: Torque pulsations in the overmodulation II region; $\omega_s = 0.985$ *p.u.*

Figure 4.25 summarizes the steady state torque quality of the proposed method in the entire operating region. The equations (4.6-4.9) and (4.12) are used to estimate the nature of torque ripple at different operating angular velocities. The analytical value of the magnitude of torque ripple $|m_{e(rip)}(k)|$ is given by equation (4.12), in a sample. Using this value, the average magnitude of torque pulsations can be obtained using equation 4.20. As the average magnitude $|\Delta m_{e(ss)}|$ of torque

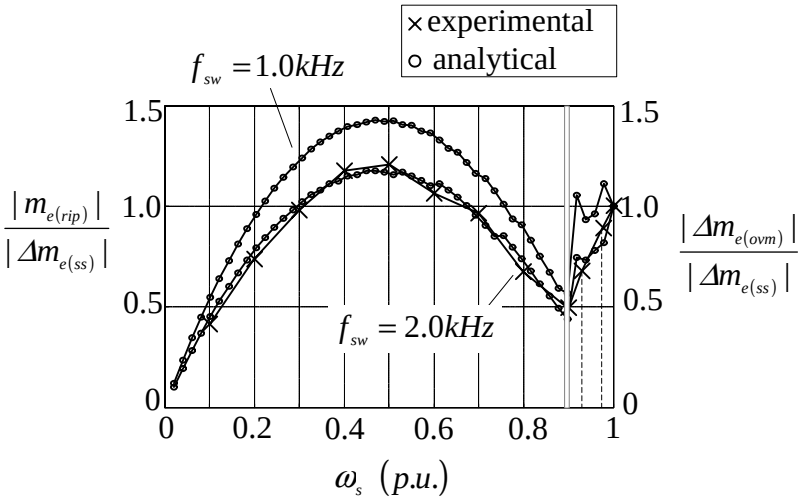

Figure 4.25: Variation of torque ripple (q-component of $\boldsymbol{\psi_{s(rip)}}$ vector) with operating angular velocity

pulsations during six-step operation is independent of the type of PWM, the ripple at any angular velocity can be represented as a fraction of this value. In the figure 4.25, $|\Delta m_{e(ss)}|$ is the average peak to peak torque pulsation during six-step operation. In the normal range, the maximum value of torque ripple occurs at an operating angular velocity of around 0.5 $p.u.$ The experimental peak to peak torque ripple at a switching frequency $f_{sw} = 2kHz$ is also shown in the figure. It is important to note that during normal range of operation ($\omega_s < 0.907$) the graph gives the normalized value of torque ripple. On the other hand in overmodulation region, the graph shows the normalized value of torque pulsation $\Delta m_{e(ovm)}$. In normal range, the predominant frequency of torque ripple is around the switching frequency, figure 4.21, while in overmodulation and above, the torque pulsations have a frequency equal to six times the stator frequency.

4.8.2 Dynamic torque control

Dynamic condition in a torque and stator flux vector is indicated by the magnitude of the error vector $\boldsymbol{\Delta\psi}_s^*(k)$. If this magnitude is greater than the maximum value of $\frac{\pi}{3}\tau_s$, the stator flux vector is changed at the fastest possible rate by continuously switching the maximum possible voltage vector. As the positions of the stator flux vector change, the location of $\boldsymbol{\Delta\psi}_s^*(k)$ also changes and hence the status of the maximum voltage vector gets updated after every sample. This results in a dynamic response similar to the conventional DSC. Figure 4.27 shows the response to a reference torque step of 1.0 *p.u.* This value of torque is the maximum that the machine can produce using the installed voltage and current capability. For the experimental lab machine, the maximum value of torque is equal to 7.35 Nm which means $m_{e(MAX)} = 1.0$ *p.u.* torque corresponds to this value. Corresponding to this maximum value of torque the pull out slip is given by $\frac{1}{\sigma\tau_r}$ and for the parameters of the lab machine, is equal to 0.261 *p.u.* Hence the torque controller output is limited to this value of pull out slip. Torque is estimated using the following expression, [52],

$$m_e = \boldsymbol{\psi}_s \times \boldsymbol{i}_s \tag{4.21}$$

Dynamic control of torque when the motor is at standstill, is shown in figure 4.26. A similar performance is obtained when the motor is running at an angular velocity of 0.1 *p.u.* as shown in figure 4.27. As the back emf is zero or negligible in the above cases, the applied voltage vector, produces a fast torque dynamic. Selection of a single state during a torque dynamic, can be seen from the phase voltage waveforms

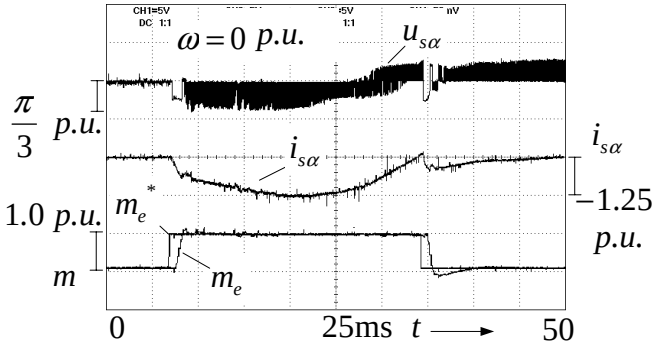

Figure 4.26: Response for step change of torque reference and the alpha component of stator voltage at standstill

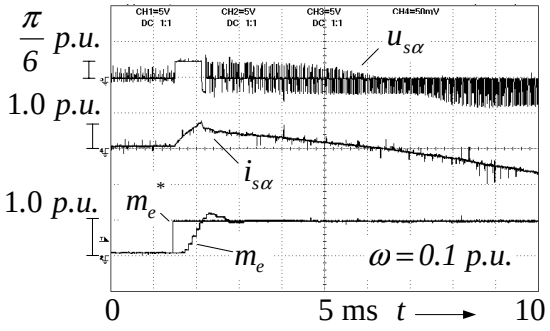

Figure 4.27: Response for step change of torque reference and the alpha component of stator voltage at an operating rotor angular velocity of 0.1 *p.u.*

of these figures. The phase current is inherently controlled. The stator flux vector trajectory under dynamic conditions is shown in figure 4.28. As the large signal algorithm holds on to a single switching state, the stator flux vector trajectory is aligned to the that switching state vector. Hence fast change of stator flux vector angle is obtained. For higher operating speeds, the dynamic torque response is slower. This can be observed from figure 4.29 when a speed step is applied from 0.65 *p.u.* to 0.9 *p.u.* Under these conditions a part of the voltage vector applied is utilized for compensating the back emf vector, resulting in a slower acceleration of the motor. Figures 4.30 and 4.31 show the dynamic torque control performance during the angular velocities corresponding to the overmodulation range. The pro-

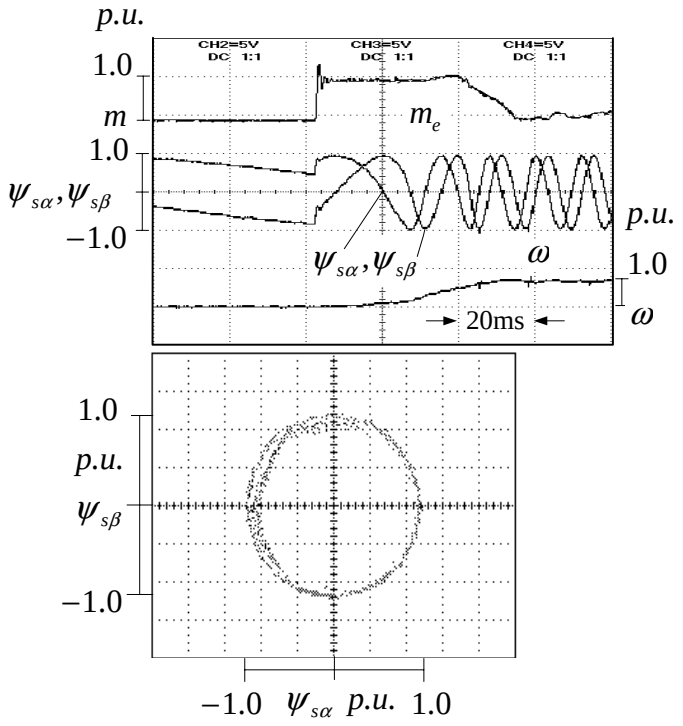

Figure 4.28: Trajectory of the stator flux vector during a torque dynamic

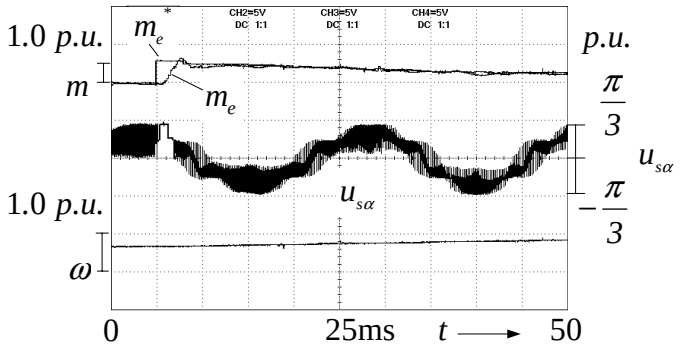

Figure 4.29: Dynamic torque control in the normal region

posed method of overmodulation switching, results in a smooth transition from one operating region to the other and in the six-step region with closed loop speed and torque control. Overmoduation regions can be clearly distinguished by observing the phase voltage waveforms.

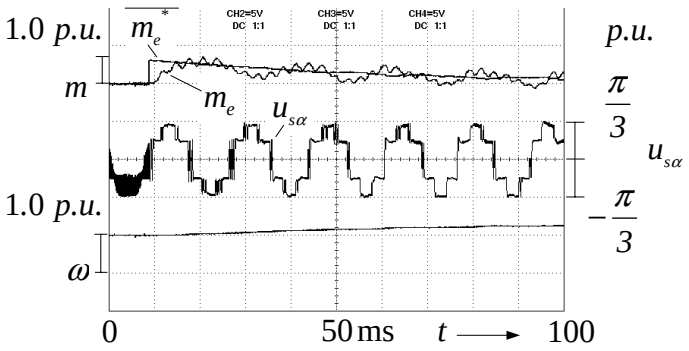

Figure 4.30: Dynamic torque control from the overmodulation region to six-step

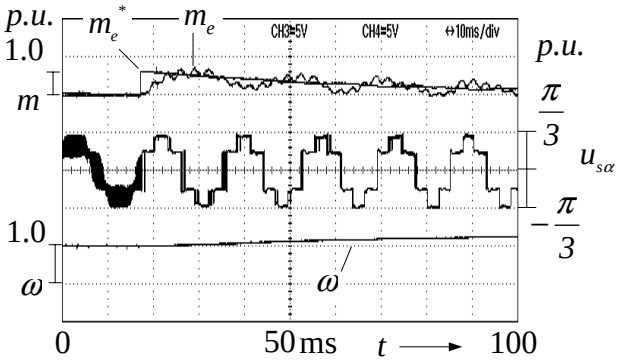

Figure 4.31: Dynamic torque control from the normal region to the six-step

4.8.3 Dynamic operation of an over fluxed machine

The proposed control system has no torque pulsations during a starting transient with a stator magnitude that is 25% greater than its rated value. Dynamic torque control with an over fluxed machine is shown in figure 4.32. This experiment was performed at a switching frequency of 5 kHz and the steady state torque is free from pulsations. If the magnitude of the reference stator flux vector is further increased, the dynamic torque and speed control performance degrades. However, the steady state torque quality is not effected. This can be observed from figure 4.33. Degradation of dynamic performance during operation at a stator flux vector

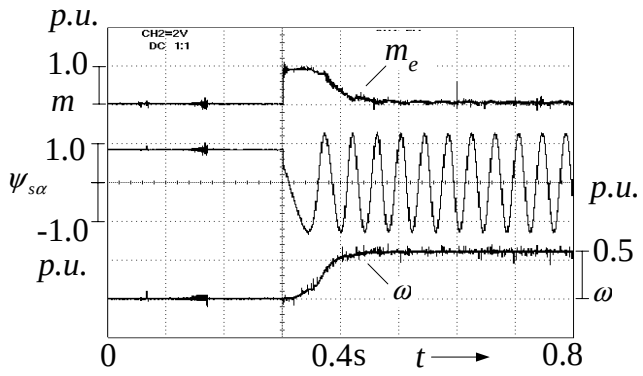

Figure 4.32: Starting transient with a stator flux vector magnitude that is 25% of the rated value: Good steady state and dynamic response

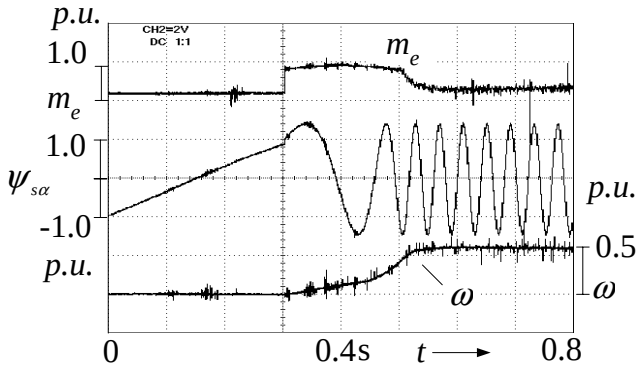

Figure 4.33: Starting transient with a stator flux vector magnitude that is 50% of the rated value: Good steady state torque quality but poor dynamic response

magnitude that is 50% more than the rated value, is due to the fact that accurate estimation of the stator flux vector cannot be achieved by using the conventional voltage model, [46], that is used in this work. This also effects the estimation of torque.

4.9 Inherent current control feature of the proposed DTC scheme

DTC aims to utilize the installed voltage and current capabilities of the inverter to eliminate the errors in torque and the stator flux vector in the shortest possible time. This is achieved by directly defining the inverter switching states using the errors in torque and stator flux vector. There is no deliberate current control. It is assumed that the current vector is inherently controlled for both the steady state and dynamic control of torque and is well within the limitation of the drive specification. Perhaps, due to this assumption, the analysis of current vector dynamic, for a transient condition in torque and stator flux vector has not been carried out in past. There is an inherent control of the current vector $\boldsymbol{i}_s$ in the proposed DTC scheme.

Given the cascaded nature of the control loop, the study of current vector dynamic during a transient in torque and stator flux vector, can be carried out in two steps. Firstly, by considering just the stator flux vector control loop and subsequently, by closing the torque loop.

4.9.1 Current control with the torque loop open

With the torque loop open, an instantaneous change in the reference stator flux vector is brought about, by a step change in its angular velocity ω_s. If magnitude of the error vector $\boldsymbol{\Delta\psi}_s^*$ is large, the control algorithm switches the maximum

voltage vector. This results in a rapid change in magnitude and angle of the current vector from its steady state value. Such a change can be expressed as the current error vector $\Delta \boldsymbol{i_s}$. The manner in which the current error vector $\Delta \boldsymbol{i_s}$ changes as the stator flux error vector $\Delta \boldsymbol{\psi}_s$ approaches zero, can be established using the fundamental equations of the machine. These equations in the stationary co-ordinate system are,

$$\begin{aligned} \boldsymbol{u}_s &= r_s \boldsymbol{i}_s + \frac{d\boldsymbol{\psi}_s}{d\tau} \\ 0 &= r_r \boldsymbol{i}_r + \frac{d\boldsymbol{\psi}_r}{d\tau} - j\omega \boldsymbol{\psi}_r \end{aligned} \tag{4.22}$$

Rotor flux vector $\boldsymbol{\psi}_r$ and the rotor current vector $\boldsymbol{i}_r$ can be expressed as,

$$\begin{aligned} \boldsymbol{\psi}_r &= \frac{1}{k_r}(\boldsymbol{\psi}_s - \sigma l_s \boldsymbol{i}_s) \\ \boldsymbol{i}_r &= \frac{1}{l_h}(\boldsymbol{\psi}_s - l_s \boldsymbol{i}_s) \end{aligned} \tag{4.23}$$

From equations (4.22) and (4.23),

$$\frac{d\boldsymbol{i}_s}{d\tau} = \frac{1}{\sigma l_s}(1 - j\omega)\boldsymbol{\psi}_s + (\frac{-k_r}{\sigma l_s}(\frac{r_r}{k_s} + \frac{r_s}{k_r}) + j\omega)\boldsymbol{i}_s + \frac{1}{\sigma l_s}\boldsymbol{u}_s \tag{4.24}$$

A perturbation about any operating point can be expressed as,

$$\begin{aligned} \frac{d(\boldsymbol{i}_s + \Delta \boldsymbol{i}_s)}{d\tau} &= \frac{1}{\sigma l_s}(1 - j\omega)(\boldsymbol{\psi}_s + \Delta \boldsymbol{\psi}_s) + \\ &(\frac{-k_r}{\sigma l_s}(\frac{r_r}{k_s} + \frac{r_s}{k_r}) + j\omega)(\boldsymbol{i}_s + \Delta \boldsymbol{i}_s) + \frac{1}{\sigma l_s}\boldsymbol{u}_s \end{aligned} \tag{4.25}$$

Assuming large inertia, it can be said that the rotor speed remains constant during this perturbation, giving $\Delta\omega = 0$. Also the applied voltage vector remains fixed to the maximum value. In conventional DTC/DSC as well, similar conditions exist.

This gives, $\Delta \boldsymbol{u}_s = 0$. Subtraction of equation (4.24) from equation (4.25) gives,

$$\begin{aligned} \frac{d\Delta \boldsymbol{i}_s}{d\tau} &= \frac{1}{\sigma l_s}(1 - j\omega)\Delta \boldsymbol{\psi}_s \\ +(\frac{-k_r}{\sigma l_s}(\frac{r_r}{k_s} + \frac{r_s}{k_r}) + j\omega)\Delta \boldsymbol{i}_s & \end{aligned} \tag{4.26}$$

or,

$$\begin{aligned} \frac{d\Delta \boldsymbol{i}_s}{d\tau} + (\frac{k_r}{\sigma l_s}(\frac{r_r}{k_s} + \frac{r_s}{k_r}) - j\omega)\Delta \boldsymbol{i}_s \\ = \frac{1}{\sigma l_s}(1 - j\omega)\Delta \boldsymbol{\psi}_s \end{aligned} \tag{4.27}$$

Solution of this equation yields,

$$\Delta \boldsymbol{i}_s = \frac{1}{\sigma l_s}(1 - j\omega)\Delta \boldsymbol{\psi}_s \epsilon^{-(\frac{k_r}{\sigma l_s}(\frac{r_r}{k_s} + \frac{r_s}{k_r}) - j\omega)\tau} \tag{4.28}$$

A step in $\Delta \boldsymbol{\psi}_s$ vector will produce a current response according to equation (4.28). It will die down as shown in the simulated result of figure 4.34. Such dynamic response is a function of rotor speed and machine parameters. This result is obtained when the rotor is at standstill and hence the affect of back emf is zero. As the sampling frequency of operation is 5 kHz, the maximum value $|\boldsymbol{\Delta \psi}_s(k)|_{max}$ is given as, 0.0657 $(\frac{\pi}{3}\tau_s)$ and is continuously applied for a few samples, by giving an angular velocity command of nominal value. From figure 4.34 it can be observed that, as $\Delta \boldsymbol{\psi}_s \rightarrow 0, \Delta \boldsymbol{i}_s \rightarrow 0$. This shows that there is an inherent control of current when predictive stator flux vector control is implemented and proves the redundancy of current controllers.

With the increase in time τ, the magnitude of the current error vector dies down to zero value. How fast the current changes from a small value to peak value

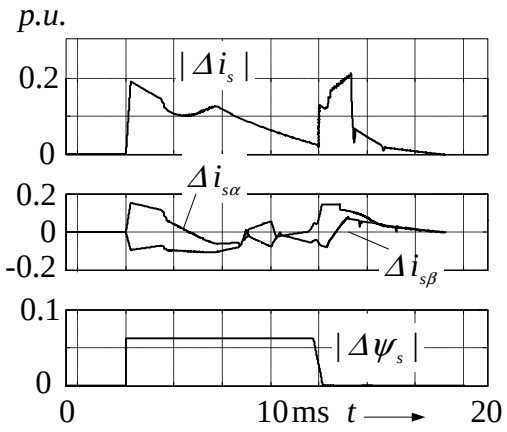

Figure 4.34: Current dynamics for a maximum step in $\boldsymbol{\Delta\psi_s}$ vector

and then to a steady state value depends upon the machine parameters as seen from equation (4.28). The peak current for any machine can be obtained using equation (4.28) and considering the worst possible conditions of zero rotor angular velocity and switching of the maximum flux error vector. The current vector at any sampling instant can be obtained by knowing the current error vector. Hence,

$$\boldsymbol{i}_s(k) = \boldsymbol{i}_s(k-1) + \Delta\boldsymbol{i}_s(k) \tag{4.29}$$

For the lab machine under test (data given in chapter 6), figure 4.35 gives the variation of current vector magnitude, when the machine is continuously subjected with the maximum value of the flux error vector. The current rises to a peak value of around 1.6 *p.u.* and then stabilizes. The current error vector approaches zero as shown in figure 4.36.

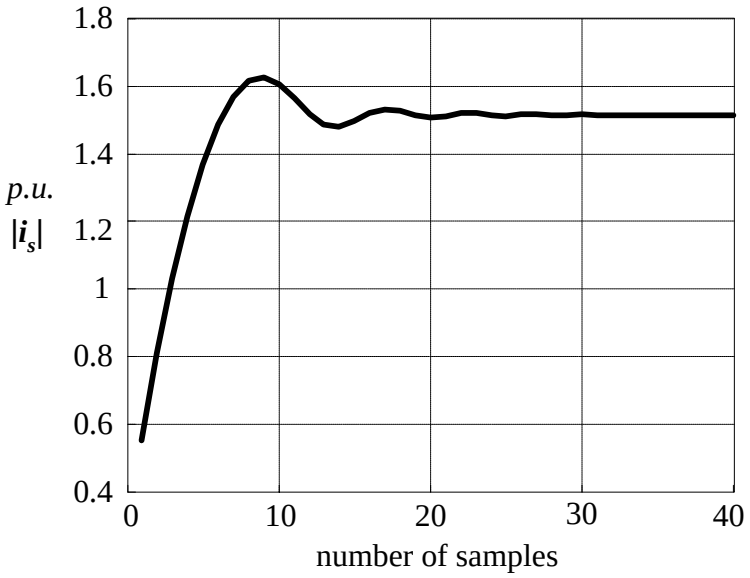

Figure 4.35: Maximum current for continuous application of $|\boldsymbol{\Delta\psi}_s(k)|_{max}$ on the machine

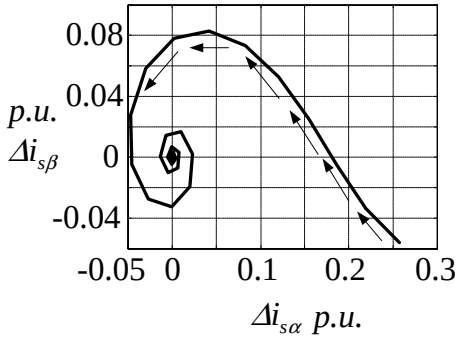

Figure 4.36: Change in the current error vector $\boldsymbol{\Delta i}_s$ for continuous application of $|\boldsymbol{\Delta\psi}_s(k)|_{max}$ on the machine

4.9.2 Study of the current error vector dynamic for machines of different specifications

To study the affect of machine parameters, a $\Delta\boldsymbol{\psi_s}$ step was applied on machines of different ratings. The parameters of these machines are given in table 4.1 and the responses to this step are given in figure 4.37. In the table, τ_{mech} is the mechanical time constant, [52], or the normalized moment of inertia. Following

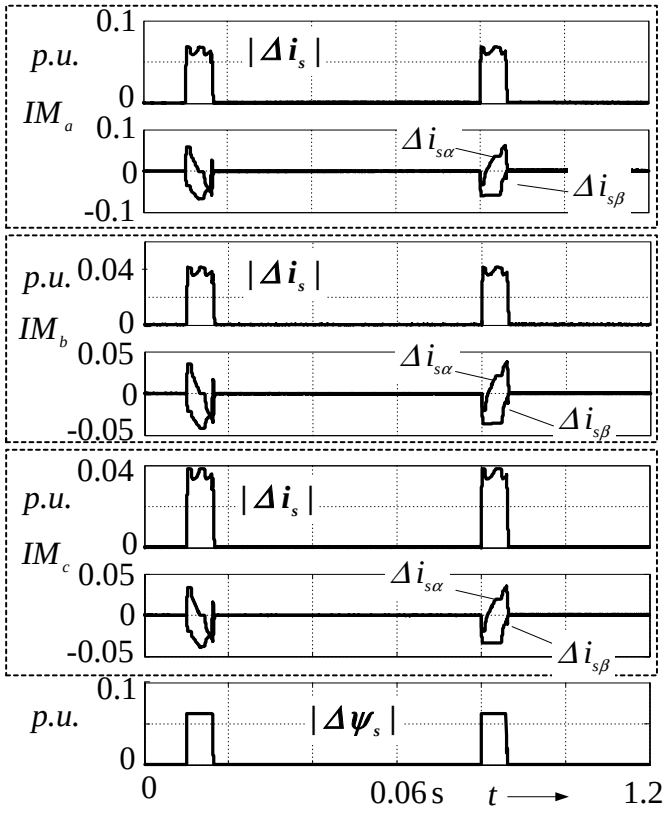

Figure 4.37: Current dynamics for a maximum step in $\Delta\psi_s$ vector (simulated)

Table 4.1: Normalized Parameters of test machines (Rating in kW)

Motor	*Rating*	r_s	r_r	l_s	l_r	l_h	τ_{mech}
IM_{lab}	0.75	0.131	0.096	2.95	2.95	2.76	7.5
IM_a	37.5	0.015	0.04	2.35	2.35	2.31	596.9
IM_b	375	0.0185	0.0132	3.9	3.9	3.81	397.31
IM_c	1687.5	0.009	0.007	4.21	4.21	4.14	509.86

observations can be made. (1) The maximum magnitude of current error vector, depends upon the factor σl_s. Since $\boldsymbol{i}_s(k{+}1) = \boldsymbol{i}_s(k){+}\boldsymbol{\Delta i}_s(k)$, this indicates that the current vector $\boldsymbol{i}_s$ will attain higher per unit magnitude for machine IM_a than the other two machines, IM_b and IM_c. (2) The time taken by the current error vector to become zero depends upon the factor F, where $F = \frac{k_r}{\sigma l_s}(\frac{r_r}{k_s} + \frac{r_s}{k_r})$. For the machines under observation, this factor is in the order, $F(IM_a) > F(IM_b) > F(IM_c)$.

Hence the time taken by the current transient to die down will be smallest for the machine IM_a that has a larger value of the factor F.

When torque control is included, the rate of change of the flux error vector and therefore the current vector depends upon the error in torque. However, with the given control structure, this error in torque translates in a flux error vector. Hence a similar dynamic response of the current error vector can be expected.

4.10 Inherent current control with the torque loop closed

The electromagnetic torque is given as, [52],

$$m_e = \boldsymbol{\psi}_s \times \boldsymbol{i}_s = -\frac{k_r}{\sigma l_s}\boldsymbol{\psi}_s \times \boldsymbol{\psi}_r \tag{4.30}$$

To increase robustness and minimize computation, the cross product of the stator flux vector with the measured stator current vector is used. Simplification of equation (4.30) gives,

$$m_e = \psi_{s\alpha} i_{s\beta} - \psi_{s\beta} i_{s\alpha} \tag{4.31}$$

A small disturbance Δm_e from the steady state value of torque equation (4.31) gives,

$$\begin{aligned} m_e + \Delta m_e = (\psi_{s\alpha} + \Delta\psi_{s\alpha})(i_{s\beta} + \Delta i_{s\beta}) - \\ (\psi_{s\beta} + \Delta\psi_{s\beta})(i_{s\alpha} + \Delta i_{s\alpha}) \end{aligned} \tag{4.32}$$

From equations (4.31) and (4.32) and neglecting the higher order terms,

$$\Delta m_e = \psi_{s\alpha}\Delta i_{s\beta} + \Delta\psi_{s\alpha} i_{s\beta} - \psi_{s\beta}\Delta i_{s\alpha} - \Delta\psi_{s\beta} i_{s\alpha} \tag{4.33}$$

Also, the magnitude of stator flux vector is given as,

$$|\boldsymbol{\psi}_s|^2 = \psi_{s\alpha}^2 + \psi_{s\beta}^2 \tag{4.34}$$

A small disturbance about an equilibrium point results in,

$$(|\boldsymbol{\psi}_s| + |\Delta\boldsymbol{\psi}_s|)^2 = (\psi_{s\alpha} + \Delta\psi_{s\alpha})^2 + (\psi_{s\beta} + \Delta\psi_{s\beta})^2 \tag{4.35}$$

From equations (4.34) and (4.35) and after neglecting the higher order terms,

$$|\boldsymbol{\psi_s}||\Delta\boldsymbol{\psi_s}| = \psi_{s\alpha}\Delta\psi_{s\alpha} + \psi_{s\beta}\Delta\psi_{s\beta} \tag{4.36}$$

Further, equation (4.28) can be written as follows,

$$\Delta\boldsymbol{\psi_s} = \frac{\sigma l_s}{1+\omega^2}(1 + j\omega)\epsilon^{(F+j\omega)\tau}\Delta\boldsymbol{i_s} \tag{4.37}$$

Let,

$$B = \frac{\sigma l_s \epsilon^{F\tau}}{1+\omega^2} \tag{4.38}$$

This gives,

$$\Delta\boldsymbol{\psi}_s = B((Q\Delta i_{s\alpha} - R\Delta i_{s\beta}) + j(R\Delta i_{s\alpha} + Q\Delta i_{s\beta})) \tag{4.39}$$

Here,

$$Q = \cos\omega\tau - \omega\sin\omega\tau$$

$$R = \sin\omega\tau + \omega\cos\omega\tau \tag{4.40}$$

Substituting the real and imaginary parts of $\Delta\boldsymbol{\psi_s}$ in equation (4.33) and equation (4.36),

$$\Delta m_e = T\Delta i_{s\alpha} + U\Delta i_{s\beta}$$

$$|\Delta\boldsymbol{\psi_s}||\boldsymbol{\psi_s}| = R\Delta i_{s\alpha} + W\Delta i_{s\beta} \tag{4.41}$$

Here,

$$T = -\psi_{s\beta} - BRi_{s\alpha} + BQi_{s\beta}$$

$$U = \psi_{s\alpha} - BRi_{s\beta} - BQi_{s\alpha}$$

$$S = BQ\psi_{s\alpha} + BR\psi_{s\beta}$$

$$W = BQ\psi_{s\beta} - BR\psi_{s\alpha} \tag{4.42}$$

Solving equations (4.41) for the values of $\Delta i_{s\alpha}$ and $\Delta i_{s\beta}$,

$$\Delta i_{s\alpha} = \frac{U|\Delta\boldsymbol{\psi}_s||\boldsymbol{\psi}_s| - W\Delta m_e}{US - WT}$$
$$\Delta i_{s\beta} = \frac{T|\Delta\boldsymbol{\psi}_s||\boldsymbol{\psi}_s| - S\Delta m_e}{WT - US} \tag{4.43}$$

The factor $WT - US$ can be expanded as,

$$WT - US = Q\frac{\sigma l_s\epsilon^{F\tau}}{1+\omega^2}(\psi_{s\beta}^2 - \psi_{s\alpha}^2) +$$
$$(\sigma l_s\epsilon^{F\tau})^2(\psi_{s\alpha}i_{s\alpha} + \psi_{s\beta}i_{s\beta}) = X \tag{4.44}$$

As $\tau \to \infty$, $(WT-US) \to$ a non-zero value. Now from equations (4.43) and noting that,

$$|\Delta\boldsymbol{i}_s|^2 = \Delta i_{s\alpha}^2 + \Delta i_{s\beta}^2 \tag{4.45}$$

the following expression can be obtained,

$$|\Delta\boldsymbol{i}_s|^2 = \frac{(W^2+S^2)\Delta m_e^2 - 2|\Delta\boldsymbol{\psi}_s||\boldsymbol{\psi}_s|\Delta m_e(WU+ST)}{X^2 - |\boldsymbol{\psi}_s|^2(U^2+T^2)(\frac{\sigma l_s\epsilon^{F\tau}}{\sqrt{1-\omega^2}})} \tag{4.46}$$

From equation (4.46) it can be seen that as $\Delta m_e \rightarrow 0$, $|\Delta \boldsymbol{i}_s| \rightarrow 0$. Fig. 4.38 shows a simulated result for a unit step input in the commanded torque. This figure shows the per unit values of $i_{s\alpha}$, $i_{s\beta}$ and magnitude of the current error vector $|\Delta \boldsymbol{i}_s|$ for the torque step.

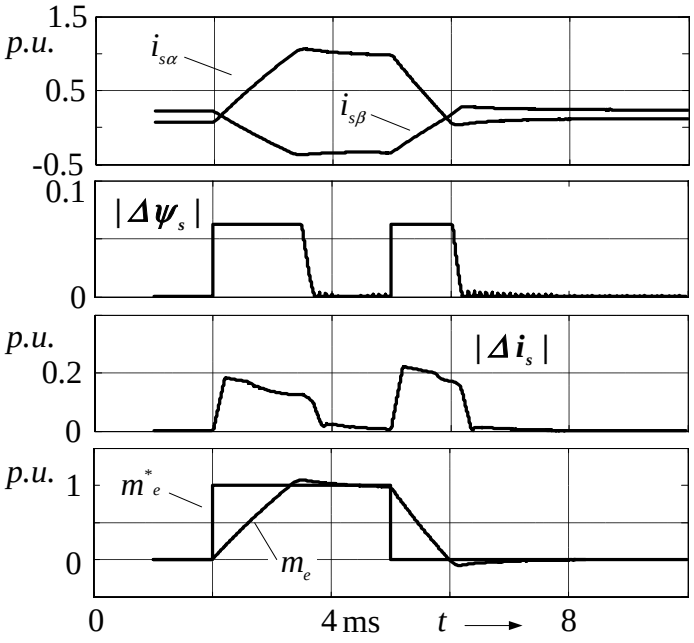

Figure 4.38: Current response for step change of torque reference

4.11 Comparison of Current Control dynamics for different machines

The affect of applying a large torque step, on the machines of table 4.1 can be studied for the worst case of zero rotor angular velocity. The duration of torque step is 5 ms and the initial assumption that $\Delta\omega = 0$ is valid as the motors have considerably large mechanical time constant. Using equations (4.43) and (4.46), it can be observed that the magnitude and duration of the $|\Delta \boldsymbol{i}_s|$ transient under

these conditions is proportional to the factor $\frac{1}{B}$. For $\omega = 0$, B can be expressed as,

$$B = \sigma l_s \epsilon^{F\tau} \tag{4.47}$$

Table 4.2 gives the numerical data for the test machines. The dynamic response of the current error vector magnitude for unity torque step is shown in figure 4.39. As expected from the machine data, magnitude of current vector transient for machine IM_a is the largest (smallest value of σl_s). However, this transient lasts for the shortest duration (given by comparatively larger value of the factor F). Similarly, the transient response for the motors IM_b and IM_c matches with their respective values of the factor B. For the test machines selected, $k_s = k_r$. This

Table 4.2: Elements of the transient factor B of the test machines (Rating in kW)

$Motor$	$Rating$	k_s	k_r	σl_s	F
IM_a	37.5	0.981	0.981	0.09	0.62
IM_b	375	0.979	0.979	0.1635	0.1936
IM_c	1687.5	0.983	0.983	0.142	0.114

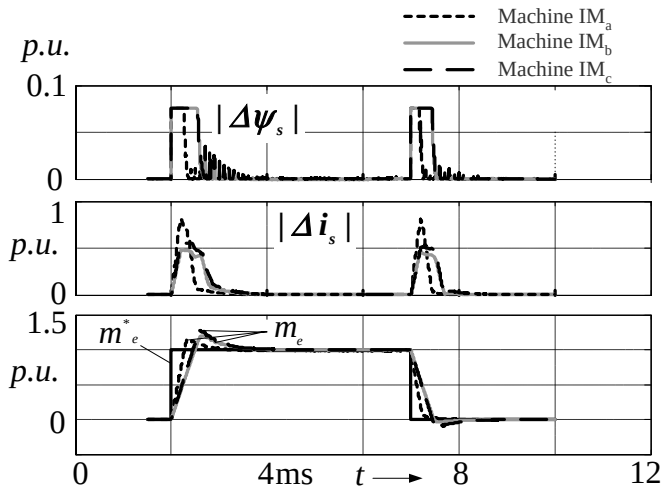

Figure 4.39: Step in torque and the resulting current error vector transients: a comparative study

gives, $F = \frac{r_s + r_r}{\sigma l_s}$. An increase of stator and rotor resistance (due to temperature rise) decreases the transient response time of the current vector.

Though it is observed that the control of current error vector is inherent to the proposed DTC-SVM, it is important to investigate whether such a condition will ensure that the peak value of current is always within its limit. The change of peak value of current for different machines when used with the proposed scheme was also studied. A simulation to obtain the torque response was carried out for machines given in table 4.1 and the results are shown in figure 4.40. For machines with power rating ranging from few kW to several hundred kWs the peak current during the torque change from 0 to 1 *p.u.* is within 1.5 *p.u.* Hence for closed loop stator flux vector and torque control proposed, an inherent current limit control always exists.

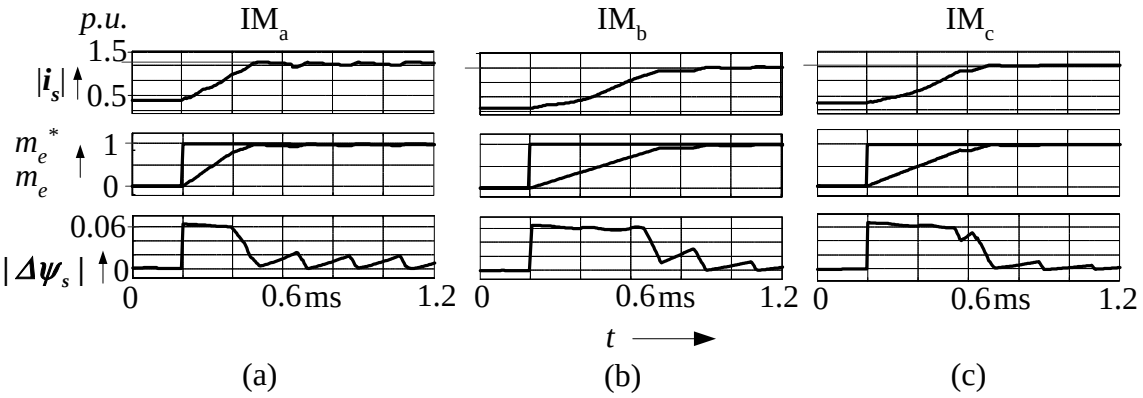

Figure 4.40: Change in the current error vector $\boldsymbol{\Delta i}_s$ for continuous application of $|\boldsymbol{\Delta\psi}_s(k)|_{max}$ on the machine

4.12 Principle of current limiting DTC-SVM

It has been shown earlier that limiting the stator flux error vector also limits the stator current. The stator flux error vector in figure 4.41, has different magni-

tudes for steady state, figure 4.41 (a) and dynamics, figure 4.41 (b). As the flux error vector gets translated in the acceleration of the stator flux vector, the selection of switching states and their times of application can be controlled by limiting the error vector magnitude or the angular velocity commanded by the torque controller. If the command value is not limited and the maximum voltage vector is

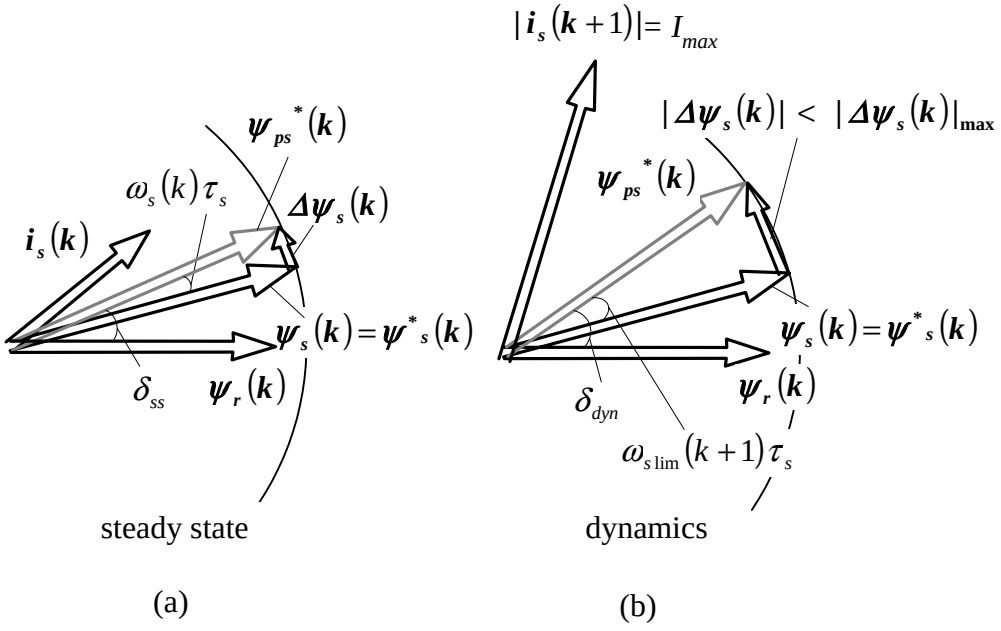

Figure 4.41: Principle of current limiting direct torque control

continuously applied during dynamic, a maximum current magnitude of 1.5 *p.u.* may result. This usually occurs in all DTC methods where there is no limit on the change in the stator flux vector angle or in other words where a maximum voltage vector is applied during dynamic.

If however, the output of the torque controller is deliberately limited, the flux error vector also gets limited. This limit in angle is expressed as $\omega_{s(lim)}\tau_s$ in the figure 4.41. Thus the rate of change of torque is slower. This will limit the current

below 1.5 *p.u.* The basic control structure is still the same. The above principle has been experimentally verified and the results are presented in the next section.

4.13 Experimental results of inherent current control

4.13.1 Inherent current control during a torque and stator flux vector dynamic

Figure 4.42 shows the transient response of the drive for a step change in the angle of the stator flux vector. Worst case experimental condition of zero rotor angular velocity has been considered to study the current transients. This experi-

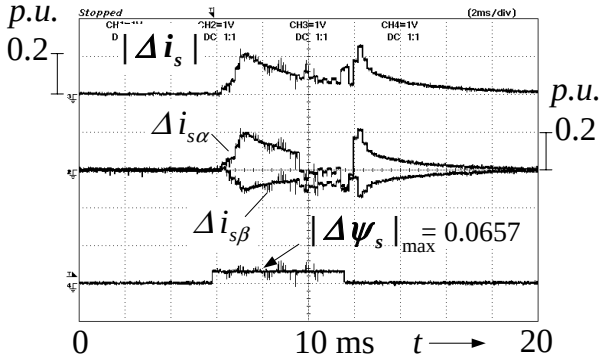

Figure 4.42: Current dynamics for a maximum step in $\boldsymbol{\Delta\psi_s}$ vector

mental result matches with the simulation result obtained when the lab machine is excited with the maximum step in the flux error vector under similar conditions, figure 4.34. The maximum magnitude attained by the current error vector and time duration of its decay, depends upon the machine parameters and rating of the machine. As the lab machine (table I), used is of relatively smaller rating and

has a smaller value of the factor F, the decay of the current vector error transient takes longer time. Current transients for a reference torque step of unit magnitude

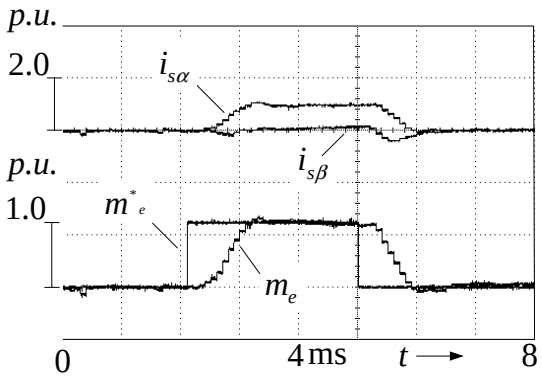

Figure 4.43: Step in torque and the resulting transients in the currents

is shown in figure 4.44. Again, this step is applied at zero rotor angular velocity. In this experiment, no limit is imposed upon the magnitude of the current vector. This result matches with the one obtained by simulating similar conditions on the lab machine. As analytically established in figure 4.38, the current vector is controlled inherently. Moreover, its magnitude exceeds the rated peak value of the machine to bring about a fast dynamic response. The initial time delay in the current response is due to dynamic of the analog filter used. During a step in torque, the behavior of the current error vector $\boldsymbol{\Delta i}_s$ can be seen from figure 4.44. Such a dynamic is expected as a step in torque is translated as a step in the $\boldsymbol{\Delta \psi}_s$ vector. However, there is a distinct difference between this dynamic and the one with just the stator flux vector control, figure 4.42. As the error between the reference and actual torque reduces, the magnitude of the flux error vector reduces as well. This increases the rate of decay of the current error vector. Direct torque control with an upper limit on the magnitude of the current vector is shown in

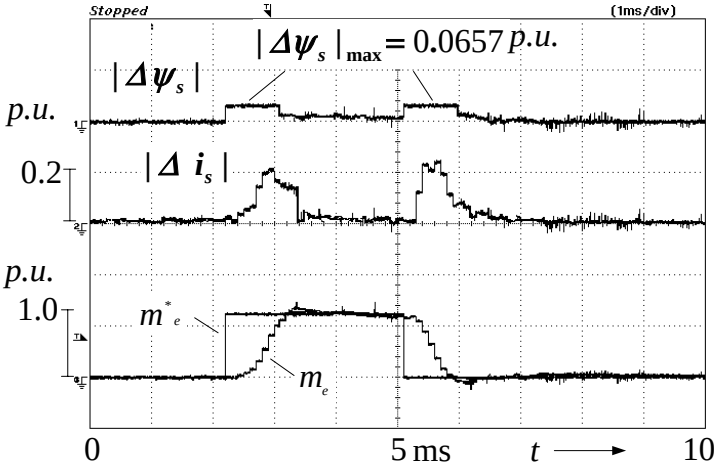

Figure 4.44: Current error vector for a step in torque

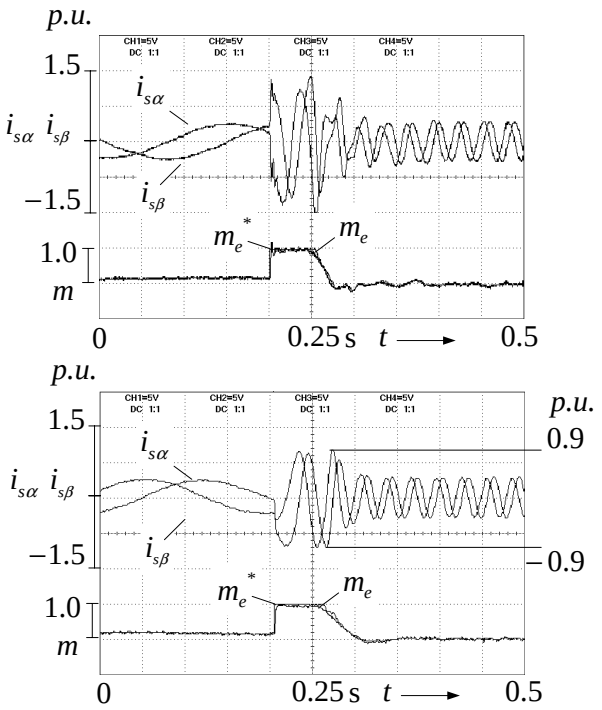

Figure 4.45: Current limiting direct torque control control

figure 4.45 (figure in the bottom) and a comparison of this result is given with the case when no limit is imposed (figure on top). Faster dynamic response, but with a higher magnitude of the current vector results in the normal case. The result also verifies the simulation presented earlier which showed that the maximum current

under such condition for any unsaturated machine is below 1.5 *p.u.* On the other hand, when the flux error is limited by limiting the output of the torque controller, the dynamic torque response is much slower. For this experiment, the torque controller output was limited to pull out slip. The difference between these two cases,

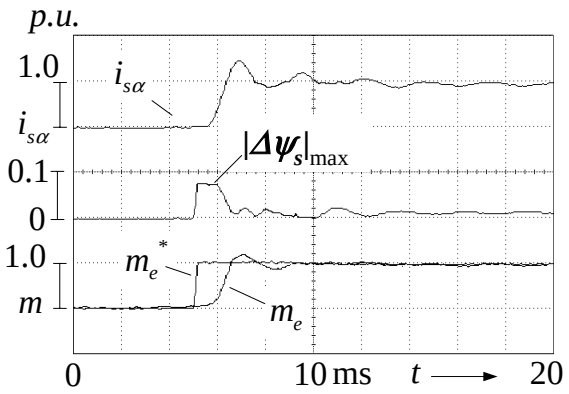

Figure 4.46: Torque step with no limit on the flux error vector magnitude, $T_s = 200\mu s$

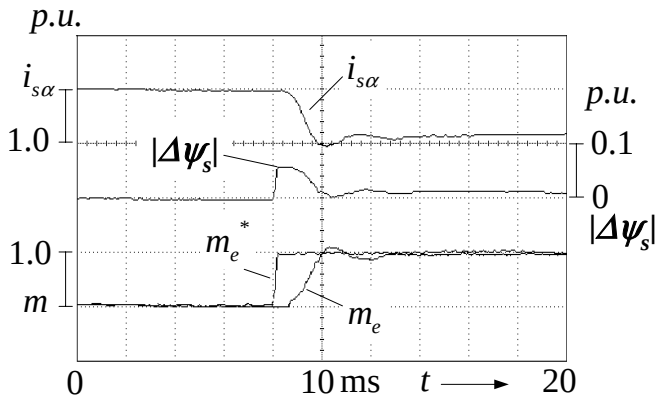

Figure 4.47: Torque step with the magnitude of flux error vector limited to 90% of the maximum value, $T_s = 200\mu s$

lies in the criterion of selection of the switching states under dynamic conditions. When normal DTC is implemented, the control algorithm selects the maximum voltage vector and has no deliberate restriction on the current vector. This moves the stator flux vector $\boldsymbol{\psi}_s$ at the fastest possible rate giving a rapid torque dynamic

as shown in figure 4.46. On the other hand, rate of change of stator flux vector during current limiting control is slower, and depends upon the current control requirement. This makes the response slower as shown in figure 4.47

4.14 Summary

Instantaneous change in torque is influenced by the switching states of the inverter. However, torque control can be achieved if the average value of torque is equal to its reference. In the normal range, a constant average torque can be obtained at every PWM sampling period. However, the instantaneous change in torque within a PWM period produces torque ripple. The magnitude of the torque ripple is a function of switching frequency and operating angular velocity. Hence in the proposed DTC SVM, where the switching frequency is constant, torque ripple varies only with the operating angular velocity. On the other hand, in classical DTC, as the torque ripple is maintained within hysteresis band, the switching frequency changes with the angular velocity. Thus using constant switching frequency, a desired torque ripple can be achieved at any operating angular velocity. Hence, the maximum switching capability of the inverter is exploited.

During overmodulation the average value of torque in a PWM period cannot be held constant. However, with the proposed switching strategy in this region, the average value of torque is maintained constant over the sector. This causes torque pulsations at six times the stator frequency. Even then average torque control is

achieved in every sector. Thus the proposed scheme is able to achieve average torque control from zero speed to six-step without needing a change in the control structure. Overmodulation in steady state and large signal algorithm in dynamic state are able to utilize the maximum voltage capability of the inverter. Though there is no deliberate control of current, the current vector is inherently controlled and is well within the drive specifications.

Hence the proposed scheme has merits of both the classical DTC and the fixed frequency space vector modulation. Due to its simple structure it can be easily implemented on available embedded DSPs. The next chapter will analyze the proposed scheme for operation at high angular velocities and in the field-weakening region.

Chapter 5

Dynamic Torque Control at Large Angular Velocities

Study of dynamic torque control at large operating angular velocities can be carried out under two categories. (1) Dynamic control of torque at large angular velocities but below base speed or in the overmodulation region and (2) Dynamic control of torque above base speeds or in the field weakening region with six-step operation. Figure 5.1 shows the block diagram of the control scheme. For

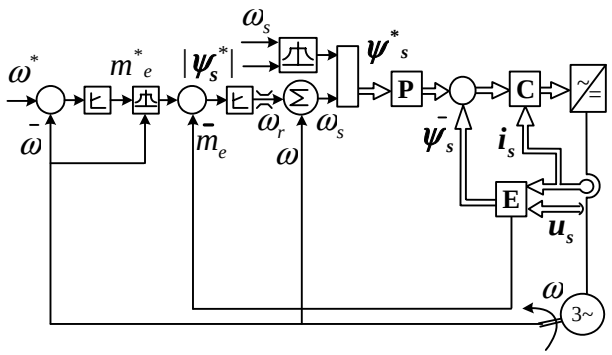

Figure 5.1: Control scheme for operation in the field weakening range

operation above base speeds, the reference torque is adjusted corresponding to the

operating rotor angular velocity to maintain constant rated power operation, [2]. The magnitude of the stator flux vector is weakened as per the $\frac{\psi_{sR}}{\omega_s}$ rule, where ψ_{sR} is the rated magnitude of the stator flux vector. As the angular velocity ω_s is commanded by the torque controller, the desired stator flux vector magnitude level depends upon the torque control requirement.

To achieve fast dynamics and operate in the field-weakening, the drive is constraint by certain limitations. One is the DC-link voltage. It determines the voltage limit of the inverter. In this work this voltage limit is 1.0 $p.u.$ and is given as $\frac{2}{\pi}U_{dc}$ where U_{dc} is the DC-link voltage of the inverter and $\frac{2}{\pi}U_{dc}$ is the fundamental component of the six-step voltage. This limit is called the voltage limit. The current limit depends on the duration of operation. For continuous operation the continuous current rating of the motor is used. In this work it is 1.0 $p.u.$ and is called the motor current limit. For short term, the motor current can exceed this value. However it cannot exceed the inverter over current limit. In this work the inverter over current limit is considered to be 2.0 $p.u.$

5.1 Dynamic torque control in the overmodulation region

In overmodulation, the voltage limit starts effecting closed loop torque and stator flux vector control. This happens because of the large back emf vector that reduces the voltage reserve. Switching strategies are suggested by Habetler et.

al, [1], Mochikawa et. al, [33] and Jul et. al, [35] to exploit the inverter voltage limit. The main objective of these methods is to improve the dynamic torque response. The methods described in [33] and [35] have been tested with the FOC method whereas the one described in [1] has been tested for a DTC-SVM scheme. All these methods report the application of overmodulation switching only under dynamic operating conditions and therefore are also called dynamic overmodulation methods, [36].

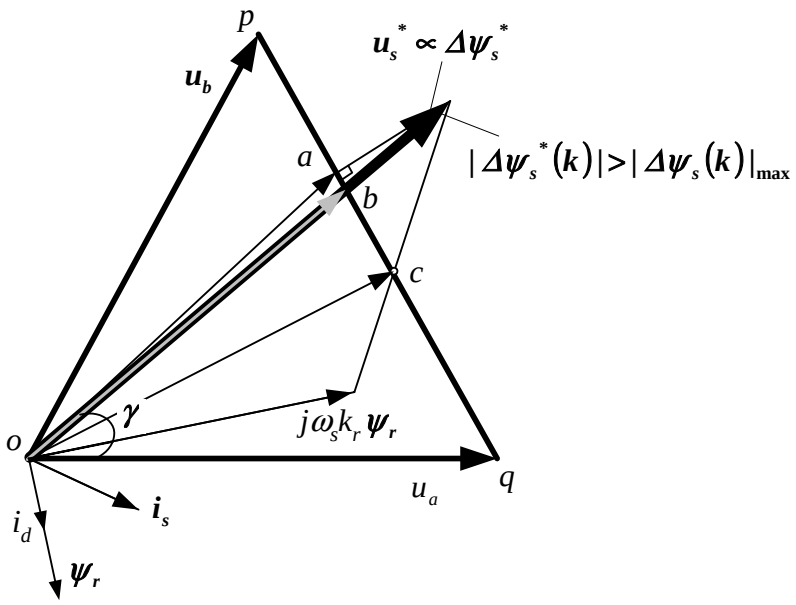

Figure 5.2: Switching strategies for dynamic torque control in the overmodulation region

During a dynamic condition in the overmodulation region, the voltage vector $\boldsymbol{u}_s^*$ required for torque control is outside the hexagonal voltage limit of the inverter, figure 5.2. As the inverter cannot provide this voltage, the switching strategy approximates it with a vector that lies on the hexagonal boundary. The different methods of obtaining this approximation can be distinguished from each other by

the criterion of selecting the voltage vector. In [1], the approximated voltage vector is such that there is no phase difference between the required voltage vector $\boldsymbol{u}_s^*$ and the readjusted reference voltage vector. Such vector is shown as *ob* in figure 5.2 as a grey line. Implementation of this switching strategy is very straightforward but the dynamic response is slow, [35]. On the other hand, the methods proposed in [33] and [35] are computationally intensive approaches, [36]. In [33], the approximated voltage vector is such that, the error between the magnitude of this vector and that of the required voltage vector $\boldsymbol{u}_s^*$ is minimum. This is shown as vector *oa* in the figure 5.2. In [35], the vector formed by the superposition of the back-emf vector and the PI current controller output vector $\boldsymbol{u}_s^*$ at the point of intersection of the line connecting these two vectors with the hexagon side. The intersection point of the PI controller vector with the hexagon side defines the tip point of the modified reference voltage vector. This vector is shown as *oc* in the figure. The improvement in the dynamic torque control performance of these methods ([33] and [35]) is marginal (as reported in [36]), when compared with the method of [1]. The reason for the marginal improvement lies in the difference in the way torque control is carried out. For instance, methods [33] and [35] have been implemented in a FOC scheme that necessitates the selection of voltage vector such that the field orientation condition is always met and the saturation of current controllers is prevented. On the other hand the dynamic overmodulation method of [1], has been implemented in a DTC-SVM scheme that relies on fastest possible change in the flux vector during a torque dynamic. Selection of any arbitrary voltage vector along the hexagonal boundary, may result in coupling and saturation of the current

controllers in the case of an FOC scheme. However since DTC-SVM does not use decoupled current controllers, it will not face these constraints. Hence DTC-SVM will have a better dynamic response compared with the FOC based method.

5.2 Effect of applying different voltage reference vectors on dynamic torque control performance

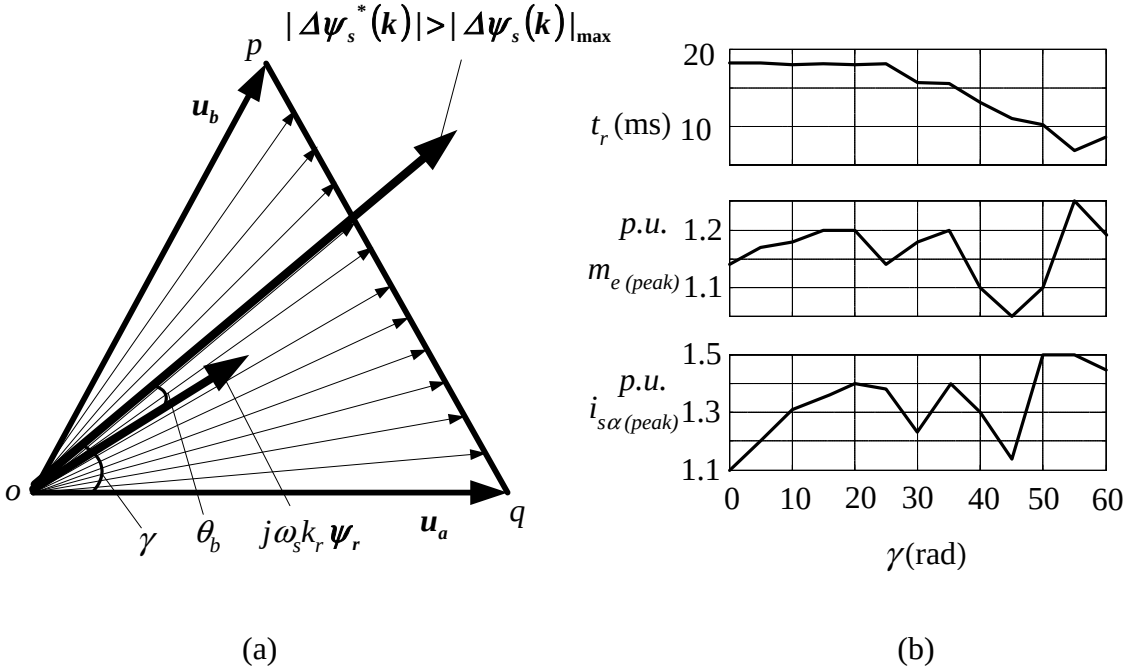

Figure 5.3: Peak torque, torque rise time and peak current when different voltage vectors are selected along the hexagonal boundary

In figure 5.3 (a) a dynamic overmodulation condition is depicted when the control is carried out using the proposed DTC-SVM scheme. This condition is initiated by applying a rotor angular velocity step of 0.45 $p.u.$ when the motor is operating at a rotor angular velocity of 0.9 $p.u.$ The reference stator flux error vector

$\boldsymbol{\Delta\psi}_s^*$ is outside the hexagonal boundary. Note that the vector $\boldsymbol{\Delta\psi}_s^*$ corresponds to the reference voltage vector $\boldsymbol{u}_s^*$ of figure 5.2. At the instant of the step, the back-emf $j\omega_s k_r \boldsymbol{\psi}_s$ was displaced from the reference stator flux error vector $\boldsymbol{\Delta\psi}_s^*$ by an angle θ_b of approximately 4.2^o, as shown in figure 5.3 (a). The hexagonal boundary is a locus of all possible vector displacements and any one of these can be used for switching, instead of the vector $\boldsymbol{\Delta\psi}_s^*$. The possible displacement vectors selected for testing the dynamic torque response differ from each other by an angle of 5^o, figure 5.3 (a). Continuous application of each of these vectors during dynamic conditions, results in a performance that is shown in figure 5.3 (b). The torque rise time represented as t_r in the figure is slowest, when the vector $\boldsymbol{u}_a$ is applied and improves as the adjusted reference voltage vector approaches $\boldsymbol{u}_b$. On the other hand, the peak torque that can be obtained varies between 1.05 to 1.25 $p.u.$ The variation of peak current during the dynamic, is between 1.1 to 1.5 $p.u.$ This analysis shows that the application of voltage vectors lying closer to the vector $\boldsymbol{u}_b$ result in a faster response, while application of voltage vectors closer to $\boldsymbol{u}_a$ result in a lower current. To elaborate on these effects and to observe the effect of application of reference voltage vectors $\boldsymbol{u}_a$ and $\boldsymbol{u}_b$ on the stator flux vector magnitude, simulation results of figure 5.4 will be used. In figure 5.4 (a), the vector displacement was done by continuously switching the voltage vector $\boldsymbol{u}_a$ for operation in a sector during the dynamic condition. This resulted in an increase in the stator flux vector magnitude above the nominal value during dynamic overmodulation. The rate of rise of currents was slow and the magnitudes of currents were around 1.0 $p.u.$

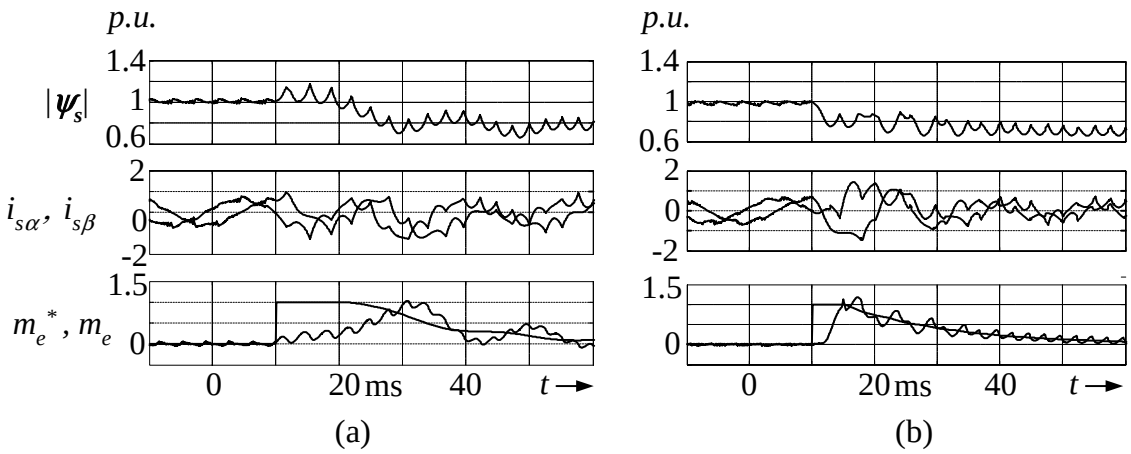

Figure 5.4: A study of different switching strategies for dynamic overmodulation. (a) when vector $\boldsymbol{u}_a$ is continuously switched and (b) when vector $\boldsymbol{u}_b$ is continuously switched

As a second option, voltage vector $\boldsymbol{u}_b$ was continuously switched. Figure 5.4 (b) shows that the dynamic response was very fast with dynamic field weakening (or reduction of the stator flux vector magnitude during dynamics). The magnitude of the stator flux vector monotonically reduces. The magnitudes of currents rise to a value of approximately 1.5 $p.u.$

5.2.1 Proposed method

The lack of the voltage reserve during dynamic overmodulation conditions, slows down the dynamic torque response of a DTC-SVM scheme. Such deficiency can be partly compensated by applying a voltage vector that moves the stator flux vector by a large angle. If the required reference stator flux error vector $\boldsymbol{\Delta\psi}_s^*$ is large, it will have a large magnitude and a large angle. Under these conditions, the angle γ of the vector $\boldsymbol{\Delta\psi}_s^*$ exceeds $\pi/6$ in a sector and the voltage vector $\boldsymbol{u}_b$ is continuously switched. This results in a sharp rate of rise of torque and currents

as shown in figure 5.5. However, as the operation shifts to a new sector, the angle γ has a value which is less than $\pi/6$. Under these conditions voltage vector $\boldsymbol{u}_a$ is continuously switched. This checks the rate of rise of currents. The switching of vectors $\boldsymbol{u}_a$ and $\boldsymbol{u}_b$ can be identified from the figure 5.5. Immediately after the step, there is a weakening of the stator flux vector magnitude, due to the fact that the vector $\boldsymbol{u}_b$ is being applied. However, instead of a continuous reduction, the stator flux vector magnitude stabilizes indicating the application of the vector $\boldsymbol{u}_a$. Hence, instead of doing PWM between two active vectors as in schemes [1], [33] and [35], continuous switching of the voltage vectors is proposed here.

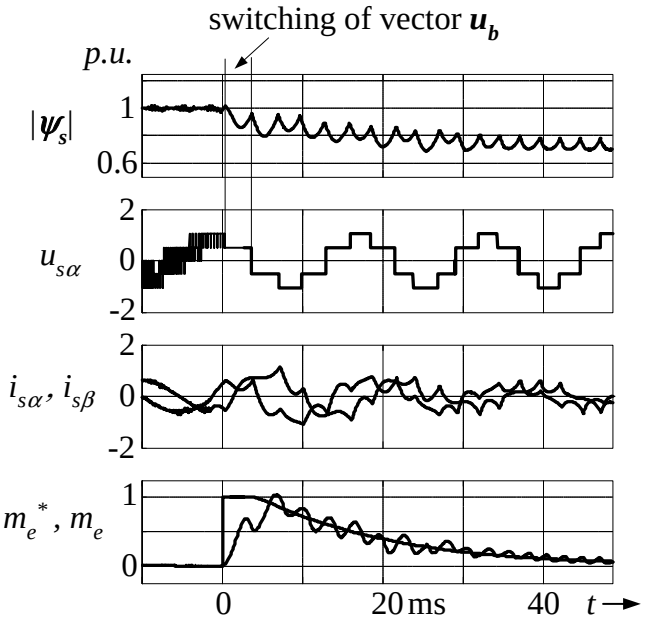

Figure 5.5: Result with the proposed method of switching

On the other hand, figure 5.6 shows the effect of applying the voltage vector as proposed in [1] (vector *ob* of figure 5.2). To apply such a vector, both $\boldsymbol{u}_a$ and $\boldsymbol{u}_b$ are switched in every sampling period. Such a switching results in a slower

dynamic response when compared to the proposed scheme. The magnitude of the stator flux vector reduces during the dynamic but this weakening is very slow. The current magnitudes are equal to 1.0 *p.u.* and the rate of rise of currents is gradual.

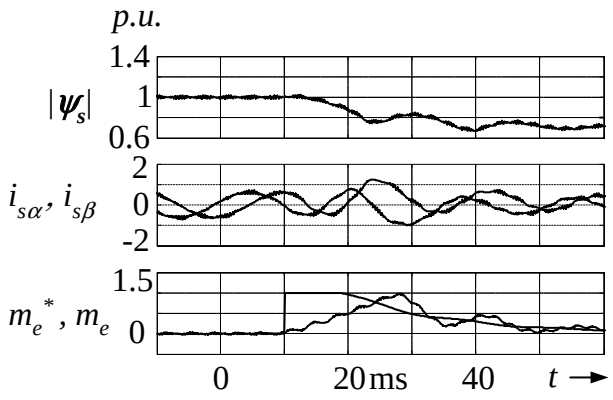

Figure 5.6: Result with the method proposed in [1]

It should be noted from figures 5.4 (b) and 5.5 that the dynamic response obtained using the proposed switching is slower than the one obtained in figure 5.4 (b) when only vector $\boldsymbol{u}_b$ was continuously switched. However, one important advantage of the proposed scheme is that the peak currents are less than 1.5 *p.u.* which is within the current rating of 2.0 *p.u.* of the inverter.

From the above analysis it can be said that, if the adjustment of the reference voltage vector is done based on any of the schemes, [1], [35] or [33], it will result in a voltage vector along the hexagon boundary even for very large reference stator flux error vector $\boldsymbol{\Delta\psi}_s^*$. To implement such an adjusted voltage reference vector, PWM between the active states needs to be carried out. Therefore when these methods are employed in a DTC-SVM scheme, the acceleration of the stator flux

vector will be slow. Hence the dynamic response time of the methods proposed in these references will be slower compared with the proposed method.

5.3 Analysis of dynamic overmodulation switching strategies

Any voltage vector on the hexagonal limit, is obtained by a suitable combination of the voltage vectors, $\boldsymbol{u}_a$ and $\boldsymbol{u}_b$. Figure 5.7 compares the affect of selecting

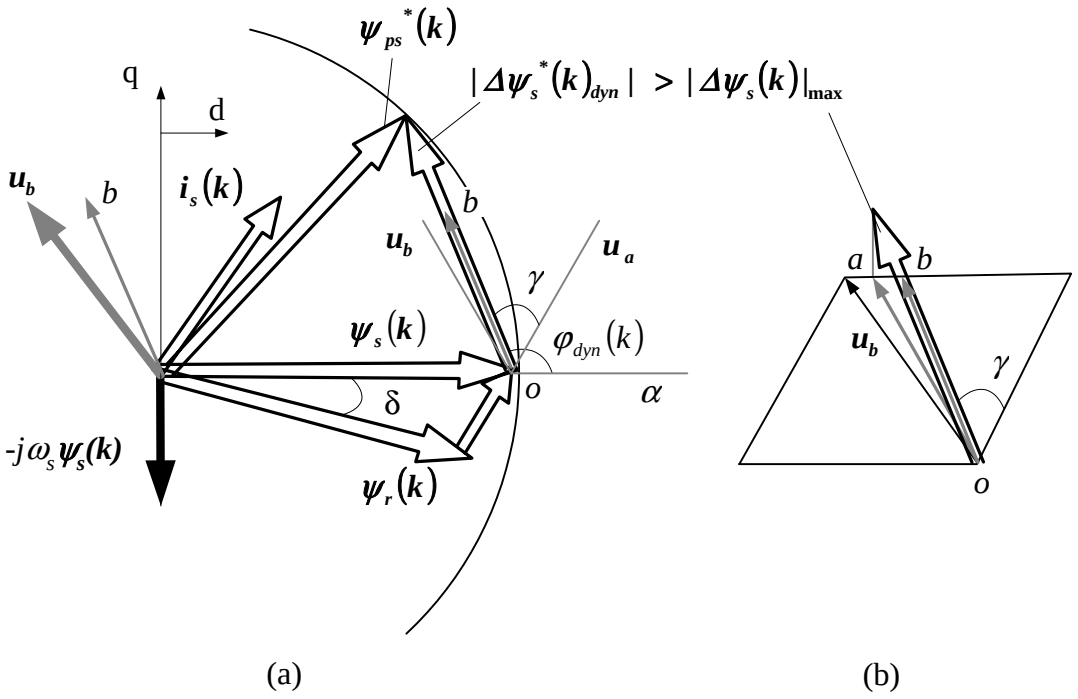

Figure 5.7: Analysis of different switching strategies during a torque dynamic in the overmodulation region

different switching options for the dynamic conditions depicted in the figure. Here vector *ob* is the voltage vector used in [1] and the other vectors are $\boldsymbol{u}_a$ and $\boldsymbol{u}_b$. For analyzing the affect of switching these vectors, the stator voltage equation will be

used. This equation can be arranged as follows,

$$\boldsymbol{i}_s = \frac{\boldsymbol{u}_s - j\omega_s \boldsymbol{\psi}_s}{r_s} = \frac{\boldsymbol{u}_s - \boldsymbol{u}_i}{r_s} \tag{5.1}$$

here, $\boldsymbol{u}_i$ is the induced-emf vector that is proportional to the back-emf vector of the machine. Vector $\boldsymbol{u}_s$ can be either $\boldsymbol{u}_a$, *ob* or $\boldsymbol{u}_b$. To understand the affect of switching, a d-q co-ordinate system can be considered such that the d-axis is aligned with the stator flux vector. Hence, $u_{iq} = \omega_s \psi_{sd}$. This gives,

$$i_{sd} + j i_{sq} = \frac{u_{sd}}{r_s} + j\frac{u_{sq} - u_{iq}}{r_s} \tag{5.2}$$

Following observations can be made from the figures, 5.7, 5.8 and equation 5.2.

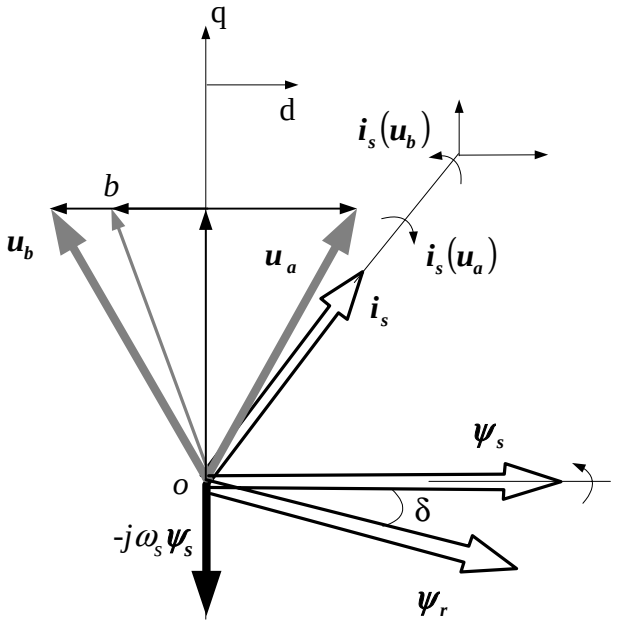

Figure 5.8: Current dynamics for application of the different voltage vectors under dynamic conditions

- Switching of the voltage vector $\boldsymbol{u}_a$ creates a positive q-axis component of the voltage vector along with a positive d-axis component. From equation 5.2,

this increases the positive d-axis current component resulting in an increase in the stator flux vector magnitude, figure 5.4 (a). At the same time the magnitude of the vector $\boldsymbol{u}_i$ is also increased, reducing the q-axis current and slowing down the dynamic torque response.

- Looking from the stationary co-ordinate system, the rate of change of torque is proportional to the rate of change of angle between the stator flux vector and the stator current vector. The affect of switching the voltage vector $\boldsymbol{u}_a$ can be explained using figure 5.8. Though the current magnitude and the stator flux vector magnitude increase, the angle between the stator current vector and the stator flux vector reduces resulting in a slower torque dynamic, figure 5.4 (a).

On the other hand, for the switching of voltage vectors $\boldsymbol{u}_b$ or *ob*, following observations can be made using equation 5.2 and figures 5.7 and 5.8.

- The extent of dynamic field weakening for the switching of voltage vector $\boldsymbol{u}_b$ is larger than when the voltage vector *ob* is applied. This is because of a larger magnitude of the negative d-axis component of the current vector. As a result, the magnitude of the vector $\boldsymbol{u}_i$ gets reduced, causing a sharp increase in q-axis component of the current vector.

- The rate at which the angle between the stator current vector and the stator flux vector increases, is much larger for the switching of $\boldsymbol{u}_b$ than when the vector *ob* is switched, giving a rapid dynamic torque response, figures 5.8, 5.4

(b).

To conclude, it can be said that the affect of applying the voltage vectors $\boldsymbol{u}_a$ and $\boldsymbol{u}_b$ are completely different. Continuous switching of $\boldsymbol{u}_b$ produces a fast torque dynamic. In [1] the application of vector *ob* will result in the switching of both $\boldsymbol{u}_a$ and $\boldsymbol{u}_b$ vectors in every sample but this combination of switching, results in a slower dynamic response. The fast dynamic characteristic of vector $\boldsymbol{u}_b$ is partly neutralized by the slower dynamic response characteristic of the vector $\boldsymbol{u}_a$ in every sampling period. The same condition holds true for the schemes [35] or [33] where PWM is done between the two voltage vectors during dynamic overmodulation. On the other hand, continuous switching of $\boldsymbol{u}_b$ speeds up the dynamic response whereas continuous switching of $\boldsymbol{u}_a$ stabilizes current. In the proposed method both these conditions exist based on the angle γ of the vector $\boldsymbol{\Delta\psi}_s^*$ in a sector. Thus vector $\boldsymbol{u}_b$ is switched when $\gamma > \pi/6$ giving fast acceleration and when $\gamma < \pi/6$ and sector transition has taken place, the vector $\boldsymbol{u}_b$ of the previous sector becomes vector $\boldsymbol{u}_a$ in the next sector, thus decelerating the stator flux vector. Hence a time optimal torque response is produced.

5.4 Dynamic torque control in the field-weakening region

At high angular velocity, the induction motor is operated in field weakening range due to voltage limit of the inverter. In this region of operation, two methods

of torque control are prominent (a) by Kim et. al in reference [42] that is implemented using FOC and (b) by Depenbrock in reference [11] that is implemented in the DSC method of direct torque control.

In [42], the controllable magnitudes of the d-axis and q-axis current references are obtained based on the available voltage reserve. Instead of weakening the rotor flux vector magnitude using the conventional $1/\omega$ rule, the authors use the continuous current rating of the motor and a voltage limit of 0.9 $p.u.$ of the inverter voltage limit, to decide the rotor flux magnitude level. The control scheme achieves a better performance than the conventional method of rotor flux vector magnitude weakening. However, steady state current and voltage limits are used for deciding the reference values of the d-axis and q-axis currents. The current limit used in

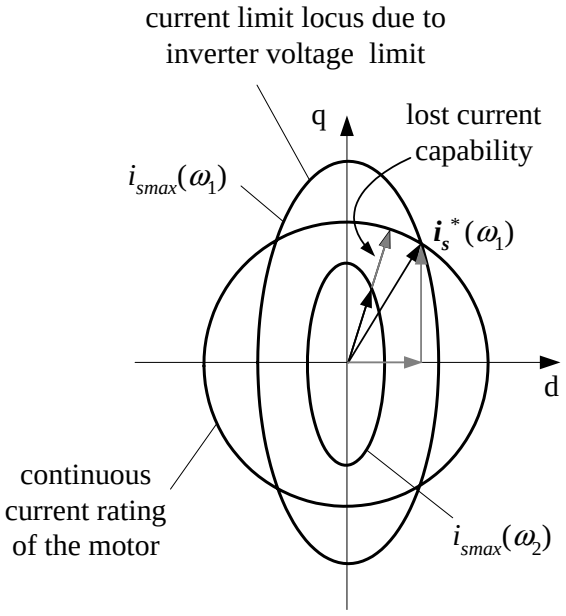

Figure 5.9: Reference current vector for field oriented current control does not exploit the installed voltage and current capability. Here $\omega_2 > \omega_1$

[42] is expressed as a circular locus while the current limit due to the voltage limit

is expressed in the form of an ellipse, figure 5.9. As the operating angular velocity increases, the size of this ellipse reduces and therefore the controllable d-axis and q-axis current magnitudes reduce as well. Since the control structure uses motor current limit and 0.9 *p.u.* of voltage limit, the current and voltage capability of the inverter cannot be exploited under dynamic conditions. The parameter sensitivity of this method was corrected by Harnefors et. al in reference [43]. However, the authors still use the current limit as suggested by the reference [42] and therefore there is no significant improvement in the dynamic response. In a similar approach, Griva et. al, [44] use the same voltage limit to generate the torque reference while the reference flux vector magnitude is determined using the d-q components of the current vector under limiting conditions. Hence their method requires co-ordinate transforms.

In Depenbrock's paper, [11], the method of field weakening depends upon the requirement of torque control. The optimum stator flux vector magnitude is calculated based upon the estimated rotor and stator flux vectors and the maximum possible change in the stator flux vector that can be achieved. To this end, simultaneous equations are solved in every sampling period that require the information of the rotor flux vector. Selection of switching state vectors is done based upon the calculated value of the reference stator flux vector magnitude and the error in torque. Unlike the FOC methods, DSC employs the weakening of the stator flux vector magnitude. This has the advantage of retaining the optimal torque capability, [59], [2] during field weakening region. Moreover, it is easier to incorporate in

a direct torque control structure.

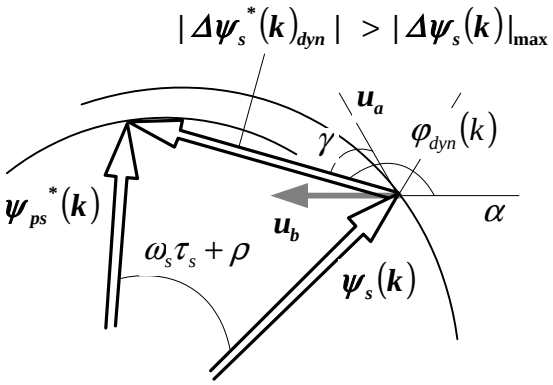

Figure 5.10: Dynamic operation in the field weakening region

In the proposed method, operation in the field-weakening range is carried out in the six-step mode and the synchronous angular velocity ω_s is used for field weakening. Figure 5.10 shows the principle of operation during a dynamic in the field-weakening region. If a rotor angular velocity step is given, the output of the torque controller produces a step increase in the angular velocity ω_s of the reference flux vector. This results in (a) a reduction in the magnitude of the predicted reference and (b) sharp increase in the angle (φ_{dyn}) of the error vector $\boldsymbol{\Delta\psi}_s^*$. The step change in the angle of the vector $\boldsymbol{\psi}_{ps}^*$ is represented as $(\omega_s\tau_s+\rho)$. Under these dynamic conditions, vector $\boldsymbol{u}_b$ is continuously switched. With the reduction in the error vector $\boldsymbol{\Delta\psi}_s^*$, normal six-step switching is carried out. As the synchronous angular velocity is commanded by the torque controller, the appropriate magnitude of the reference stator flux vector during a dynamic in torque is decided by the requirement of torque control. Since no limit is imposed upon the current vector magnitude, the current capability of the inverter is exploited.

In Depenbrock's method, [11], the calculation of (a) optimum stator flux vector magnitude and (b) change in the stator flux vector angle required for fast torque dynamic is based upon the information of the slip angular frequency. Calculation of slip angular frequency requires the information of the rotor flux vector which is not readily available in a DSC structure. However, in the proposed method, the slip angular frequency information is given by the torque controller. This avoids the use of rotor parameters which deviate from their normal range values during the field-weakening. Therefore the proposed method that uses slip and field weakening algorithm which seeks fast reduction in the stator flux vector magnitude, is simple to implement. It exploits the inherent advantages of the DSC structure without needing the parameter dependant calculation of the rotor flux vector. As compared to FOC methods, it does not have problems of controller saturation or low frequency harmonics. Moreover due to the inherent coupled structure of the induction motor during field-weakening, a decoupled control as in FOC is not very suitable for dynamic field-weakening.

5.5 Experimental results

Figure 5.11 gives a comparison of the dynamic torque control performance between the proposed method and the method described in [1]. The motor was operating under steady state when a step change in the rotor angular velocity command is given. The dynamic response is much faster in the proposed method due to sharp flux weakening and rate of rise of currents during the dynamic overmodu-

lation. Note that the currents are within the motor rated current of 1.0 *p.u.* In the region of operation above base speed, the reference torque is limited to a value of $m_{e(max)}$ such that constant rated power operation is maintained. Dynamic control

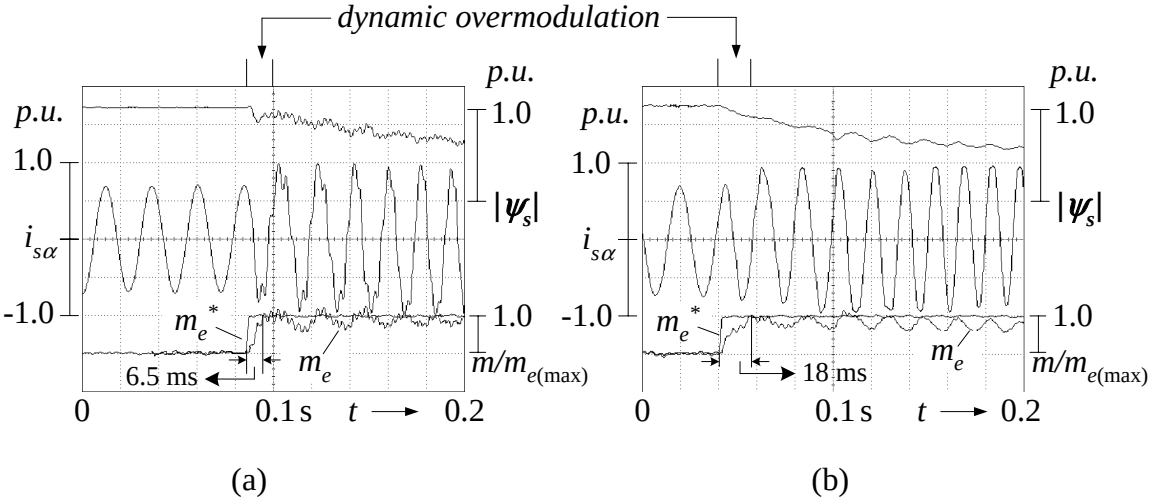

Figure 5.11: Dynamic response for a speed step from 0.85 to 1.35 *p.u.* (a) proposed method (b) method suggested in [1]

of the magnitude of the stator flux vector and torque is shown in figure 5.12. As the phase angle of the error vector at the instant of application of the step is large there is an initial dip in the stator flux vector magnitude. The stator flux vec-

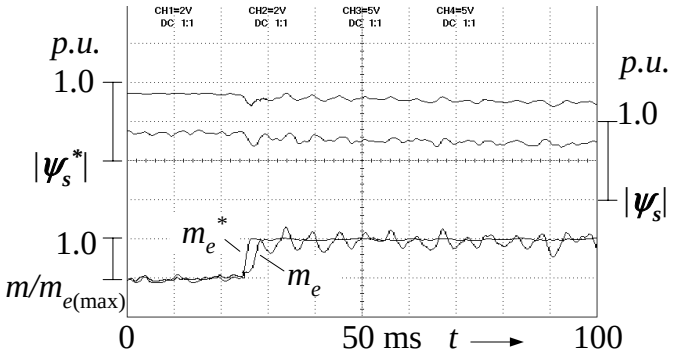

Figure 5.12: Control of torque and flux vector magnitude for a step change in the rotor angular velocity from 1.25 *p.u.* to 2.0 *p.u.*

tor magnitude is defined by the synchronous angular velocity commanded by the

torque controller. Flux vector trajectory for a step increase in the rotor angular velocity command during six-step operation is depicted in figure 5.13. The reduction in the flux vector magnitude during the transient period, is more than the steady state value attained by it after the transient has died down. This dynamic field weakening causes the current vector magnitude to increase to bring about a fast torque dynamic with six-step operation.

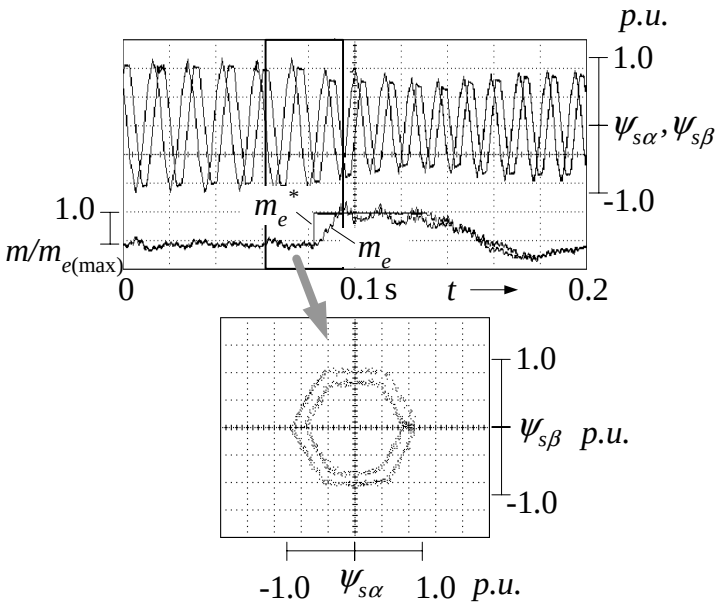

Figure 5.13: Flux vector trajectory for a dynamic in the six-step region, rotor angular velocity command 1.3 *p.u.* to 1.75 *p.u.*

In figure 5.14, the magnitude of the current vector for a torque dynamic in the field-weakening region is shown to be within the upper limits of 2.0 *p.u.* of the inverter. Figure 5.15 gives the dynamic torque response in the field weakening range of operation while figure 5.16 shows the inherent current control feature during dynamic torque control in the field weakening region. Unlike FOC methods, current control is not done and no deliberate limit is imposed upon the maximum

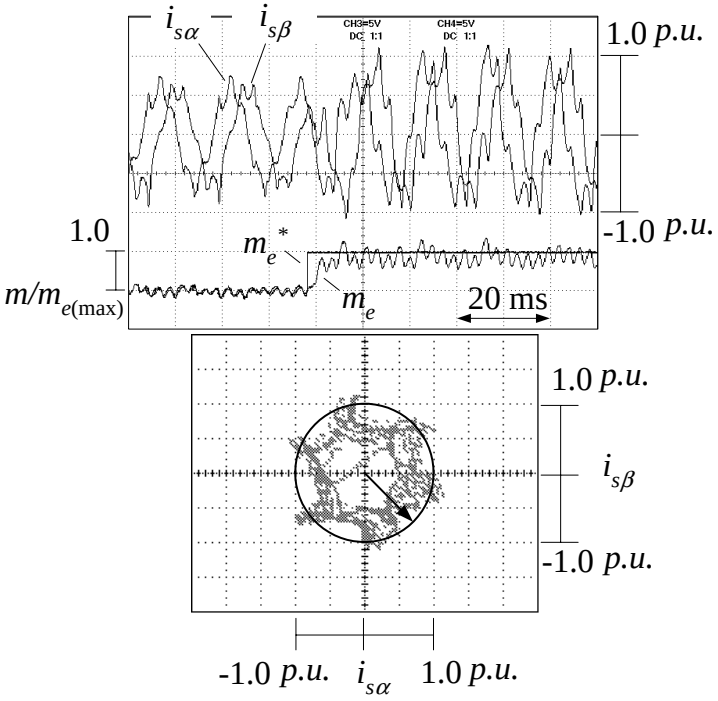

Figure 5.14: Test result showing phase current for a torque dynamic during six-step operation when a speed step from 1.34 *p.u.* to 1.7 *p.u.* is given

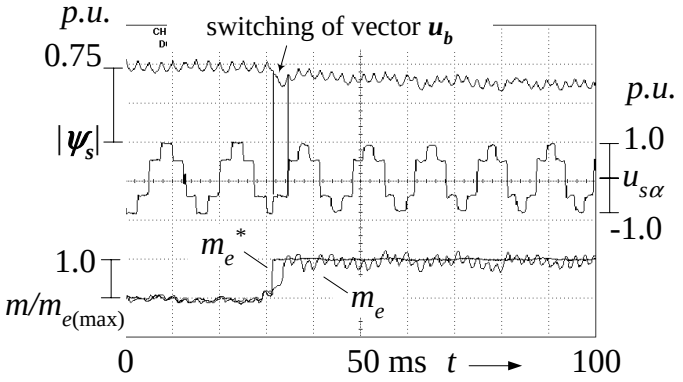

Figure 5.15: Test result of Torque control for a speed step from 1.34 *p.u.* to 1.7 *p.u.*

value of phase currents. As voltage limit is already exhausted, the currents rise to a value that ensures that the rate of change of active power drawn by the motor is increased during the dynamic period. This implies that the current limit of the inverter is exploited during the dynamics.

The result of figure 5.17 shows that smooth control of speed and torque can

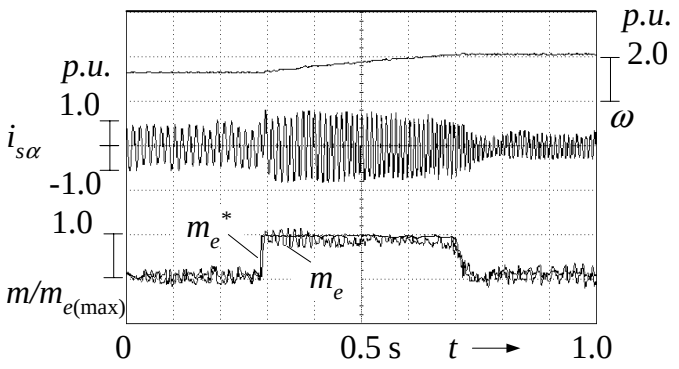

Figure 5.16: Test result showing current with torque dynamic during six-step operation for a speed step from 1.34 *p.u.* to 2.15 *p.u.*

be achieved in the field-weakening region. In this experiment a large speed step of 3.8 *p.u.* was given at an operating angular velocity of 0.1 *p.u.*. This experiment was performed at a voltage that is half the rated DC-link voltage of the inverter so as to maintain the 4 times rated speed below the mechanical limit of the test drive. These results demonstrate the ability of the proposed scheme to optimally control

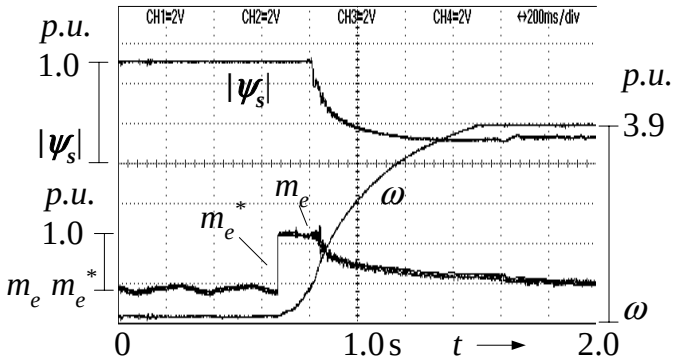

Figure 5.17: A rotor angular velocity step from 0.1 *p.u.* to 3.9 *p.u.*

the torque by completely exploiting the physical constraints of the inverter.

5.6 Summary

In this chapter, the analysis of the proposed DTC-SVM method has been extended to the field-weakening region of operation. Full utilization of the installed voltage and current capability enables fast dynamic response in the overmodulation range. When the operation is in the six-step mode, the rate of change of stator flux vector angle is maximum. Since the upper limit of the inverter voltage is reached, the current capability is exploited to bring about a fast dynamic response. This is achieved without complicating the original method of torque control. The next chapter will describe the hardware that has been used to implement the method proposed in this work.

Chapter 6

Description of hardware

6.1 Overview of the Implementation Scheme

The experimental set-up for implementing the proposed DTC-SVM scheme for induction motor has been built up, using dSPACE DSP–ds1102 processor board and rapid-prototype software tools, as shown in the block diagram of figure 6.1. The experimental set-up comprises of following units:

- A pentium PC for rapid-prototyping and real-time control.
- A DSP-ds1102 controller board for running control programs, generating control signals, sampling feedback signals and communicating with the computer.
- An interface board for logic operations, buffering, isolations, protection, etc.
- A voltage source inverter (VSI) for driving the induction motor
- An induction motor installed with an incremental encoder.

- A racking system that essentially is a hardware interfacing system. It comprises a 19" sub-racking system and several other cards which are: Digital I/O Card, Control-PWM Card and Analog-signal Cards

- Sensing devices. These include current sensors, voltage sensors and position encoder. Current and voltage sensors are enclosed in the sensor box connected in between the inverter and the induction motor. The position encoder is mounted on the end of the shaft of the motor.

- A loading system (DC generator) for producing load torque to the induction motor.

6.2 Controller board

The dSPACE DS1102 controller-board is specifically designed for the development of high-speed multivariable digital controllers and real time simulations in various fields such as motor drives, [60], [61], [62]. The board consists of a floating-point DSP TMS320C31, a DSP-microcontroller TMS320P14 based digital-I/O subsystem, A/D & D/A converters and encoder interfaces. The main DSP processes the numeric intensive algorithms and the DSP-microcontroller has the function of PWM generation. The A/D converters can be used to convert analogue feedback signals such as stator-current signals to digital signals. The encoder interface is specially designed to interface with the incremental encoder to acquire rotor-position data. The controller board is designed like an expansion card that can be inserted

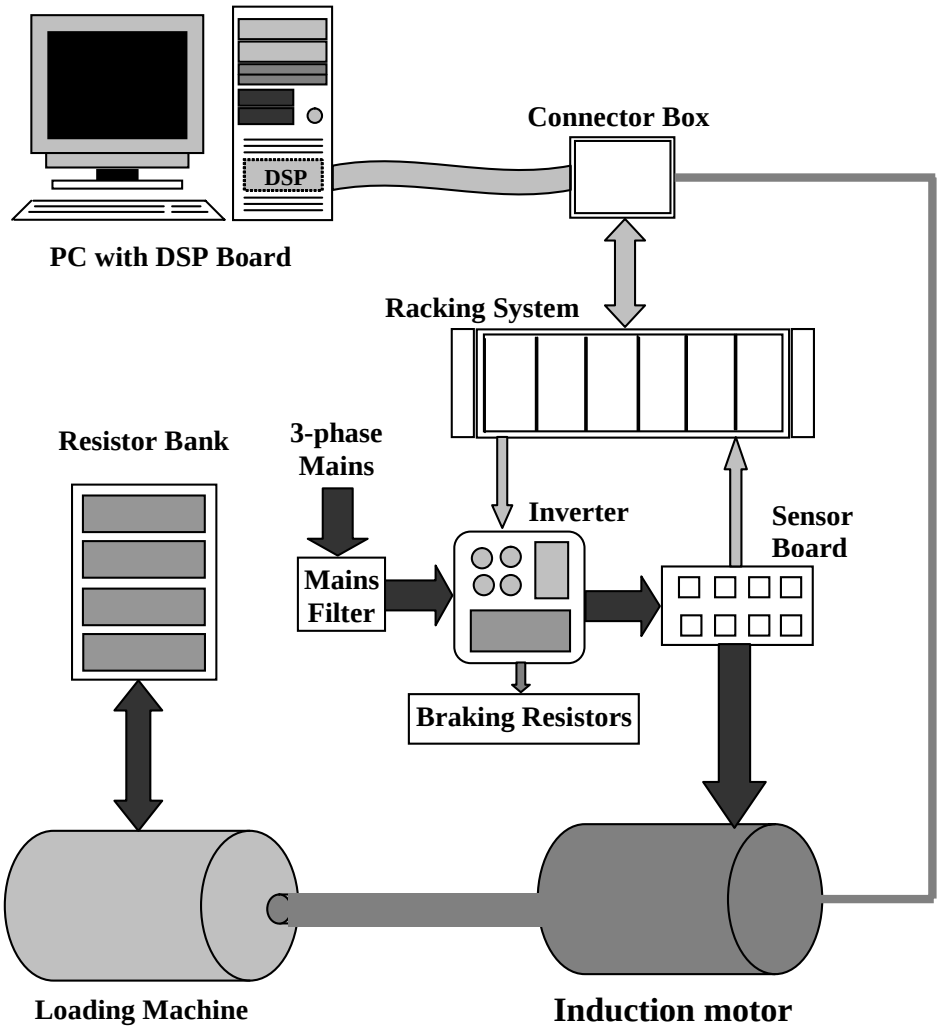

Figure 6.1: Platform used for hardware implementation

in the expansion slot of the personal computer. Depending on the communication between the PC and the DSP, users can debug the program as well as tune parameters and trace execution results in real-time. Figure 6.2 shows the block diagram of the architecture of DSP ds1102 controller board.

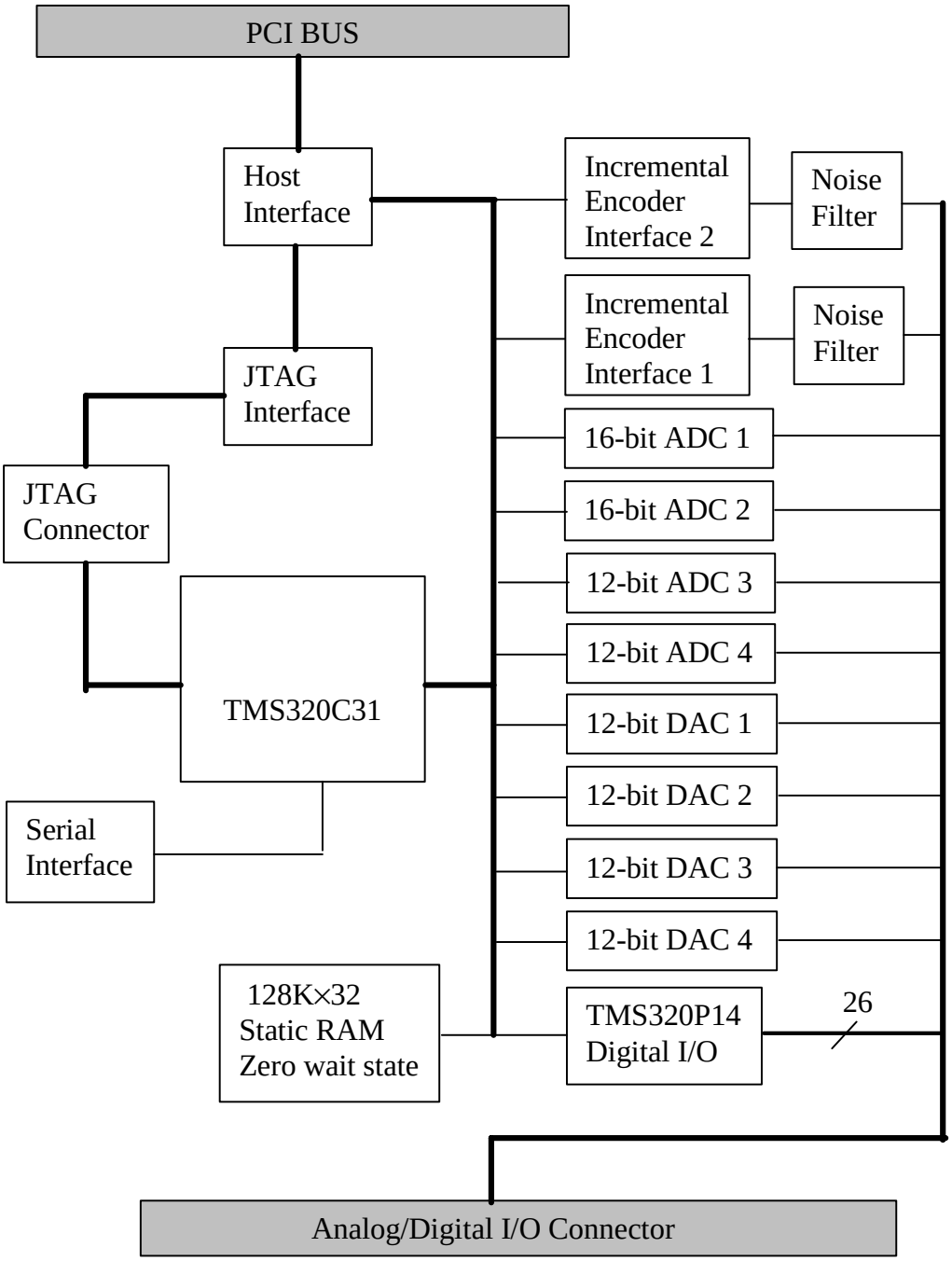

Figure 6.2: Configuration of the controller board used for hardware implementation

6.3 The Peripheral Interface Circuit

It is necessary to design a hardware interface circuit to perform the following functions,

- Using EX-OR gates to generate mid-symmetrical PWM signals
- Generating six PWM signals to control the six switches of the PWM inverter
- Incorporating dead-time in the PWM signals
- Using current sensors for stator currents
- Buffering the pulse signals generated from the incremental encoder
- Setting over-current/voltage protections and reset/stop functions.

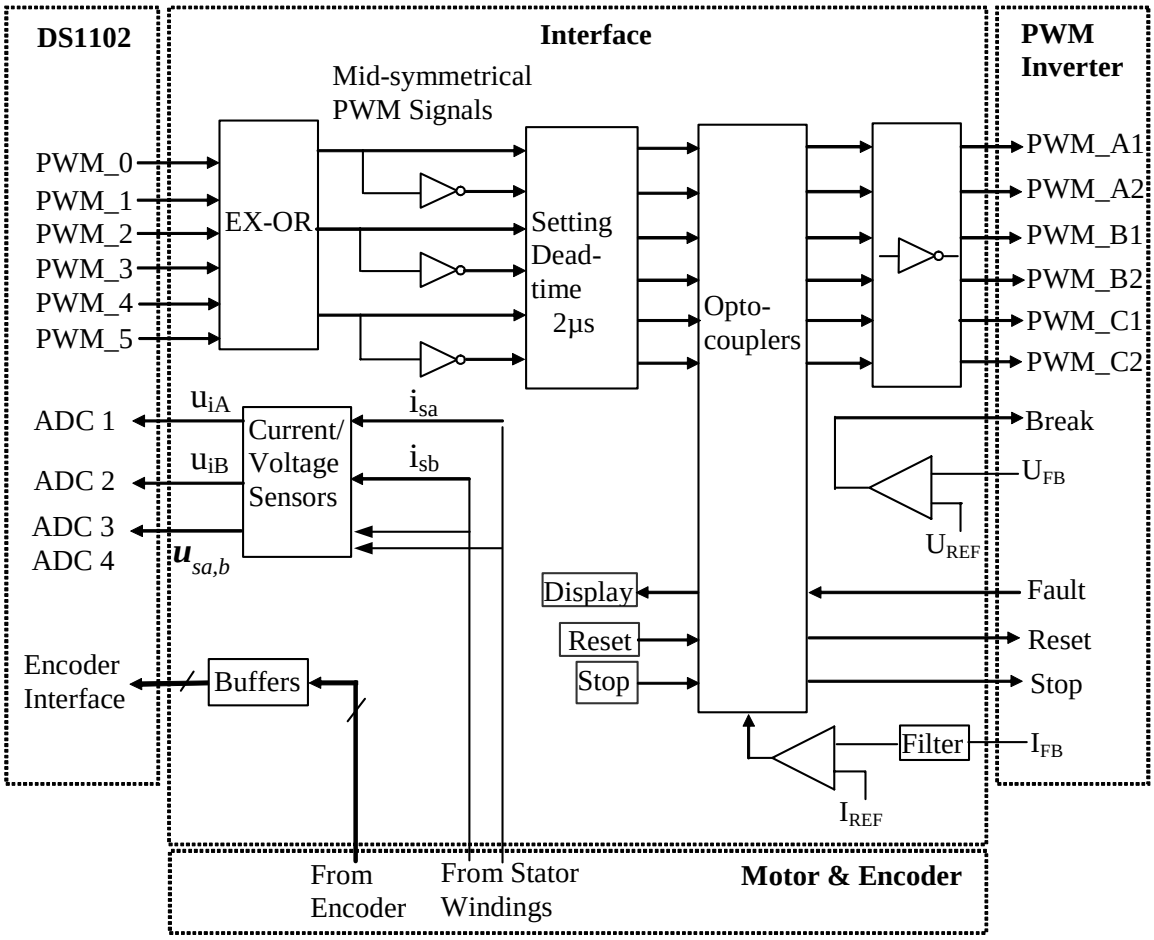

Figure 6.3: Interfacing the controller board with the control circuit

The block diagram of the peripheral interface circuit is shown in Signals of the six PWM channels, which are ch0 and ch1 for phase A, ch2 and ch3 for phase B, and ch4 and ch5 for phase C, are EX-ORed and become three mid-symmetrical PWM signals. Another three complementary signals are obtained from three logic inverters. Proper "dead time" is then incorporated in these six PWM signals to avoid "mutual-ON" of the upper and lower switches on the same phase of the inverter. The opto-couplers transfer the six PWM signals and isolate the low-side circuit from the high-side circuit. The six PWM signals are inverted in "low-active" signals as required by the inverter and then sent to the inverter. Signals of "Reset" and "Stop" are also sent through opto-couplers to control the inverter. Voltage comparators are used to detect over voltage and over current. "Fault" signals generated by the inverter and the voltage comparators are sent through opto-couplers to the low-side circuit to inhibit the transfer of the PWM signals. The installed current sensors and resistors convert the current signals in voltage signals for the use of A/D converters of ds1102. Signals from the incremental encoder are sent through buffers to shape the waveforms and to drive the encoder interface circuit of ds1102.

6.4 Generation of the SVM switching pattern using the dSPACE ds1102 card

The SVM switching pattern is not provided in the ds1102 card. Therefore, a switching logic has been developed to implement SVM switching with the already

available configuration. For the generation of the train of pulses for SVM technique the "variable switching frequency configuration" that is available from the dSPACE card is used. The function $ds1102\_p14\_pwmvar(longchannel, floatduty)$ is used to generate variable frequency PWM duty cycle. This duty cycle of the selected channel is updated to the new value specified by the parameter *duty*, which must be a value in the range $0-1.0$. The parameter *channel* must be in the range $1-6$.

In the conventional SVM switching, one sampling cycle τ_s is divided in a set sub-cycle and a reset sub-cycle. In the set sub cycle the sequence of switching is, $\frac{\tau_0}{4} - \frac{\tau_a}{2} - \frac{\tau_b}{2} - \frac{\tau_0}{4}$ while in the reset sub cycle it is, $\frac{\tau_0}{4} - \frac{\tau_b}{2} - \frac{\tau_a}{2} - \frac{\tau_0}{4}$. Here, τ_0, τ_a and τ_b are the switching state times that are already available to implement switching. The nature of variation of the switching states S_a, S_b and S_c for operation in the sector 0 is shown in figure 6.4. These states signify whether the upper switches

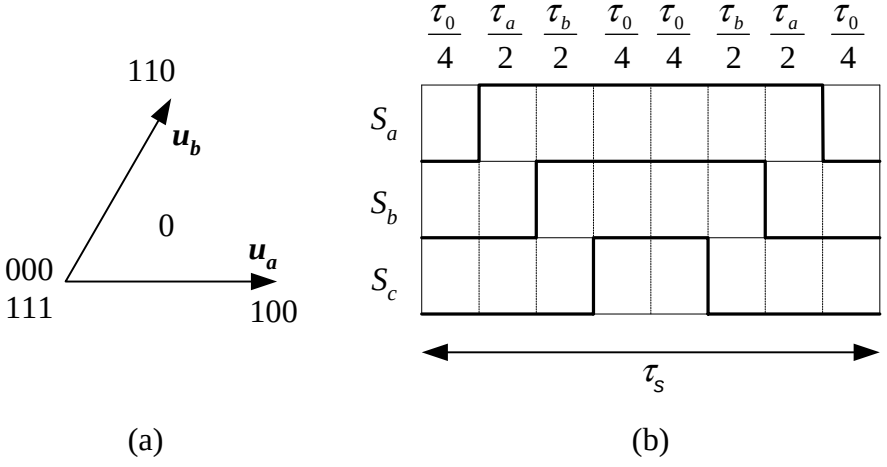

Figure 6.4: SVM switching pattern for operation in sector 0

of a three phase two level inverter are ON or OFF. For instance, 100 means, the upper switch of the first inverter leg is ON while those of the other two legs are

OFF. If it is desired to obtain the variation of state S_a as shown in figure 6.4 (b), two pulses P_1 and P_2 need to be defined in the control algorithm such that their duty ratios d_{1a} and d_{2a} are,

$$d_{1a} = \frac{\tau_0/4}{\tau_s}$$
$$d_{2a} = \frac{\tau_s - \tau_0/4}{\tau_s} \tag{6.1}$$

respectively. Using function $ds1102\_p14\_pwmvar(longchannel, floatduty)$ the pulses

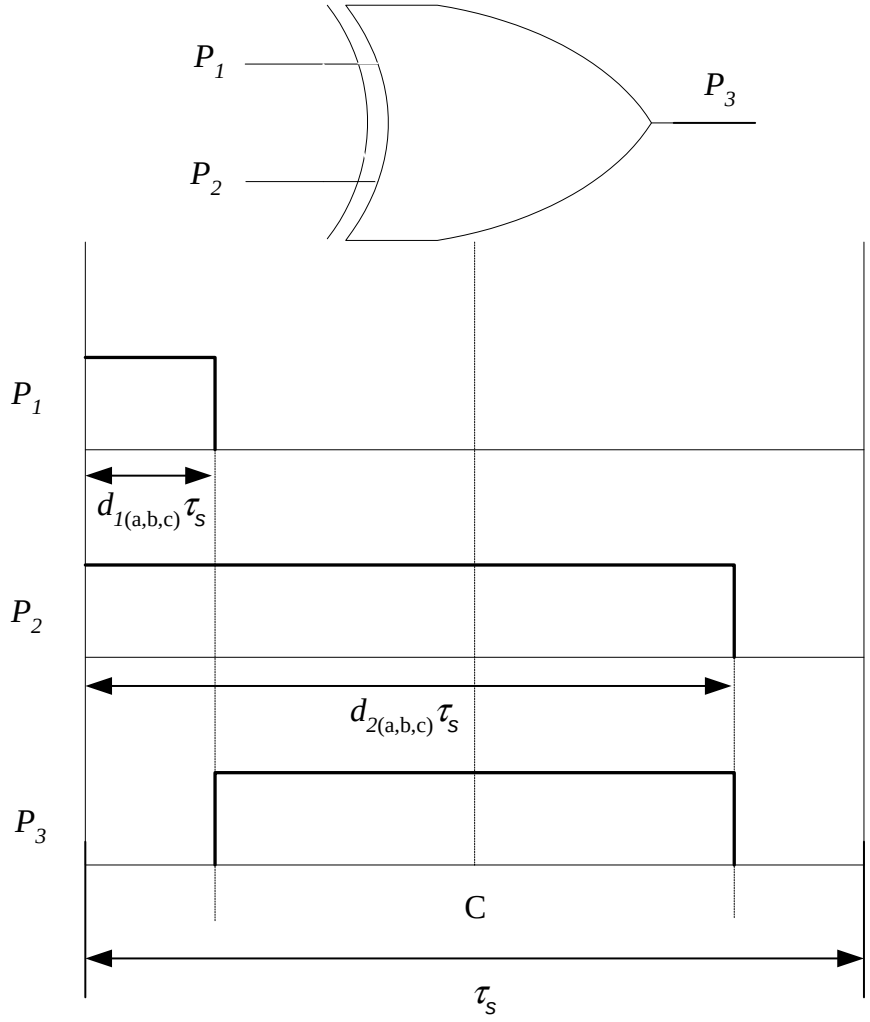

Figure 6.5: Mid-symmetrical pulse generation using an EX-OR gate

with duty ratios d_{1a} and d_{2a} are output from channels 1 and 2 to the EX-OR gates

of figure 6.3. The EX-OR combination of these two pulses will result in a pulse S_a as shown in figure 6.5.

Similarly for sector 0 suitable pulses P_1 and P_2 to generate S_b and S_c can be obtained from figure 6.4 (b) and stored. For example, the duty ratios of the pulses required to generate S_b are given as,

$$\begin{aligned} d_{1b} &= \frac{\tau_0/4 + \tau_a/2}{\tau_s} \\ d_{2b} &= \frac{\tau_s - (\tau_0/4 + \tau_a/2)}{\tau_s} \end{aligned} \tag{6.2}$$

and to generate S_c,

$$\begin{aligned} d_{1c} &= \frac{\tau_s/2 - \tau_0/4}{\tau_s} \\ d_{2c} &= \frac{\tau_s/2 + \tau_0/4}{\tau_s} \end{aligned} \tag{6.3}$$

are the respective duty ratios. Figure 6.6 shows the experimental result that is

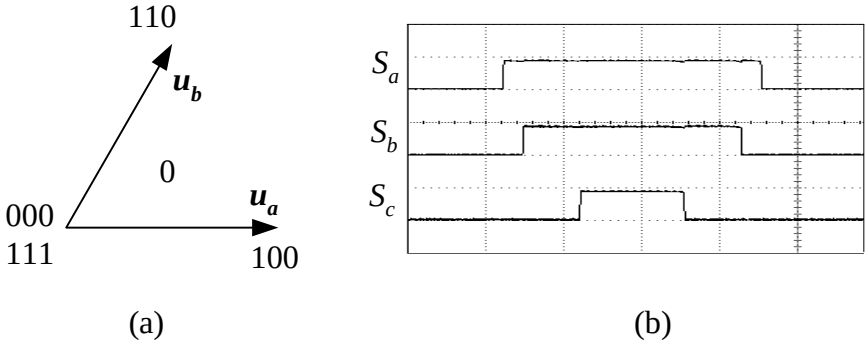

Figure 6.6: SVM switching pattern for operation in sector 0, figure (b) shows the experimental result

obtained with the proposed method using a ds1102 card.

To obtain the duty ratios for switching in the other sectors, the timing diagrams like the one for sector 0 (figure 6.4 (b)) have been used. The variable duty

ratios are stored in the control algorithm itself. Hence the algorithm first checks the sector of operation and then uses the appropriate sets of duty ratios to implement SVM.

6.5 Inverter

The PWM inverter used for the hardware implementation is called PowIRTrain, which is an integrated subsystem from International Rectifier, combining all power conversion and power control that is functionally required for building state-of the-art AC drives and controls in modules or assemblies. PowIRTrain includes all required power semiconductor devices and associated circuitry in one package. It consists of a 3-phase input rectifier, a 3-phase IGBT inverter stage with a braking switch, gate drive, power terminations, DC link capacitor with soft charge scheme, surge suppression, current/voltage/temperature sensing with associated protection circuits, system power supply as well as control interface. According to the power rating of the test motor (0.75 kW) and model, a 2.2 kW model named IRPT2062C is selected for the hardware implementation.

6.6 Motor Specifications

The experimental induction motor is 0.75 kW, 4-pole, 3-phase squirrel cage induction motor having the following specifications.

Table 6.1: Parameters of test machine

$Motor$	$Rating$	R_s	R_r	L_{ls}	L_{lr}	L_h	J
IM_{lab}	0.75	8.35Ω	6.12Ω	0.03596H	0.03596H	0.5633H	0.0024

Chapter 7

Conclusions

DTC-SVM in this thesis is achieved using stator flux vector control in stationary co-ordinates. Steady state and dynamic control of torque has been carried out using a cascaded control structure with an inner stator flux vector control loop and outer torque and rotor angular velocity loops. Following are the important features of the proposed DTC-SVM scheme.

- Chapter 3 of this dissertation describes the closed loop stator flux vector control method. Using a simple method of prediction, the problem of phase error that exists in the DTC-SVM schemes of Habetler et. al, [1] and Casadei et. al, [20] has been eliminated. The proposed overmodulation algorithm results in lower distortion of flux waveform and in comparison with the existing methods, achieves control of average angular velocity of the stator flux vector, throughout the overmodulation region as seen in figures 3.22 and 3.23. Control of average angular velocity of the stator flux vector eliminates the

phase error in overmodulation. This solves the problem of current control using FOC in the overmodulation region, without requiring an inverse model as proposed in reference [32]. Fast dynamic response for a change in the stator flux vector angle and magnitude is obtained, as the control scheme selects an appropriate voltage vector that causes the magnitude and phase angle of the stator flux vector to change at the maximum possible rate.

- In Chapter 4, steady state and dynamic control of torque in the normal and overmodulation regions have been described. The proposed scheme achieves direct torque control at constant switching frequency. Hence the switching capability of the inverter is fully exploited. This is an advantage over the classical DTC/DSC methods in which the switching frequency varies with rotor angular velocity and is maximum at 0.5 $p.u.$ The torque ripple analysis in the normal region shows that the ripple in torque is a function of operating angular velocity, in any constant switching frequency DTC-SVM scheme. Only a few schemes can achieve overmodulation with closed loop torque control. The proposed overmodulation switching strategy maintains a constant average torque over the sector during steady state operation.

  A large signal algorithm is used during the dynamic operation. This produces a torque response which is similar to that obtained with the classical DSC as seen in figures, 4.27 and 4.20. This ensures that the inverter voltage and current capabilities are fully utilized.

- Dynamic control of torque at large operating angular velocities is discussed

in the fifth chapter. Steady state and dynamic torque control during field-weakening is carried out with six-step operation. When the voltage reserve decreases in field-weakening region, the current capability of the inverter is fully utilized to obtain a fast torque dynamic. As noted in chapter 5, the FOC based schemes presented in references [42], [43] and DTC-SVM based scheme by Griva et. al in reference [44] work at an inverter voltage limit which is 90% of the installed capacity.

- Using the fundamental equations of machine and the errors in torque and stator flux vector, the analysis presented in chapter 4 shows how the inherent current control works in any DTC method. Such analysis has been missing in the literature. It is shown how the current vector magnitude can be limited by limiting the rate of change of the stator flux vector angle.

Study of current vector dynamic in a DTC scheme is important because the currents are not deliberately controlled and also because there is no limit imposed on the magnitude of the current vector. On the other hand, steady state and dynamic control of torque in a rotor FOC scheme necessitates decoupled control of the torque and rotor flux vector producing current components. It would be of interest to know how the current vector behaves during dynamic in proposed DTC-SVM method, when observed from the rotor flux co-ordinate system.

7.1 Relation between the proposed DTC-SVM and rotor FOC scheme

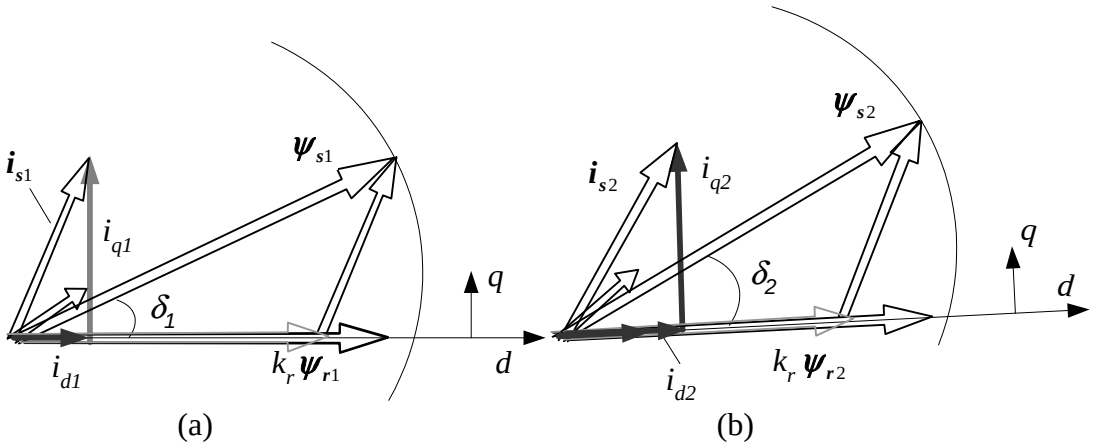

Figure 7.1: (a)Dynamic operation using FOC method (b)Dynamic operation using DTC-SVM method

Figure 7.1 shows the dynamic torque control using FOC and DTC-SVM methods. Figure 7.1 (a) shows the dynamic operation using a rotor FOC method while figure 7.1(b) shows a dynamic condition using a DTC-SVM method. Torque in a DTC scheme is interpreted as the vector product between the stator and rotor flux vectors. In a rotor FOC method, it is given by the product of the q-axis current component and the rotor flux vector magnitude. During a dynamic in torque, the stator flux vector is changed at the fastest possible rate. This results in a current vector that responds in a manner as shown in figure 7.1 (b). Figure 7.2 simulates a dynamic torque condition using the proposed method while the current vector dynamic is observed with respect to the rotor co-ordinates. Both d-axis and q-axis current components change. This can be reasoned in the following manner. In a DTC-SVM scheme, the magnitude and phase angle of the stator flux vector are

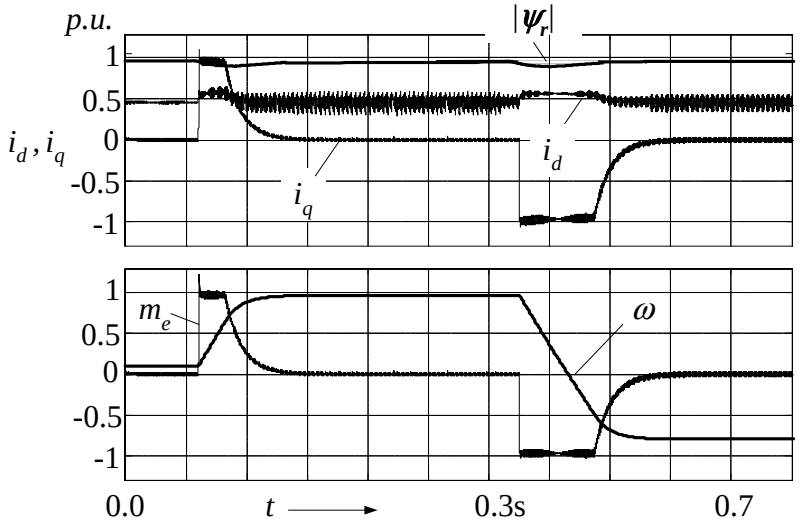

Figure 7.2: Current dynamics with respect to the rotor flux vector for a step change in torque using the proposed DTC-SVM method of torque control

controlled. During dynamics, a voltage vector is applied to produce fast change in angle of the stator flux vector. As the stator flux vector follows this voltage vector, the current vector gets adjusted so as to bring about the commanded change in the stator flux vector. This results in a small change in the d-axis current component, when viewed from the rotor co-ordinates. On the other hand, in rotor FOC the applied voltage vector will control the current vector so as to maintain the d-axis current constant and will increase the q-axis current, figure 7.1 (a). As a result, the stator flux vector will change such that the current control requirements are met.

Although co-ordinate transforms are not used, the extent of dynamic decoupling of a DTC-SVM method when viewed from rotor co-ordinates is much better when compared with a simple V/f scalar control.

7.2 Speed sensorless operation

Speed sensorless operation has not been the focus of the present work. However, a simple sensorless control was implemented by exploiting the control structure of the proposed DTC-SVM method. The control strategy is shown in the block diagram of figure 7.3. The flux error vector $\boldsymbol{\Delta\psi}_s(k)$ is used to obtain the

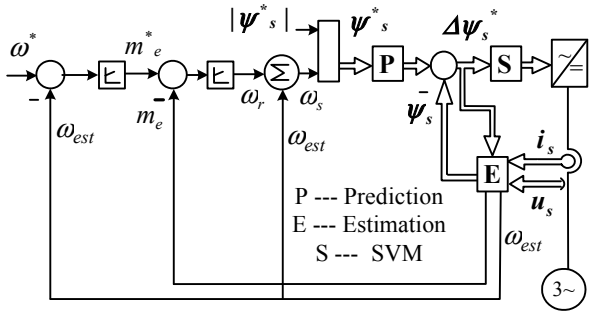

Figure 7.3: Block diagram for speed sensorless dynamic torque control using the proposed method

synchronous angular velocity ω_s. Hence,

$$|\boldsymbol{\Delta\psi}_s(k)| = |\boldsymbol{\psi}^*_{ps}(k) - \boldsymbol{\psi}_s(k)| = 2.|\boldsymbol{\psi}_s(k)|\sin(\omega_s\tau_s/2). \tag{7.1}$$

(7.2)

This gives,

$$\omega_{s(est)} = \frac{2}{\tau_s}\sin^{-1}\frac{|\Delta\boldsymbol{\psi_s(k)}|}{2|\boldsymbol{\psi^*_s(k)}|} \tag{7.3}$$

This synchronous angular velocity is filtered to eliminate the switching harmonics. Rotor angular velocity ω is estimated using the expression $\omega = \omega_s - \omega_{rest}$. Here ω_{rest} is the estimated slip frequency and is given as $m_e r_r/|\boldsymbol{\psi}_r|^2$. Figure 7.4 shows the dynamic torque control for a rotor angular velocity step of 0.34 pu. The estimated

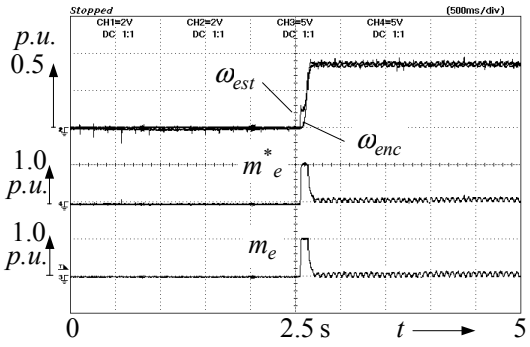

Figure 7.4: A step of 500 RPM from standstill, using estimated rotor angular velocity for closed loop drive operation

rotor velocity is equal to the angular velocity obtained from the encoder, except at values near zero, as shown in the figure.

Hence without changing the original control structure, a speed sensorless control is possible with the proposed method.

To conclude, this dissertation has presented a DTC-SVM method that has the advantages of both the classical DTC and constant switching frequency SVM. Predictive control of stator flux vector solves the phase error problem in normal region while average angular velocity control of the stator flux vector helps to achieve closed loop torque and stator flux vector control in the overmodulation region. Exploitation of the voltage and current capabilities of the inverter helps to achieve good dynamic response in the entire speed range of operation.

Bibliography

[1] T. G. Habetler, F. Profumo, M. Pastorelli, and M.Tolbert, "Direct torque control of induction machines using space vector modulation," *IEEE Trans. on Industry Applications*, vol. 28, pp. 1045–1053, Sept/Oct 1992.

[2] R. Krishnan, *Electric Motor Drives Modelling, Analysis and Control*. New Jersey: Prentice Hall, first ed., 2001.

[3] D. W. Novotny and T. A. Lipo, *Vector Control and Dynamics of AC Drives*. Oxford: Oxford Science Publications, first ed., 1996.

[4] F. Blaschke, "The principle of field orientation as applied to the new transvektor closed loop control system for rotating field machines," *Siemenes Review*, p. 217, 1972.

[5] K. Hasse, "Zur dynamik drehzahlgeregelter antriebe mit stromrichtergespeisten asynchron-kurzschlusslaufermachinen. phd thesis, th darmstadt," 1969.

[6] R. Gabriel, W. Leonhard, and C. Nordby, "Microprocessor control of the converter-fed induction motor," *Process Automation*, p. 35, 1982.

[7] T. M. Rowan and R. J. Kerkman, "A new synchronous current regulator and analysis of current-regulated pwm inverters," *IEEE Transaction on Industry Applications*, vol. 22, no. 4, pp. 678–690, 1986.

[8] H. Shierling, "Self commissioning- a novel feature of modern inverter-fed induction motor drives," in *In IEE conference on power electronics and variable speed drives, London, U.K.*, pp. 287–290, 1988.

[9] L. Garces, "Parameter adaptation for the apeed control static ac drive with a squirrel cage induction motor," in *IEEE transactions on Industry Applications*, pp. 173–178, March/April 1980.

[10] A. M. Khambadkone and J. Holtz, "Vector-controlled induction motor drive with a self-commissioning scheme," *IEEE Transactions on Industrial Electronics*, vol. 38, pp. 322–327, October 1991.

[11] M. Depenbrock, "Direct self control(dsc)of inverter-fed induction machines," *IEEE Trans. on Power Electron.*, vol. 3, pp. 420–429, Oct. 1988.

[12] I.Takahashi and T.Noguchi, "A new quick response and high-efficiency control strategy of an induction motor.," *IEEE Trans. on Industry Applications*, vol. IA-22, pp. 820–827, Sept/Oct. 1986.

[13] M. Jaenecke, R. Kremer, and G. Steuerwald, "Direct self-control (dsc), a novel method of controlling asynchronous machines in traction applications," in *European Power Electronics conference EPE89,Conference records, Aachen*, pp. 75–81, 1989.

[14] J. Holtz and S. Stadtfeld, "A predictive controller for the stator current vector of ac machines fed from a switched voltage source," in *International Power Electronics Conference, IPEC, Tokyo*, pp. 1665–1675, 1983.

[15] J. Holtz and E. Bube, "Field-oriented asynchronous pulsewidth modulation for high performance ac machines operating at low switching frequency," in *Conference Record, IEEE-IAS Annual Meeting, Pittusburgh*, pp. 412–417, 1988.

[16] M. Kazmierkowski and M. A. Dzienialkowski, "Novel current regulators for vsi-pwm inverters," in *European Power Electronics Conference, EPE'89, Conference Records, Aachen*, pp. 23–28, 1989.

[17] A. M. Khambadkone and J. Holtz, "Low switching frequency and high dynamic pulsewidth modulation based on field-orientation for high-power inverter drive," *IEEE Transactions on Power Electronics*, vol. 7, pp. 627–632, October 1992.

[18] J. Holtz, "Pulsewidth modulation - a survey," *IEEE Trans. on Industrial Electronics*, vol. 38, no. 5, pp. 410 – 420, 1992.

[19] G. Juhasz, S. Halasz, and K. Veszpremi, "New aspects of a direct torque controlled induction motor drive," in *Industrial Technology 2000. Proceedings of IEEE International Conference on*, pp. 43–49, Jan 2000.

[20] D. Casadei, G. Serra, and A. Tani, "Implementation of a direct torque control algorithm for induction motors based on discrete space vector modulation," *IEEE Transaction on Power Electronics*, vol. 15, pp. 769–777, July 2000.

[21] A. Purcell and P. Acarnely, "Enhanced inverter swicthing for fast response direct torque control," *IEEE Transactions on Power Electronics*, vol. 16, pp. 382–389, may 2001.

[22] L. Xu and M. Fu, "A sensorless direct torque control technique for permanent magnet synchronous motors," in *IEEE Industry Applications Conference*, vol. 1, pp. 159–164, 1999.

[23] J.-K. Kang and S.-K. Sul, "New direct torque control of induction motor for minimum torque ripple and constant switching frequency," in *IEEE transactions on Industry Applications*, vol. 35, pp. 1076–1082, sept-oct 1999.

[24] L. Cristian, I. Boldea, and F. Blaabjerg, "A modified direct torque control for induction motor sensorless drive," in *IEEE transactions on Industry Applications*, vol. 36, pp. 122–130, January/February 2000.

[25] N. Mohan, T. Undeland, and W. Robbins, "Power electronics converters, applications and design," John Wiley, 1985.

[26] M. P. Kazmierkowski and G. Buja, "Review of direct torque control methods for voltage source inverter-fed induction motors," in *Industrial Electronics Society, IECON '03. The 29th Annual Conference of the IEEE*, november 2003.

[27] J. Holtz, W. Lotzkat, and A. M. Khambadkone, "On continuous control of pwm inverters in overmodulation range including six-step," *IEEE Transaction on Power Electronics*, vol. 8, pp. 546–553, 1993.

[28] A. R. Bakhshai, Géza, Joós, P. K.Jain, and H. Jin, "Incorporating the overmodulation range in space vector pattern generators using a classification algorithm," *IEEE Trans. on Power Electronics*, vol. 15, pp. 83 – 91, January 2000.

[29] D.-C. Lee and G.-M. Lee, "A novel overmodulation technique for space-vector pwm inverters," *IEEE Trans. on Power Electronics*, vol. 13, no. 6, pp. 1144–1151, 1998.

[30] S. Bolognani and M.Zigliotto, "Novel digital continuous control of svm inverters in the overmodulation range," *IEEE Trans. on Industrial Applications*, vol. 33, no. 2, pp. 525–530, 1997.

[31] G. Narayanan and V. T. Ranganathan, "Overmodulation algorithm for space vector modulated inverters and its application to low switching frequency pwm techniques," in *Electric Power Applications, IEE Proceedings*, vol. 148, November 2001.

[32] A. M. Khambadkone and J. Holtz, "Current control in overmodulation range for space vector modulation based vector controlled induction motor drives," (Nagoya, Japan), pp. 1334–1339, October 2000.

[33] H. Mochikawa, T. Hirose, and T. Umemoto, "Overmodulation of voltage source pwm inverter," in *JIEE-Ind Society conference records*, 1991.

[34] D. R. Seidl, D. A. Kaiser, and R. D. Lorenz, "One-step optimal space vector

pwm current regulation using a neural network," in *IEEE-Industrial Application Soc. Conf. Rec.*, 1994.

[35] S.Jul-Ki and S. Sul, "A new overmodulation strategy for induction motor drive using space vector pwm," in *IEEE Applied Power Electronic Conference*, March 1995.

[36] A. M. Hava, S.-K. Sul, R. J. Kerkman, and T. A. Lipo, "Dynamic overmodulation characteristics of triangle intersection pwm methods," in *IEEE transactions on Industry Applications*, vol. 35, pp. 896–907, July/August 1999.

[37] P. Tenti, A. Zuccato, L. Rossetto, and M. Bortolotto, "Optimum digital control of pwm rectifiers," in *IEEE-IECON Conference records*, 1994.

[38] A. M. Hava, R. J. Kerkman, and T. A. Lipo., "Carrier-based pwm-vsi overmodulation strategies: analysis, comparison, and design," *IEEE Transactions on Power Electronics*, vol. 13, pp. 674–689, July 1998.

[39] M. Depenbrock, *Pulsewidth control of a three phase inverter with non-sinusoidal phase voltages*, pp. 399–403. 1977.

[40] S. Ogasawara, H. Akagi, and A. Nabae, "A novel pwm scheme of voltage source inverter based upon space vector theory," in *European Power Electronics Conference records*, 1989.

[41] R. J. Kerkman, T. M. Rowan, D. Leggate, and B. J. Seibel, "Control of pwm voltage inverters in pulse dropping range," *IEEE Industry Application Magazine*, vol. 2, pp. 24–31, Sept-Oct 1996.

[42] S. H. Kim and S.K.Sul, "Maximum torque control of an induction machine in the field weakening region," *IEEE transactions on Industry Applications*, vol. 31, no. 4, 1995.

[43] L. Harnefors, K. Pietilinen, and L. Gertmar, "Torque-maximizing field-weakening control: Design, analysis, and parameter selection," in *IEEE Transactions on Industrial Electronics*, vol. 48, February 2001.

[44] G. Griva, F. Profumo, M. Abrate, A. Tenconi, and D. Berruti, "Wide speed range dtc drive performance with new flux weakening control [for induction motor drives]," in *Power Electronics Specialists Conference, 1998. PESC 98 Record. 29th Annual IEEE*, vol. 2, pp. 1599 – 1604, May 1998.

[45] D. Casadei, G. Serra, A. Tani, L. Zarri, and F. Profumo, "Performance analysis of a speed sensorless induction motor drive based on a constant switching frequency dtc scheme," in *IEEE transactions on Industry Applications*, vol. 39, pp. 476–484, March/April 2003.

[46] M. P. Kazmierkowski and H. Tunia, *Automatic Control of Converter-Fed Drives*. Amsterdam: Elsevier science publishers, 1994.

[47] J.Hu. and B.Wu, "New integration algorithms for estimating motor flux over a wide speed range," *IEEE transactions on Power Electronics*, vol. 13, no. 5, pp. 694–700, 1998.

[48] M. H. Shin, D. S. Hyun, and S. Y. Choe, "An improved stator flux estimation

for speed sensorless stator flux orientation control of induction motors," in *IEEE Transactions on Power Electronics*, vol. 15, pp. 312 –318, march 2000.

[49] J. Holtz and J. Quan, "Sensorless vector control of induction motors at very low speed using a nonlinear inverter model and parameter identification," in *Industry Applications Conference, Thirty-Sixth IAS Annual Meeting*, vol. 4, pp. 2614 –2621, sept-oct 2001.

[50] M. Hinkkanen and J. Luomi, "Modified integrator for voltage model flux estimation of induction motors," in *Industrial Electronics Society, IECON '01. The 27th Annual Conference of the IEEE*, vol. 2, pp. 1339 –1343, sept-oct 2001.

[51] N. Idris and A. Yatim, "An improved stator flux estimation in steady state operation for direct torque control of induction machines," *IEEE transactions on Industry Applications*, vol. 38, no. 1, 2002.

[52] P. K. Kovacs, *Transient phenomenon in Electrical Machines.* Amsterdam: Elsevier science publishers, 1984.

[53] D. Lee and G.-M. Lee, "A novel overmodulation technique for space-vector pwm inverters," *IEEE Transactions on Power Electronics*, vol. 13, pp. 1144–1150, Nov. 1998.

[54] S. Bolognani and M. Zigliottio, "Novel digital continuous control of svm inverters in the overmodulation range," *IEEE Transations on Industry Applications*, vol. 33, no. 2, pp. 525–530, 1997.

[55] P. G. Handley and J. T. Boys, "Practical real-time pwm modulators: an assessment," *IEE-Proceeduings Part B, Electric Power Applications*, vol. 139, pp. 96–102, march 1992.

[56] R. Wu and G. R. Slemon, "A permanent magnet motor drive without a shaft sensor," in *IEEE Industry Applications Conference*, vol. 1, pp. 553–558, 1990.

[57] B.-S. Lee and R. Krishnan, "Adaptive stator resistance compensator for high performance direct torque controlled induction motor drives," in *Industrial Applications Society, IAS '1998. The Thirty-Third IAS Annual Meeting*, vol. 1, pp. 423–430, Oct 1998.

[58] H. Krishnamurthy, G. Narayanan, R. Ayyanar, and V. Ranganathan, "Design of space vector-based hybrid pwm techniques for reduced current ripple," in *Applied Power Electronics Conference and Exposition, 2003. APEC '03*, vol. 1, pp. 583 –588, February 2003.

[59] X. Xu and D. W. Novotny, "Selection of the flux reference for induction machine drives in the field weakening region," in *IEEE Transactions on Industrial Applications*, vol. 28, November/December 1992.

[60] dSPACE, "Squirrel cage induction motor control with ds1102," in *Application Note*, vol. 1.0, 1994.

[61] dSPACE, "General software installation guide," vol. 2.0, 1994.

[62] dSPACE, "Floating-point controller board - ds110. user's guide," vol. 2.0, 1994.

[63] D.-W. Chung and S.-K. Sul, "A new dynamic ovemodulation strategy for high performance torque control of induction motor," in *Fourteenth Annual Applied Power Electronics Conference and Exposition, 1999. APEC '99.*, vol. 1, pp. 264 –270, March 1999.

List of Publications

Published/Accepted for Publication

Journals

1. Anshuman Tripathi, Ashwin M. Kambadkone and Sanjib K. Panda, "Stator Flux based Space Vector Modulation and Closed Loop Control of the Stator Flux Vector in Overmodulation into Six-Step Mode," *Published in IEEE transactions on Power Electronics*, Vol. 19, No. 3, May 2004, pp.775 - 782.

2. Anshuman Tripathi, Ashwin M. Kambadkone and Sanjib K. Panda, "Torque Ripple Analysis and Dynamic Performance of a Space Vector Modulation Based Control Method for AC-Drives," *Published in IEEE transactions on Power Electronics*, Volume 20, Issue 2, March 2005 Page(s):485 - 492.

3. A. Tripathi, A. M. Khambadkone and S. K. Panda, "Direct Method of Overmodulation with Integrated Closed Loop Stator Flux Vector Control," *Accepted for publication in IEEE transactions on Power Electronics.*

4. A. Tripathi, A. M. Khambadkone and S. K. Panda, "Analysis of Current

Dynamics in a Direct Torque Control Scheme," *Accepted for publication in IEEE transactions on Industrial Electronics.*

Conferences

1. A. Tripathi, A. M. Khambadkone and S. K. Panda, "Space-vector based, Constant Frequency, Dead Beat Stator Flux Control of AC Machines," *Power Electronics and Drive Systems, 2001. Proceedings., 2001 4th IEEE International Conference on*, October 2001, pp.329 - 334.

2. Anshuman Tripathi, A. M. Khambadkone and S. K. Panda, "Space-vector based, Constant Frequency, Direct Torque Control and Dead Beat Stator Flux Control of AC Machines," *IEEE International Conference on Industrial Electronics, Control, Instrumentation and Automation, IECON*, Vol. 2, November 2001.

3. A. Tripathi, A. M. Khambadkone and S. K. Panda, "Predictive Dead-beat Stator Flux Control with Overmodulation and Dynamic Torque Control at Constant Switching Frequency in Ac - drives," *IEEE Industry Application Conference,* 37^{th} *IAS annual meeting*, October 2002, pp.2080–2085.

4. Tripathi A., Khambadkone A.M. and Panda S.K., "Analysis and Performance of Direct Flux Control Scheme for Dynamic Torque Control in AC Drives," *IEEE International Conference on Electric Machines and Drives, IEMDC'03*, Vol. 2, June 2003, pp.709 -714.

5. Liu Qinghua, Khambadkone A.M. and Tripathi A. and Jabbar M.A., "Torque Control of IPMSM Drives using Direct Flux Control for Wide Speed Operation," *IEEE International Electric Machines and Drives Conference*, June 2003, pp.188 - 193.

6. Tripathi A., Khambadkone A.M. and Panda S.K., "Speed Sensorless Control of AC Machines using Direct Flux Control Scheme," *Power Electronics and Drive Systems, 2003. Proceedings., 2003 4th IEEE International Conference on*, November 2003, pp.1647 - 1652.

7. Tripathi A., Khambadkone A.M. and Panda S.K., "Dynamic Torque Control Performance of the Direct Flux Control Scheme in Field Weakening Range," *IEEE International Conference on Industrial Electronics, Control, Instrumentation and Automation, IECON*, November 2003, pp.220 - 225.

8. A. Tripathi, A. M. Khambadkone and S. K. Panda, "Direct Method of Overmodulation with Integrated Closed Loop Stator Flux Vector Control," *35th Annual IEEE Power Electronics Specialists Conference*, June 2004, pp. 4196 - 4201.

Submitted for Review

1. A. Tripathi, A. M. Khambadkone and S. K. Panda, "Dynamic Torque Control Performance of the Direct Flux Control Scheme in Field Weakening Range," *Submitted for review for publication in IEEE transactions on Power Electron-*

ics.